Measuring techniques of Induced Polarization regarding data quality with an application on a test-site in Aarhus, Denmark and the tunnel construction at the Hallandsås Horst, Sweden

Carl-Henrik Månsson & Jonas Siikanen

Examensarbeten i Geologi vid Lunds universitet - Kvartärgeologi, nr. 217

Tillika:
Examensarbeten i Fysik vid Lunds universitet
Teknisk geologi vid Lunds Universitet / LTH
(ISRN: LUTVDG/TVTG--5110--SE)

Geologiska institutionen
Centrum för GeoBiosfärsvetenskap
Lunds universitet
2007

Measuring techniques of Induced Polarization regarding data quality with an application on a test-site in Aarhus, Denmark and the tunnel construction at the Hallandsås Horst, Sweden

Master Thesis

Carl-Henrik Månsson
Jonas Siikanen

Department of Geology | Engineering Geology | Department of Physics

Lund University
2007

Contents

Cover Picture: The Hallandsås Horst, Site 2. Picture is taken during fieldwork.

Preface

The work has been divided as follows:

Jonas Siikanen has been responsible for the interpretation and discussion of the field tests at Lund and Aarhus, chapter 6.5 and 7.5.

Carl-Henrik Månsson has been responsible for the interpretation and discussion of the field test at the Hallandsås Horst, chapter 8.5.

The rest of the work has been done together.

Measuring techniques of Induced Polarization regarding data quality with an application on a test-site in Aarhus, Denmark and the tunnel construction at the Hallandsås Horst, Sweden

CARL-HENRIK MÅNSSON & JONAS SIIKANEN

Månsson, C-H., 2007: *Examensarbeten i geologi vid Lunds universitet*, Nr. 217, 54 pp. 20 points.

Siikanen, J., 2007: *Examensarbeten i fysik vid Lunds universitet*, 54 pp. 20 points.

Abstract: It has been shown that surveys of Induced polarization (IP) often contain data of low quality, because it is highly sensitive against different noise sources. When measuring induced polarization, where the method uses multicore cables and continuous electrode sounding (CVES, Continuous Vertical Electrical Sounding), noise phenomena such as capacitive coupling effects have to be considered. It is possible to decrease the capacitive coupling effect by using separated cables. This noise occur between transmitting current cable and potential reading cable. Also, other effects such as electromagnetic coupling effects will generate bad quality of data. This appears between the current electrodes and the electrical properties of the subsurface. It is strongly dependent on the length of the array. However, to obtain data of good quality, the electrode contact has to be taken into account as well. The purpose with this thesis is to examine the quality of data when measuring IP, with different techniques, and then apply the obtained experience in two different geological environments, Aarhus, Denmark and the tunnel construction at the Hallandsås Horst. The geophysical methods used were CVES 2D sounding of IP and resistivity. For a better interpretation and analysis, the results of the resistivity measurement are used as a complement to the results of IP. To achieve the purpose, measurements with both normal layouts, i.e. multicore cable, and separated cables has been made. Also different types of electrode configurations have been examined. Analysis of negative data and distribution of chargeabilities gives a good picture of the data quality. Once, electrode contact resistance was measured; this was done by measuring the resistance of each electrode. The survey was performed on a lawn at the Institute of Engineering, Lunds University, Lund. From earlier measurements it has been indicated that the area of investigation in Aarhus contains something that gives IP effect. This was examined with experience from the measurements in Lund. The survey area at the Hallandsås Horst has never earlier been examined with the method that is used in this work. Therefore, this site was chosen to complement the last part of the tunnel area and also use the knowledge from the measurements in Lund. This thesis shows that the capacitive coupling is manifested for example by negative data, which affect the measured IP effects negatively. Bad electrode contact is probably a strong candidate to the low quality of data, as well as the inductive coupling effects. The technique of using separated cables contributes to data of good quality IP data, but are logistically complicated and time consuming. It was shown, both in Aarhus and at the Hallandsås Horst, that if the geology in an area contributes to a good electrode contact, the results are satisfying when using normal cable layout. The survey in Aarhus gave a strong IP-effect that is interpreted as a pipeline. This is situated about 5 to 10 m under the ground surface. The results from the measurement at the Hallandsås Horst have given three major structures: One dolerite dike that crosses the tunnel, a probable fracture zone that may be partly clay weathered and partly water bearing. Finally, one more clay weathered fracture zone was interpreted which might contain amphibolite. The upper boundary is in level with the tunnel.

Keywords: Induced Polarization, capacitive coupling, separated cables, chargeability, CVES, the Hallandsås Horst

Carl-Henrik Månsson, Department of Geology, GeoBiosphere Science Centre, Lund University, Sölvegatan 12, SE-223 62 Lund, Sweden. E-mail: ch.mansson@hotmail.com

Jonas Siikanen, Department of Physics, Lund University, Sölvegatan 14C, SE-223 62 Lund, Sweden. E-mail: siikanen@hotmail.com

Mättekniker av Inducerad Polarisation med avseende på data-kvalitet samt tillämpning på ett testområde i Århus, Danmark och tunnelbygget på Hallandsås, Sverige

CARL-HENRIK MÅNSSON & JONAS SIIKANEN

Månsson, C-H., 2007: *Examensarbeten i geologi vid Lunds universitet*, Nr. 217, 54 sid. 20 poäng.

Siikanen, J., 2007: *Examensarbeten i fysik vid Lunds universitet*, 54 sid. 20 poäng.

Sammanfattning: Undersökningar med Inducerad Polarisation (IP) är mättekniskt sett mycket känsliga mot olika störningskällor och innehåller därför ofta data av dålig kvalitet. När man mäter inducerad polarisation, och använder sig av multiledare och kontinuerlig mätning (CVES, Continuous Vertical Electrical Sounding), uppstår brus orsakat av kapacitiv koppling. Denna effekt genereras mellan strömledare och mätande potentialkabel. Det är möjligt att minska den kapacitiva kopplingen genom att separera dessa kablar. Även andra störkällor påverkar datakvaliteten negativt. Elektromagnetisk (induktiv) koppling är en sådan effekt som uppstår mellan strömelektrod och markens ledande egenskaper, denna effekt är också beroende av längden på kabelutlägget. Det är viktigt att ha en god elektrodkontakt för att uppnå data av god kvalitet. Syftet med examensarbetet är att undersöka datakvaliteten i IP-mätningar när olika typer av mättekniker använts, för att sedan applicera dessa erfarenheter på två olika geologiska miljöer, Århus, Danmark och tunnelbygget vid Hallandsås. De geofysiska metoder som användes var CVES 2D-undersökning av IP och resistivitet. Resistivitetsresultaten användes som komplement till IP-resultaten för en bättre analys och tolkning. För att uppnå syftet har mätningar med både normalt utlägg, d.v.s. en enkel multiledarkabel, och separerade kablar utförts och analyserats. Även olika elektrodkonfigurationer har undersökts. Analys av negativa värden och distributioner av IP effekter i pseudosektioner ger en god bild av datakvalitet. Elektrodkontakten har vid ett tillfälle analyserats genom att resistansen mättes vid varje elektrod. Analyserna är utförda på en gräsmatta vid Teknisk geologi, Lunds Universitet, Lund. Det fanns indikationer från tidigare mätningar att undersökningsplatsen i Århus innehöll något som gav IP effekt. Detta undersöktes med erfarenheter från de tidigare mätningarna i Lund. Undersökningsplatsen på Hallandsås har ej tidigare undersökts med denna metod. Därför valdes denna plats för att komplettera den sista biten av tunnelsträckningen, samt tillämpa erfarenheterna från mätningarna i Lund. Resultaten bekräftar att kapacitiv koppling orsakar t.ex. negativa data som påverkar resultaten av IP effekter negativt. Elektrodkontakten är förmodligen också en stark bidragande orsak till dålig kvalitet på data, likaså den elektromagnetiska kopplingen. Tekniken med att använda separerade kablar ger god kvalitet på IP data men är också en väldigt logistiskt komplicerad och tidsmässigt krävande metod. Det har visats sig, både i Århus och på Hallandsås, att om geologin i ett undersökningsområde är av sådan karaktär att god elektrodkontakt kan uppnås, är kvaliteten på data tillfredställande även när en normal mätning med en kabel är utförd. Undersökningen i Århus gav en stark IP-effekt vilket tolkas som ett rör och ligger ca 5 till 10 m under markytan. Resultaten från Hallandsås har visat tre huvudsakliga geologiska formationer: En diabasgång som skär tunneln, en trolig sprickzon som kan vara delvis lervittrad och delvis vattenförande. Denna ligger huvudsakligen under tunnelnivån. Slutligen hittades ytterligare en sprickzon som bör innehålla amfibolit och troligtvist är lervittrad. Sprickzonens övre gräns är i nivå med tunneln.

Nyckelord: Inducerad polarisation, kapacitiv koppling, separerade kablar, CVES, Hallandsås

Carl-Henrik Månsson, Geologiska Institutionen, Centrum för GeoBiosfärsvetenskap, Lunds Universitet, Sölvegatan 12, 223 62 Lund, Sverige. E-post: ch.mansson@hotmail.com

Jonas Siikanen, Fysiska Institutionen, Lunds Universitet, Sölvegatan 14C, 223 62 Lund, Sverige. E-post: siikanen@hotmail.com

1. Introduction

1.1 Background

In geophysics, measurement of Induced Polarization (IP) is a method that uses the sub-surface capability to act as a capacitor. The first who described the IP effect was Conrad Schlumberger (1878-1936) in 1920. He claimed though that background noise was so extensive that it tended to overshadow the IP effect. This led to that research on IP was discouraged for many years (Sumner 1976).

During the 20th century, the use of IP in environmental, hydrogeological and mineral prospecting purposes has been more popular, but the method is still at a research stage (Reynolds (1997).

Besides background noise, there are other noise sources that are more prevalent when using e.g. multicore cables and CVES (Continuous Vertical Electrical Sounding) technique. One is the capacitive coupling effect, which depends on for example the separation of the electrodes. Another one is the Electromagnetic (inductive) coupling effect (EMC).

These effects will affect the quality of data negatively. Unfortunately, it is problematic to reduce these effects by mathematical corrections. This study will show the difference in quality by physically reducing the capacitive coupling effect when using separated cables for current transmitting and potential reading cables in the layout. Also, the EMC will be discussed. However, it is a time-consuming and logistically complicated method to use separated cables.

In this study, an investigation regarding data quality was performed. This was surveyed at a site close to the Lund Institute of Technology.

The obtained experience was applied on two other sites, a test-line in Aarhus and the tunnel construction on the Hallandsås Horst.

The test-line in Aarhus has a moderate ground resistivity and the subsurface may contain something that gives IP-effect. The data quality was investigated by using both single cable and separated cable arrays.

Constructing a tunnel requires a good knowledge about the subsurface, especially the quality of the rock and the hydrogeological conditions. One way to get this information is to drill boreholes and examine the drilling cores. However, this is a very expensive way to get this information and will only provide discrete points of information. Geoelectrical methods provide continuous information about the subsurface that is feasible in point of economy.

In 1988 a decision was made by the Swedish government that the traffic in Sweden should be safer, more effective and ecofriendly. Therefore, the decision, among other things, led to a project of constructing a railway tunnel in the Hallandsås Horst, to make the railway net more modern. This tunnel should reduce the transport problems due to sharp curves and steep slopes that are present today (www.banverket.se). In 1989 the pre-study of the geological and hydrogeological conditions took place and was surveyed by different geophysical methods. Between year 1995-1998, investigation with CVES were performed (Banverket 2002).

One part of the site is still not investigated either by resistivity nor IP measurement. This site is situated south of the Southern Marginal Zone (SMZ), at the southern part of the tunnel.

The measurement of this site will complete the last part of the geoelectrical measurements of the Hallandsås Horst. Both resistivity and IP will be measured and the data quality will be investigated as well.

1.2 Purpose and limitations

The purpose of this study is to:

- Investigate the data quality when measuring Induced polarization (IP) for optimizing field techniques.
- Applying and evaluate the technique in a field measurement at a test site in Aarhus and the tunnel project at Hallandsås Horst.

This study will discuss primary the results of induced polarization, but the results of resistivity will be taken into account as well, especially in the measurement of the Hallandsås Horst.

In the first stage, the test-line in Lund, Sweden, concentration on the data quality is the primary object. Therefore, the geological description is not so detailed.

In the second and third stage, applying the technique in a field test in Aarhus, Denmark and on the Hallandsås Horst, Sweden, the geological description is more detailed.

2. Study areas

2.1 Test-line Lund

The site is situated on the backside of building V, Faculty of Engineering, Lund University, Sweden. It is approximately a 120 m long and 5 m wide grass covered area with some trees on a line. The site is in an urban environment with buildings and paved courts; hence the subsurface contains filling material and electrical power-cables etc. The area is expected to be a high noise area and the data acquisition will probably give data of rather low quality. The different types of measurements will probably appear with significant differences.

2.2 Test-line Aarhus, Denmark

The study area is located just outside the city of Aarhus on the eastern coast of Jutland, Denmark. The area of investigation is a grass path between a pea field and a forest with deciduous trees. The subsurface contains material which gives IP-effect. This will be investigated with experience from the measurements in Lund and analysis of data quality can be made.

2.3 The Hallandsås Horst

The Hallandsås Horst is situated in the north-western part of Scania, Sweden. It is the northernmost of the scanian horsts (Wikman and Bergström 1987).

The area of interest is the southern part of the tunnel. It is situated north of Förslöv, a small village on the Bjäre peninsula.

The field site is approximately 1 km long. The first 200 m of the site is located on a rather flat meadow. The site is then interrupted by a road, where measurements can not be made. After the road the topography increases and a beech forest covers the ground for about 100 m. The next 400 m consists of a grass field and the last 200 m goes over a ploughed field.

3. Geology and hydrogeology

Geological timescale is shown in Fig. 3.1.

3.1 Lund, Sweden

The geology is built up of clayey till with intrabeds of sand and silty sand overlying shale, according to measured log 25 m west of the line (Table 3.1). The quaternary deposits are up to 50 meters thick (Persson (Alm) 1985). Paved courts are situated on both sides, so probably there are some filling materials as well (Dahlin 1999).

Table 3.1 Lithology in borehole LTH1, Sweden (Persson (Alm) 1985)

Depth (m)	Material
0.0 – 8.0	Boulder clay
8.0 – 11.0	Sandy layer
11.0 – 13.5	Boulder clay.
13.5 – 28.0	Sand and silty sand.
28.0 – 29.3	Silty sand and sand with stones and gravel.
29.3 – 41.8	Boulder clay.
41.8 – 51.3	Sand.
51.3 – 52.5	Sand and gravel.
52.5 – 64.0	Shale and limestone.
64.0 – 66.0	Silty sandstone.
66.0 – 73.5	Shale and limestone.
73.5-	Dolerite

3.2 Aarhus, Denmark

Geological development

Thick layers of tertiary and quaternary deposits cover the middle part of Jutland. The depth to the underlying Cretaceous limestone decreases northward. The Fennoscandian border zone, a NW – SE trending fault zone that marks the south-western end of the Fennoscandian shield, crosses Northern Jutland. The Precambrian bedrock south of it has subsided gradually during long time; more or less at same time the overlaying Mesozoic layers were formed. This resulted in the Danish basin with thick layers of Mesozoic bedrock. There are several salt domes that penetrate the Mesozoic layers. The salt was formed during Permian, when the climate was very dry, and later uplifted by the pressure of overlaying sedimentary bedrock. The salt domes do not reach higher than 200 m below ground level. During the Tertiary period heavy layers of clays were deposited in a deep-sea environment, in some places these layers are more than 1 km thick. Towards the end of the Tertiary period the land was uplifted and during the Quaternary period several ice sheets deposited till material. Mid-Jutland have actually sediment from all known glacials and interglacial's in Denmark (Larsen and Kronborg 1994).

Quaternary and Tertiary deposits

The Tertiary formation consists of mud and low-permeable clays with chalk and sand. The thickness of the Tertiary formation in the Aarhus area can be up to 200 m and is formed during the Eocene and Oligocene.

The Quaternary deposits, are in some part of the Aarhus area, made of unconsolidated sediments that contains fine to medium and coarse-grained sand. The composition of the sand is predominantly made up of quartz. The thickness of these sediments can reach up to 100 m. Thus; this type of formation is the main aquifer in the area. These deposits are often covered by periglacial formations due to eolian, fluvial, and lacustrine processes. They are mostly composed of clay, silt, sand and gravel. In other parts the sandy Quaternary deposits are covered by glacial tills with varying contents of clay.

In the area of investigation, data from TEM (Transient Electric Method) measurements show a highly conductive layer where the top boundary is lying between 40-80 meter above sea level (m.a.s.l.) (Fig. 3.2). This formation is low-permeable clay and serves as the lower hydraulic boundary of the aquifers (Sørensen *et al.* 2003).

3.3 The Hallandsås Horst, Sweden

Geological development

The Hallandsås Horst consists mainly of Precambrian fine-grained to medium-grained gneiss, flanked by sedimentary rocks. It is situated within the Fennoscandian Border Zone. In the area there are also amphibolitic parts and several generations of NW-SE trending dolerite dikes. (Dahlin *et al.* 1999)

Amphibolites are present in the area in two different generations. The older generation of amphibolites often appears as layers or prolonged amphibolite parts in the gneiss. The origin is basaltic rock that has undergone metamorphosis and mineral transformation. When the content of amphibolitic minerals is at least 50 percent, the bedrock is considered an amphibolite. The younger generation is in fact metabasites that have not gone through a complete amphibolite transformation. This generation is more homogenous and

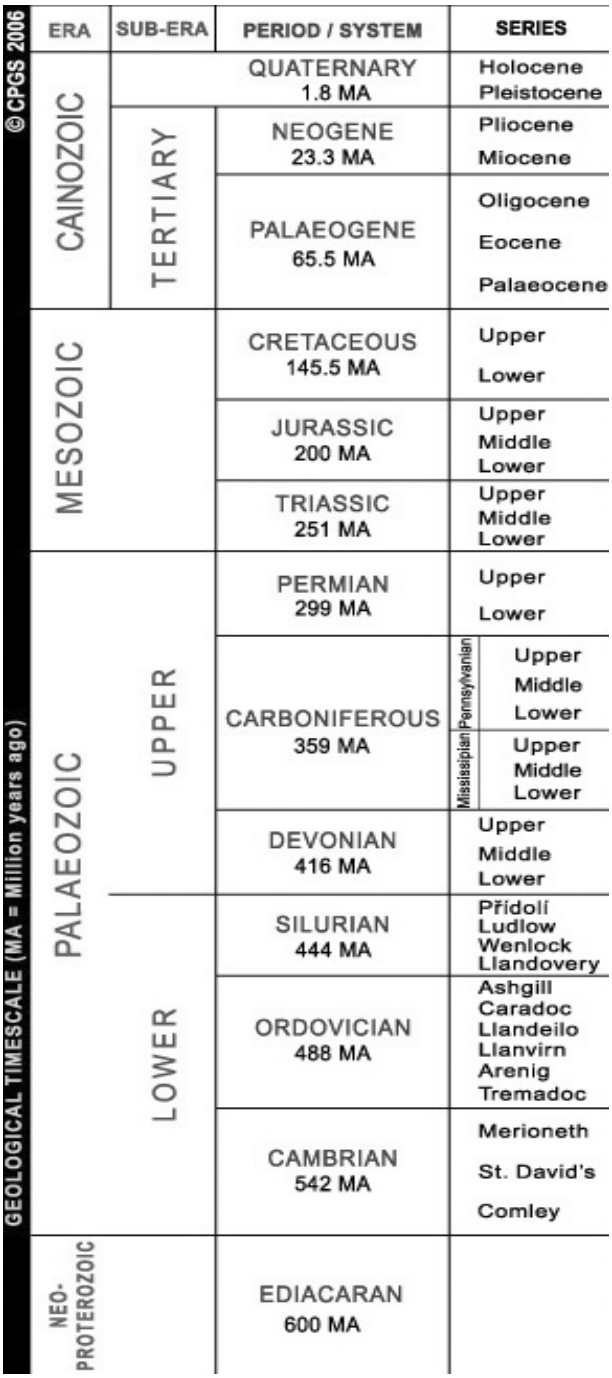

Fig. 3.1. Geological timescale (www.kabrna.com)

tends to shows up as dikes (Wikman and Bergström 1987).

The development of the Tornqvist zone resulted in a NW-SE trending fracture and fault system. The expansion started in the Cambrian-Silurian periods but the zone has also been active in later periods. In the Permian-Carboniferous periods basaltic magma slowly erupted through the fractures and formed dolerite dikes. The orientation is NW-SE to WNW-ESE and the widths of the dikes are from some decimetres to about 50 meters. In the vicinity of the dolerite dikes water bearing fractures are commonly present. However, the contact between dolerite and surrounding rock is often dry due to merging when the magma cooled. Another joint system exists roughly perpendicular to the main fracture orientation. The orientation is N-S to NNE-SSW and seems to be younger than the NW system. During Triassic, Jurassic and early Cretaceous the area underwent extensive weathering which transformed the upper bedrock layer to, among other things, kaolin (Wikman and Bergström 1987). During late Cretaceous major faulting and uplifting of the bedrock occurred which resulted in horst development. Some parts of the weathered bedrock in faulted areas was then subsided and protected from erosion by later inland ice. (Sturk *et al.* 2005).

The major fault zones that limit the Hallandsås horst are the northern and southern marginal zones. Tectonic activity has also had considerable impact on the central parts of the horst where the bedrock in places has been fissured and divided into minor plinths surrounded by weak zones. The most extensive weak zone in the central area is the Möllebacken zone (Banverket 2002).

The Southern Marginal Zone, SMZ is roughly 650 m wide (Sturk *et al.* 2005). It is a complex area which mainly consists of heavily weathered bedrock with small amounts of free water. Some sections are just partly weathered and moderately water-bearing (Banverket 2002).

Quaternary deposits

The Hallandsås horst is mainly covered by till. In places where the bedrock is partly exposed the till layer is rather thin, commonly less than 5 meters. The thickest till deposits are found in the region around Förslöv with thicknesses up to 15 – 40 m. Small areas of hummocky moraine are present above the highest coastline. These areas are most likely formed by melting dead-ice. The till is generally sandy. Medium boulder frequency dominates on the horst, while the area south of the SMZ normally has a low boulder frequency. Glacial striae and drumlin shapes indicate one main direction of glacial movement from N50°-55°E (Ringberg 1995).

The highest coastline in the area is situated ca 55 – 60 m above the present coastline. The region around the highest coastline between Grevie in northwest and Förslöv in southeast is characterized by several hills that in most cases have been classified as till. At least some of these contain glaciofluvial deposits with only a thin cover of till. The glaciofluvial material is probably kame formations that have been deposited in a dead-ice environment. Till material have then melted out from the recessing ice sheet and covered the glaciofluvial deposits. Glaciofluvial deposits are also located in the Sinarp valley and especially south of the valley as eskers trending NE-SW. Littoral sediments are found below the highest coastline. On the southwest flank of the horst littoral sediments occur between 45 and 60 m.a.s.l. Gravel is the main fraction in this area. The thickness does probably not exceed 1 – 3 m. Peat is present in forms of moss peat and swamp

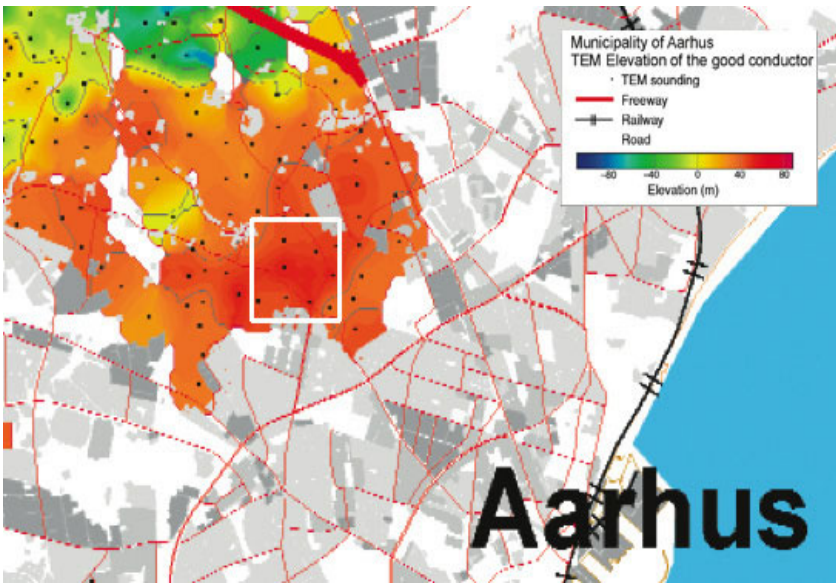

Fig. 3.2. Elevation of good conductor . TEM, White square represents the area of investigation (Modified, Sørensen *et al.* 2003).

peat. The moss peat thickness is 1 – 8 m and the swamp peat 1 – 3 m. In some of the bogs gyttja and fine-grained lake sediments is present beneath the peat (Ringberg 1995).

Hydrogeology

Groundwater is mainly connected to fracture zones in the bedrock. The contact zones between gneiss and amphibolites has normally less discontinuities than contact zones between gneiss and dolerite. Hence dolerite dikes are of great importance when interpreting the presence and quantity of water-bearing bedrock. The degree of weathering is also important. Very high degrees of weathering leads to low hydraulic conductivity, but moderate weathering leads to high or very high hydraulic conductivity.

Groundwater pressure in the tunnel varies with topography and groundwater conditions. The piezometric pressure is normally parallel to the ground surface and groundwater table is usually 0 – 15 meters beneath it. In some boreholes artesian pressures up to 10 meters above ground surface have been measured. (Banverket 2002).

4. Geoelectrical methods

4.1 Resistivity

4.1.1 Background

Conrad Schlumberger developed the technique of resistivity measurements in his first experiment in Normandy in 1912 and since the 1970s this method has become more widely used.

The technique is suitable for groundwater resource assessment and also used for surveying sub-surface cavities, fissures, faults and conductive ores (Reynolds 1997).

When measuring resistivity, the most common way is to apply a driven current through the ground, and meanwhile measure the resulting potential difference at the surface (Sharma 1997).

4.1.2 Theory

Measuring resistivity is a method that uses the capability of a material to act as an insulator and has the term ρ and the unit Ωm. Resistivity is defined as a property of a material and is a function of the amount of resistance in an electric conductor.

To describe resistivity, consider a cube that is electrically uniform with a side length of L which an amperage I is passing through (Fig. 4.1).

Depending on the properties of the material in the cube, it will somehow have an influence on the conduction of electricity and a potential difference between the opposite faces will appear.

Potential difference is caused by the resistance, R. Hence, the resistance is proportional to the length L and inversed proportional to the cross-sectional area, A (Reynolds 1997):

$$R \propto \frac{L}{A} \tag{4.1}$$

The constant of the proportionality is defined as the 'true' resistivity, ρ. This gives us:

$$R = \rho \frac{L}{A} \tag{4.2}$$

Simultaneously, according to Ohms law, resistance R is defined as:

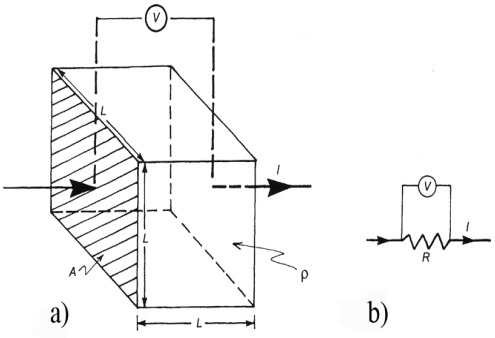

Fig. 4.1. a) Explaining model for definition of resistivity (ρ) in a homogenous cube with the sides L, where a current (I) passing thru and a potential drop (V) is created. b) Corresponding electrical circuit. R is a resistor (Reynolds 1997).

$$R = \frac{V}{I} \tag{4.3}$$

where V is the difference in potential (voltage) and I is the amperage.

By combining equation (4.2) with (4.3), resistivity (ρ) is calculated according to:

$$\rho = \frac{V}{I} \cdot \frac{A}{L} \tag{4.4}$$

The factor A/L is dependent on type of electrode configuration and electrode distance.

There are two types of conduction in a rock: electronic and electrolytic conduction.

Electronic conduction occurs when the material contains, e.g., metals, in which electrons can move rapidly and carry the charge. Electrolytic conduction is a relatively slow transportation of charge, which occurs when the material has electrolyte including ions. This type is dependent on the ionic concentration, type of ions and mobility, etc.

In a homogenous earth, the current is flowing radially from an electrode in a hemisphere. The current density, J, is proportional to the current, I, divided by the area over which the current is distributed through, in this case $2\pi r^2$. This will give:

$$J = -\rho \frac{I}{2\pi r^2} \tag{4.5}$$

Therefore, the density of the current, J, will decrease with the distance from the transmitting current electrode. This gives the possibility to calculate the voltage at any point at a distance (r) from the current source. Adding one more electrode creates a new potential distribution. This leads to a modified expression of the resistivity and a geometric factor (k) can be defined. This geometric factor is strictly dependent on the type of electrode configuration.

When measuring resistivity in field, 'true' resistivity cannot be obtained because the earth is not a homogenous body. The value that is obtained when measuring in the field is called apparent resistivity (ρ_a) and represents a set of data that can give an estimation of the resistivity distribution. To obtain 'true' resistivity, interpretation techniques have to be considered (Reynolds 1997).

The variation in resistivity of geological materials is commonly highly depending on the composition of minerals. Therefore, resistivity, in almost all geological material, depends on pore, filled pores and the resistivity of the pore liquid.

Sedimentary rocks are relatively porous types of rocks compared to crystalline rocks. Hence, the resistivity will be more dependent on the interstitial fluid than the resistivity of the host rock. Archie (1942) developed an empirical formula that gives the effective resistivity of a rock formation where the porosity, the fraction of the pores containing water and the resistivity of the water is accounted for. This is called Archie's law and is used mostly in borehole logging. However, if the medium is some kind of a gas, e.g. air (empty pore), it will increase the resistivity of a porous material. If the medium is liquid, e.g. contaminated water, it will instead decrease the resistivity (Reynolds 1997).

The resistivity in different type of earth materials is listed in Fig. 4.2.

Fig. 4.2 show that many rock types have the same resistivities and that they overlap each other. It also shows that one type of geological material can have the same resistivity as another type of geological material, e.g. both sedimentary rocks and glacial sediments have resistivity in the range of ~5 Ωm to 10 000 Ωm. Therefore, a good geological knowledge is very important when a survey with geoelectrical methods is performed.

Other things that influence the resistivity are subsurface anthropogenic materials, such as pipelines, power lines and scrap (metallic or isolating material), etc.

The field procedure when measuring resistivity is discussed in detail in chapter 5.

4.2 Induced polarization

4.2.1 Background

In 1920, Conrad Schlumberger developed a new type of sub-surface investigation method, Induced polarization (IP). He claimed though that background noise was so extensive that it tended to overshadow the IP effect. Therefore the research on IP was discouraged for many years. In the 1950's research was made on the use of IP in petroleum well logging in the Soviet Union. Since the late 1950's IP has been extensively used for ore prospecting (Sumner 1976).

In 1957 attempts were made to develop IP techniques for use in hydrogeological applications. Vacquier and his associates at New Mexico Institute of

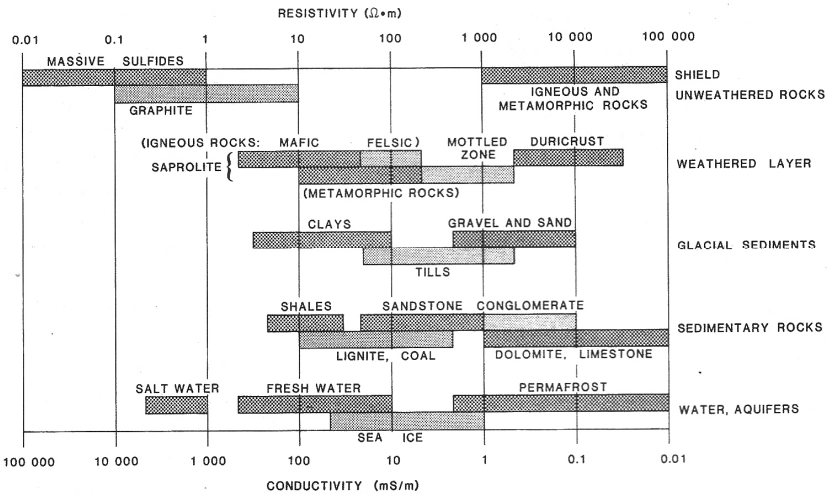

Fig. 4.2. Resistivity and the inverse (conductivity) in different earth material (Palacky 1987).

Mining and Technology discovered IP effects in contaminated sands and water-saturated clays (Sumner 1976). In recent years IP has been successfully used in hydrogeological and environmental applications, but it is still very much at a research stage (Reynolds 1997).

Some scientists claim that the name Induced polarization is not a completely correct description of the phenomenon. Induction assumes that the electrical field propagate through space without giving rise to conduction in some material. However, Induced Polarization is now an accepted term (Sumner 1976).

4.2.2 Theory

Induced Polarization is a geoelectrical method that measures the polarization characteristic of the ground and is usually measured as a function of time or a function of frequency. IP is most often used in ore prospecting applications because of the strong IP- effect in especially metal sulphides. IP is very suitable for use together with resistivity measurements. Some materials are hard to distinguish from only resistivity as the values often vary in a wide spectrum. For example fracture zones have low resistivity whether they are clay weathered or not. Clay weathering can easily be detected by IP though, since it shows high IP-effect. Resistivity is also something that is measured as a part of the procedure in IP measurements (Reynolds 1997).

The theory of Induced Polarization is very complex and not yet fully understood. There are two mechanics that describe the IP effect. These are electrode polarization and membrane polarization

Electrode polarization

Electrode (grain) polarization is a process that results from an electronically conducting mineral grain blocking a pore or a small fracture in the rock (Fig 4.3b).

When a current is applied, electrons cannot move through the grain and are therefore gathered on one side of it, making the grain polarized. When the current is switched off the ions will diffuse back through the electrolytic medium, which gives rise to voltage decay. The diffusion of ions may depend on several factors such as (Reynolds 1997):

- Pore shape and size
- Rock structure
- Permeability
- Electrolytic conductivity and ionic concentration
- Electronic conductivity of the mineral grain

Electrode polarization occurs in materials with high conductivity such as metal sulphides, oxides and graphite. IP is stronger in materials with high mineral content. Several surveys show that IP increases with increasing resistivity of the host rock (Bertin and Loeb

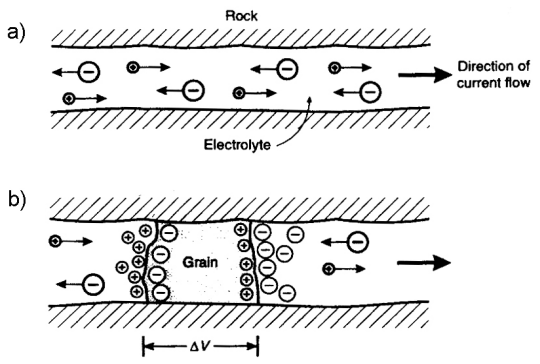

Fig. 4.3. Electrode polarization. (a) No polarization conditions. (b) Polarization of a grain blocking the channel (Reynolds 1997).

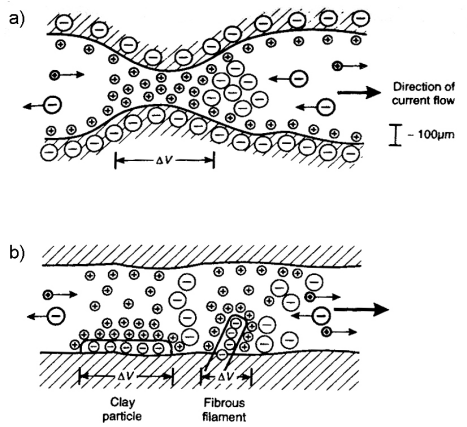

Fig. 4.4 Membrane polarization. (a) Ions creating a barrier where the channel is narrow. (b) Ions arranging due to presence of clay particles and fibrous filament (Reynolds 1997).

1976, Slater and Lesmes 2002). IP also increases as the metallic grain size decreases, maybe down to some limit. This is because the total surface area of a body increases and electrode polarization is a surface phenomenon. IP is therefore a good method to find disseminated ore bodies. Likewise homogenous ore bodies show highest IP-effect at the contact zones to the surrounding bedrock (Bertin *et al.* 1976).

Membrane polarization

Membrane polarization has two causes. One has to do with pore channel shape and the other with the presence of clay particles (Fig 4.4). Mineral surfaces are commonly negatively charged and therefore will attract positive ions from the pore fluid. A positively charged layer about 100 µm thick will develop at the mineral surface. If the pore channel is narrower than this the positive ions makes up a barrier for the negative ions and produces a potential over the pore channel (Fig. 4.4a). Diffusion takes place when the current is switched off. The other process arise when clay particles, which are negatively charged, attract positive ions and build up barriers for the negatively charged ions (Fig. 4.4b). This happens when clay particles or filaments of fibrous minerals are present in the pore space and the pore space are small enough to produce a barrier (Reynolds 1997). Membrane polarization tends to decrease with increasing pore fluid ion concentration (Bertin and Loeb 1976, Slater and Lesmes 2002).

Membrane polarization and electrode polarization give the same appearance on the overvoltage decay curve. Electrode polarization can contribute to considerably higher IP-effects though (Bertin and Loeb 1976).

Time-domain measurements

When inducing a current into the ground a voltage builds up in favourable situations as mentioned above. The voltage between two potential electrodes is then measured. When the current is turned off the voltage will decrease. The voltage is divided into primary voltage, which is the voltage that the current induce, and secondary voltage (overvoltage) that is caused by the polarization processes explained earlier. The primary voltage will vanish immediately when the current is switched off, but the secondary voltage will decrease with time in a way that is material dependent (Sumner 1976).

The most common term used in time-domain IP is chargeability (M),

$$M = \frac{V_P}{V_0} \tag{4.6}$$

where V_P is the overvoltage and V_0 the primary voltage. Chargeability is usually expressed in terms of millivolts per volt (mV/V) (Reynolds 1997).

It is almost impossible to measure the overvoltage at the moment the current is switched off. Therefore there is a time delay, usually 0.1 s, before measurement starts. The IP decay after current cut-off is then measured in several time-windows and integrated by formula 4.7, which gives the apparent chargeability (M_a) (Reynolds 1997).

$$M_a = \frac{1}{V_0}\int_{t_1}^{t_2} V_P(t)dt \tag{4.7}$$

Apparent chargeability is expressed in milliseconds (ms) or millivolts per volt (mV/V) (Reynolds 1997). The form of the overvoltage decay-curve can then be studied for more detailed information of the IP characteristics (Fig. 4.5). Field values are influenced by the volume of the earth and the array geometry and are therefore measured in apparent chargeability (Butler, 2005). What is measured is the true resistivities and absolute chargeabilities for all layers within the range of the equipment (Reynolds). Actual chargeability for each layer is interpreted in the modelling process (Butler, 2005).

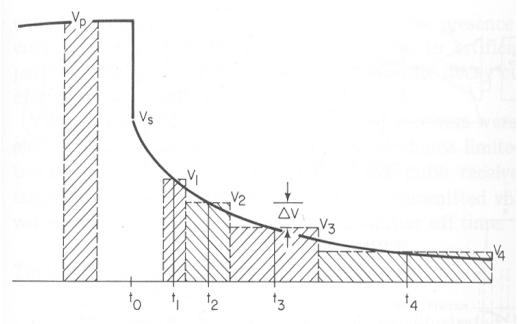

Fig. 4.5. Overvoltage decay curve (Sumner 1976).

Frequency-domain measurements

Frequency-domain IP is measured with alternating currents. Two different frequencies are measured. If the material shows large differences in apparent resistivity values for the two frequencies it means that it has a resistivity that is strongly frequency dependent . Also multifrequency IP measurement is possible. This is named Spectral IP (SIP) or complex resistivity (Reynolds 1997).

Frequency-domain measurements can be expressed as percentage frequency effect,

$$PFE = \frac{(\rho_{a0} - \rho_{a1})}{\rho_{a1}} \cdot 100 \qquad (4.8)$$

where ρ_{a0} is the apparent resistivity at low frequency and ρ_{a1} is the apparent resistivity at high frequency.

Another way to express frequency-domain IP is the metal factor.

$$MF = 2\pi 10^5 \frac{(\rho_{a0} - \rho_{a1})}{(\rho_{a0}\rho_{a1})} \qquad (4.9)$$

The numerical multiplying factor is used to place the metal factor in the same numerical range as resistivity and chargeability (Sumner 1976).

4.3 Noise

4.3.1 Capacitive coupling

Capacitive coupling is a problem when measuring Induced Polarization due to signals registered in the data acquisition that are not connected to geological parameters. This often causes errors in the IP measurement. According to Sumner (1976), capacitive coupling is a voltage change due to electrical leakage or displacement currents.

Occurrence of capacitive coupling is common when the transmitting cable is near the measuring cable in a common insulated sheath. The phenomenon that occurs is likewise an electric capacitor where the wire isolator sheath behaves as the dielectricum of a capacitor. According to Equation 4.10, the capacitance between two wires are (Sumner 1976):

$$\frac{C}{L} = \frac{27.8K_r}{\log\left[h/r \pm \sqrt{(h/r)^2 - 1}\right]} \qquad (4.10)$$

The equation shows the capacitance C per unit length L (pF/m) of two conducting wires. h is the distance, center-to-center, between the two conductors and r is the radius on the cross-section of the conductor. K_r is the relative permittivity of the material between the conductors.

There is also capacitive coupling between the cable and the ground. The potential difference that occurs is twice the value compared to the potential difference between two conductors (Sumner 1976).

When the data acquisition is carried out by using a multicore cable and a multi-channel instrument, a lot of current transmissions and potential readings are performed with a very short distance between the wires.

The capacitive coupling is relatively stable and with increasing distance between the cables, the effect will decrease quickly. Therefore, a good separation of the cables and devices will reduce the capacitive coupling (Dahlin *et al.* 2002).

4.3.2 Electromagnetic coupling

Electromagnetic coupling (EMC) is defined as the inductive response of the Earth, which manifests itself as a response over the IP signal (Partha *et al.* 2000). EMC is also called Inductive coupling (Sumner 1976).

This effect has to be considered when measuring IP. It is a noise phenomenon that has an IP-like character. Depending on array type, EMC can be a positive or negative contribution; e.g., dipole-dipole electrode configuration gives positive values and gradient electrode configuration gives negative values (Sumner 1976). Large dipole separation, i.e. long cable array, gives high EMC effects,. In frequency domain measurements, high frequencies contribute to high EMC effects. At measurements in time domain the time between the transmission and reading is of great importance. By increasing the time, the EMC effects can be reduced. The resistivity will also affect the magnitude of EMC effects where large effects can be obtained in low resistivity areas (Çağlar 2000).

A method to identify EMC is to investigate the decay curves. If the curve has increasing values in the earlier time, it is probably caused by EMC (Sumner 1976).

4.3.3 Electrode charge-up effects

In the measurement sequence, a charge is built up at the contact between the electrode and the soil. This charge-up effect contributes to significant noise in the data acquisition and can remain for tens of minutes after a current has been transmitted (Dahlin 1999). Because the measurement of IP is made shortly after the current is switched off, it is important to have low charge-up effects. Therefore, the design of the measurement protocol will contribute to more or less charge-up effects. When measuring with a normal layout, one single multicore cable, the protocol should be designed so that the reading of the potential is not performed when transmitting current has recently been made in the same electrode (Dahlin 1999). By using separated cables, charge-up effects should be nonexistent because the transmitting electrodes and potential reading electrodes are separated.

4.3.4 Other noise sources

Telluric noise

In the earth, a small, slowly varying current is flowing continuously. This is due to variation in the earth's magnetic field. This current will affect the signal in the

IP data acquisition and has to be considered. Telluric noise is often larger in high resistivity areas than in low resistivity areas. This is because the transmitting signal is larger relative to the noise in areas with low resistivity. (Sumner 1976).

Man made noise

Also power-lines, buried or airborne, will contribute to the noise in data. This is usually AC on low frequency and can therefore be low-pass filtered in the voltage-meter/receiver and thereby reduced. More problematic is man made DC-noise such as electric railways and other DC-devices (Sumner 1976).

Self potential

Depending of the contents of the subsurface, there is usually a difference in potential between two points. This will also have an influence on the collected data. The differences are weak and are caused by e.g. groundwater movement, ores and high geothermal areas (Parasnis 1997).

4.4 Negative response

Sumner (1976) points out that negative effects is dependent on type of electrode configuration used. He claims that if a polarisable body is lying between electrode pairs of the dipole-dipole array it will cause negative data. Meanwhile the gradient array, is more sensitive to EMC effects. Both type of effects will cause negative data, but to different extent. As discussed earlier, large separation of the electrodes will contribute to EMC effects which can be negative values (Martinho *et al.* 2006).

Sumner (1976) claims that negative IP response is created during the polarizing and depolarizing cycles of a polarisable body. It is not unusual to receive negative response when a conductive body is lying close to the surface. Sumner (1976) propose that negative IP response occurs if the subsurface contains horizontally multilayered structures. To get this effect, the lowest layer has to be more conductive than the layer right above and the uppermost layer has to be polarisable in some way.

If there is a horizontally three-layer situation where the geoelectrical section is of K-type ($\rho_1<\rho_2>\rho_3$) or Q-type ($\rho_1>\rho_2>\rho_3$) , negative effects can occur as well (Martinho and Almeida 2006).

Sumner (1976) suggests that large negative IP data may depend on coupling effects, if this is due to capacitive and/or electromagnetic coupling is unmentioned. Therefore, as discussed earlier, a good choice of array and a separation of cables and transmitter/receiver will give less negative response. 2D and 3D effects will also contribute to negative data points. These effects may be related to geological structures in the subsurface.

A good knowledge of the geology and the lithostratigraphy will give more understanding regarding negative responses in the data acquisition.

4.5 Electrode contact

In order to get a good data quality, a low resistance between the electrodes and the ground is needed. When measuring Induced Polarization and resistivity, it is important to obtain a high transmitting current. According to Ohm's law, a current is inversely proportional to the resistance; therefore, a low resistance is needed.

According to Sumner (1976), 'electrode resistance', R_E, is the resistance that is situated close to the electrode. The resistances between two electrodes are not linear with distance, even with the assumption of a homogenous and isotropic subsurface. In Fig. 4.3 it is shown how the total percentage resistance between two electrodes is varying. It shows that the resistance gradient is steepest close to the electrodes. This is the area that is most important when talking about electrode resistance (Sumner 1976).

To evaluate the contact resistance with the type of equipment that is used in this work, a specially designed protocol is needed (Appendix 3). With the protocol the voltage can be test measured with a fixed current between two closely spaced electrodes. The resistance on an individual electrode can then be calculated according to the equation system:

$$\begin{cases} R_a + R_b = R_{ab} \\ R_b + R_c = R_{bc} \\ R_a + R_c = R_{ac} \end{cases}$$

where R_a and R_b is the resistance on electrode *a* and electrode *b* respectively. R_{ab}, R_{bc} and R_{ac} are the measured resistances between two electrodes.
Further derivation finally gives:

$$R_a = \frac{R_{ab} - R_{bc} + R_{ac}}{2} \qquad (4.11)$$

The resistance that is calculated according Eq. 4.11 is a sum of electrode resistance and the ground resistance, se Fig. 4.3. If only the resistance of the elec-

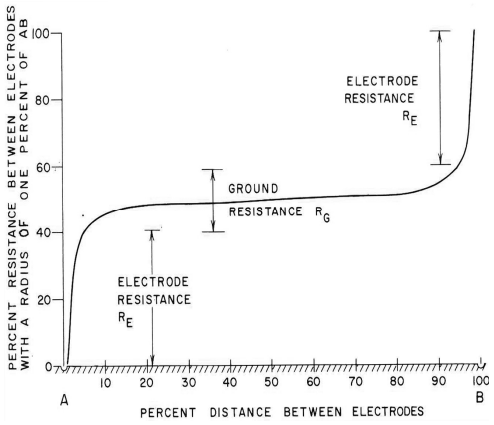

Fig. 4.3 The potential distribution between two current electrodes (Sumner 1976).

trode is wanted, the resistance of the soil volume has to be taken into account in the calculations. However, in field, this information is impossible to obtain today.

4.6 Reciprocity

When data acquisition is made in one direction, i.e. a specially set of C1, C2, P1 and P2, the recorded values should in theory be the same when measuring in the opposite direction, i.e. C1 change to P1 and C2 change to P2. But in reality it will usually not be the case, due to different types of effects. In a measurement with one single multi-electrode cable, occurrence of charge-up effects will affect the equivalence between the forward and reciprocal measurement. This is because in the measurement cycle, an electrode is used as a potential reading recently after it has been used for transmitting the current (Dahlin 1999).

By looking at the difference between the forward and the reciprocal measurement, an estimated error can be obtained. This is a good measure of the overall quality of the data. The value is presented in mV/V for the error in the IP measurement. This is because if the data points that have a value that is close or equal to zero, it will not give a meaningful error value when the ratio is calculated. In the measurement of the resistivity, percent (%) is used. For low values, a low occurrence of noise and other sources of error are present.

4.7 Geometrical effects

Depending on the shape of a conductive body, different emplacement of negative data is obtained when measuring IP (Fig. 4.4). This is due to the depolarization currents that are in opposite direction to the primary current which always goes from A+ to B-, M and N measure the IP anomaly (Bertin and Loeb 1976). Also, 2D effect can occur as negative data close to a high chargeability in the profile (Dahlin and Zhou 2005, Dahlin personal communication).

Measurements of resistivity are commonly made as a 2D profile. But in reality the ground is three-dimensional and the current that is transmitted is flowing in a hemisphere. This creates 3D effects in the data acquisition of resistivity and has to be considered when interpreting. It is known that 3D effects are really significant where the geology changes in a relative small scale. One way to decrease this effect is to place the 2D profile perpendicular against the geological structures (Danielsen and Dahlin 2004b). However, this method is not taken into account in this work.

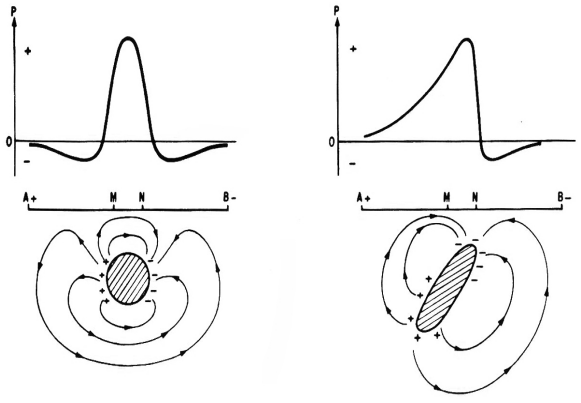

a) Polarizable Spherical Body b) Polarizable dipping body

Fig. 4.4. Negative data caused by geometrical effects (Bertin 1976).

4.8 Signal-to-noise-ratio

Obtaining a high signal-to-noise ratio is a main task in IP methodology. It has very much to do with grounding contact, i.e. the contact between electrodes and ground. The electrode has practically no resistance in itself, neither has the wetted, disturbed zone in the immediate vicinity of the electrode if present. The main contribution to electrode resistance is the undisturbed soil further down. The total current resistance R_T is

$$R_T = R_W + 2R_E + R_G \qquad (4.12)$$

where R_W is the wire resistance, R_E is the electrode resistance and R_G is the ground resistance.

Ground resistance is of high importance concerning noise behaviour. If the resistance is low a high current can be transmitted and thus, a high voltage can be received (Sumner 1976).

4.9 Normalized IP

It has been shown that in some cases it is difficult to distinguish IP-effect caused by conduction differences and IP-effect caused by lithological differences.

Laboratory tests have shown that chargeability is strongly dependent on sample resistivity. Resistivity is in turn dependent on salinity, porosity, saturation and clay content. Normalized chargeability (*MN*) is a parameter that mainly accounts for surface polarization processes, and is given by

$$MN = \sigma'_{rock} M \qquad (4.13)$$

where σ'_{rock} is rock conductivity and M is chargeability (unit is mS/m). Since conductivity is the reciprocal of resistivity, *MN* can be achieved by dividing M with resistivity (ρ) (Slater and Lesmes 2002).

Normalized chargeability is much more sensitive to lithology, e.g. clay content, than to fluid conductivity. Since surface polarization depends on the specific surface area, as well as surface charge density and surface ionic mobility, fluid conductivity has an indirect influence on normalized chargeability.

Chargeability seems to decrease with increasing fluid conductivity and therefore, decreasing resistivity. Normalized chargeability on the other hand seems to have an optimum at about 1000 mS/m (Slater and Lesmes 2002). This has been interpreted as a trade-off between increasing surface charge density and decreasing surface ionic mobility, when the solution con-

centration is increasing (Vinegar and Waxman 1984).

Field experiments in a beach environment have shown that normalized chargeability does not give any response on the transition between freshwater and saltwater, while resistivity and chargeability does. However, a glacial till formation at the same site gave a slight resistivity increase, a clear IP response and a high-normalized chargeability. This illustrates the possibility for normalized IP to differentiate between structural changes and changes due to only surface conductivity (Slater and Lesmes 2002).

4.10 Equipment

The equipment for all measurements in this study is shown in Fig. 4.5 and listed in Table 4.1. The difference between the contents of equipment in the different field tests is only the type of multicore cables. These are with 2 m or 5 m electrode distance and the total lengths are 40 m or 100 m, respectively. For the separated cables, the amount of cables are doubled. Also, a remote cable is used when measuring with pole-dipole array.

The Terraohm RIP924B is a 8 channel receiver that is equipped with 24 bit sigma-delta AD-converters.

The ABEM Terrameter Booster SAS2000 has a 40W transmitter: Max output: 400V-100mA, 200V-200mA, 80V-500mA.

The ABEM Electrode Selector ES10-64C has 10x64 relay matrix switch and the ES464 has 4x64 relay matrix switch.

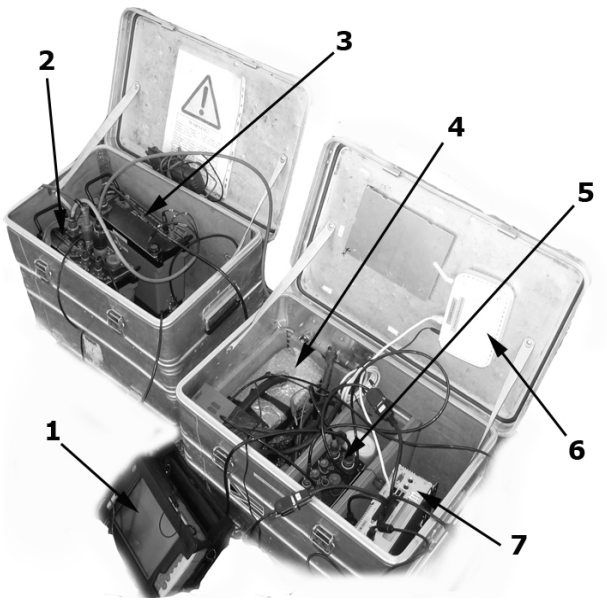

Fig. 4.5. Field equipment. (1) Operator PC. (2) ES464. (3) Booster SAS2000. (4) ES10-64C. (5) RIP942 v.2. (6) Router WLAN. (7) Acquisition PC. Photo: Siikanen J.

Table 4.1 Equipment.

Function	Type (No. in figure)
Relay switch - Potential reading	ABEM Electrode Selector ES10-64C (4)
Relay switch – Current transmitter	ABEM Electrode Selector ES464 (2)
Current transmitter	Terrameter Booster SAS2000 (3)
Instrument	Terraohm RIP924B v..2 (5)
Electrode	Stainless
Connection cable-electrode	Normal jumpers
Operator Device (OD)	Mobile touch screen PC (1)
Data Acquisition Storage (DAS)	PC (7)
Communication OD-DAS	WLAN
Power source	12 V Batteries

5 Data acquisition and processing

5.1 Electrode arrays and measuring techniques

CVES (Continuous Vertical Electrical Sounding) is a 2D measuring technique that measure both vertical and horizontal variations. Compared to 1D measuring, which only concerns the vertical variations of resistivity or IP. However, the variation that occurs perpendicular to the measuring line is not taken into account in a CVES measurement.

When measuring with the CVES method, different types of techniques can be chosen for optimizing the results by using different type of electrode configurations. These electrode configurations have their own properties and depending on the goal of the survey, electrode configuration should therefore be chosen with care.

The differences in the electrode configuration are depending on how the transmitting current electrodes (C1 and C2) are situated relative to the potential reading electrodes (P1 and P2).

The different types of electrode configuration have different distance between the electrodes (a) and different separations (n) between C and P electrodes. This combination gives the geometric factor. For example, in a dipole-dipole array, the electrodes C1 and C2 are situated pair wise in one end of the array and P1 and P2 are reading pair wise. Fig. 5.1 shows the arrangement and the geometric factor (k). In a gradient array the C1 and C2 are situated at the ends of the array and the potential is measured with a constant electrode distance between these.

The gradient array is a type of the Wenner - Schlumberger array where the potential electrodes can be placed randomly between the current electrodes. The multiple gradient array is very well suited for mul-

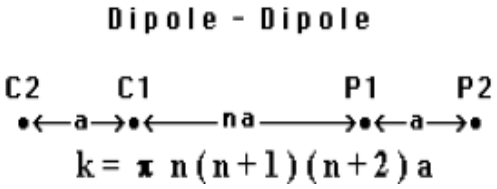

Fig. 5.1. Dipole – Dipole configuration and geometric factor (Loke 2003).

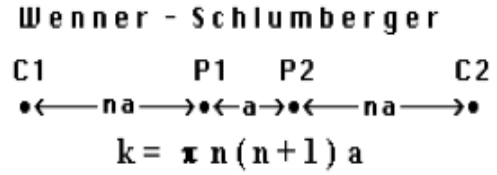

Fig. 5.2. Wenner – Schlumberger configuration and geometric factor (Loke 2003).

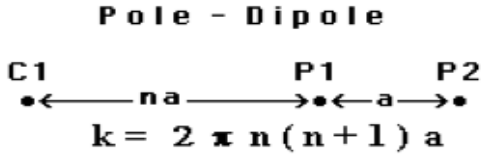

Fig. 5.3. Pole-dipole configuration and geometric factor (Loke 2003).

tichannel surveying. It allows many simultaneous measurements to be done at the same current injection which reduces the fieldwork time considerably (Dahlin and Zhou 2004). Fig. 5.2 shows the arrangement in the special case of gradient array when P electrodes are situated in the middle.

These two types of arrays have a relatively good resolution, but they are in addition quite sensitive to noise contamination. However, the dipole-dipole array has a slightly better resolution than the gradient array but the signal-to-noise ratio is lower (Dahlin and Zhou 2004).

To obtain a greater depth, pole-dipole array can be used. The pole-dipole array requires that a remote electrode be used as one of the current electrodes (C2). The distance to the remote electrode is dependent on the profile length and should be at least 5 times the maximum separation between C1 and P1 (Loke, 2003a). With a profile of 200 m the space between instrument and remote electrode has to be at least 1000 m. The pole-dipole array has roughly as good resolution as the dipole-dipole array. For some environments the signal-to-noise ratio is higher than for the other two arrays but for some environments it is lower (Dahlin and Zhou 2005). Fig. 5.3 shows the arrangement and the geometric factor (k).

Roll-along technique

The roll-along technique means that cables, for example four cables, are rolled out with the instrument placed between cable 2 and 3. When the measuring is finished the instrument is moved one cable in the profile direction and the first cable be placed as number four in the next measurement. In the first measurement cable 1 is excluded and in the last measurement cable 4 is excluded, which means that only three cables are used. This is done to obtain data in the lower corners of the profile (Fig 5.4).

Single cable measurements

Single cable measurements mean that the same cable is used for both current injection and potential readings. This is a normal and more simple technique than using separated cables because fewer cables are needed and only one relay switch is used. The disadvantage is that coupling effects that distort data quality are more prone to occur (Fig. 5.5).

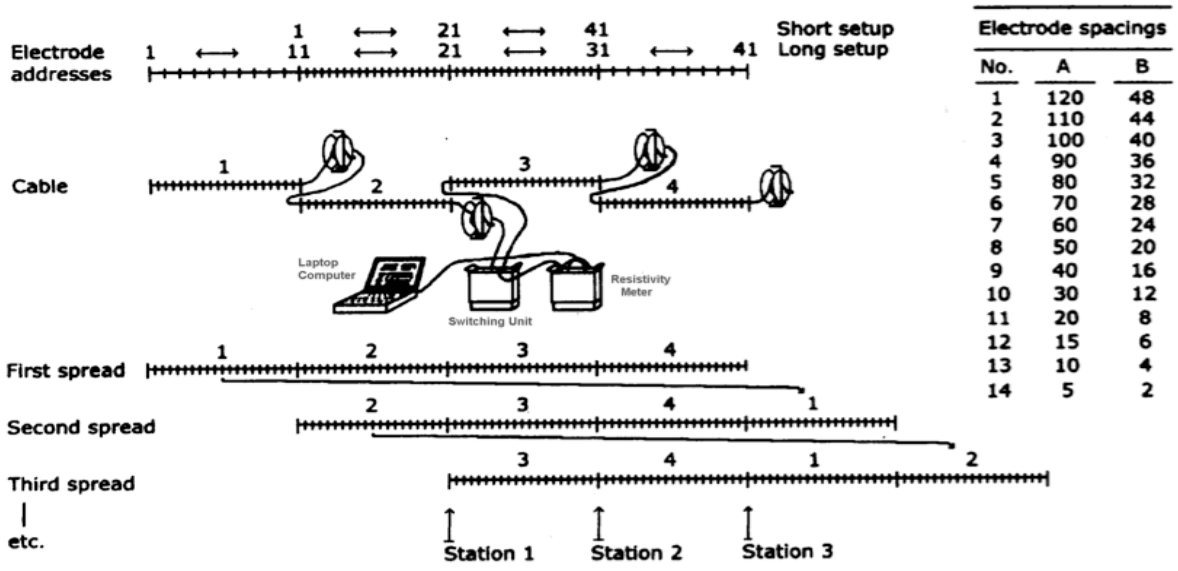

Electrode spacings		
No.	A	B
1	120	48
2	110	44
3	100	40
4	90	36
5	80	32
6	70	28
7	60	24
8	50	20
9	40	16
10	30	12
11	20	8
12	15	6
13	10	4
14	5	2

Fig 5.4. Roll-along technique (Dahlin 1999).

Separated cables measurements

The idea of separating the electrodes used for current injection and potential measurement is to minimize the capacitive coupling effects that arise between the conductors in a single cable. Electrode charge up effects that occur when an electrode previously has been used for current injection are reduced as well, as discussed in chapter 4.3.1

Measurements with separated cables is done through laying out two parallel cables and setting out electrodes with half the electrode spacing. Every second electrode is connected to the current cable and the electrodes between are connected to the potential cable. The first current electrode is placed a half electrode distance behind the first potential electrode. Two relay switches are used, one for current injection and one for measuring potentials (Fig. 5.6).

5.2 Computer software

The following programs are used for acquisition and analysing of data:

Eric v. 2.17

Eric is the program that controls the data acquisition . The software is developed by Dr T. Dahlin, Engineering geology, Lund University.

Erigraph

Erigraph converts raw data to pseudosections and handles the visualization of both pseudosections and inverted models. The software is developed by Dr T. Dahlin. Engineering geology, Lund University.

Res2Dinv

Res2Dinv is the inverse numerical modelling program. The inversion routine is based on the smoothness-constrained least-squares method. It produces 2D models of the pseudosections. The use of this program is explained in detail in chapter 5.3. The software is developed by Dr M. H. Loke, Geotomo Software.

OBSError

OBSError compares normal field values with the reciprocal ones. This is useful when estimating the data quality of a specific measurement. It requires that reciprocal measurements have been done. The software is developed by Dr T. Dahlin, Engineering geology, Lund University.

Workbench

Workbench is a GIS based resistivity and IP data handling program. It allows the user to study IP decay curves in detail. It is also possible to identify electrodes that for example cause negative data. The software is developed by the Hydrogeophysics Group, Aarhus University.

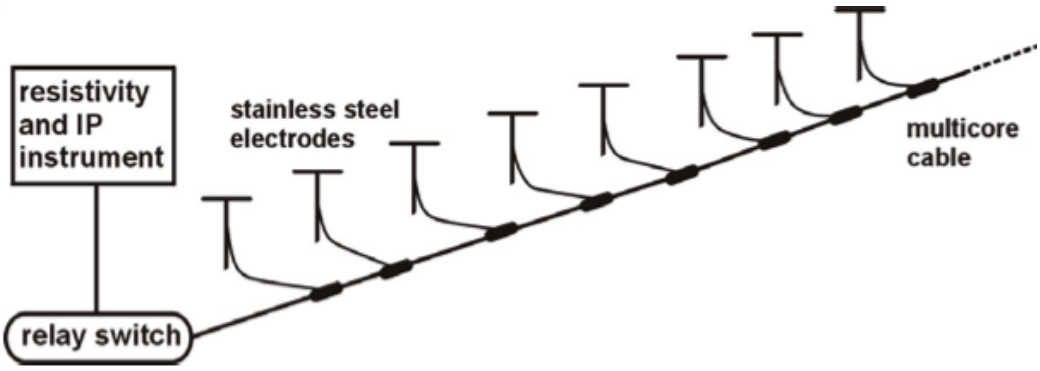

Fig. 5.5 Exampel of the single cable layout (Dahlin 2003 et. al.) .

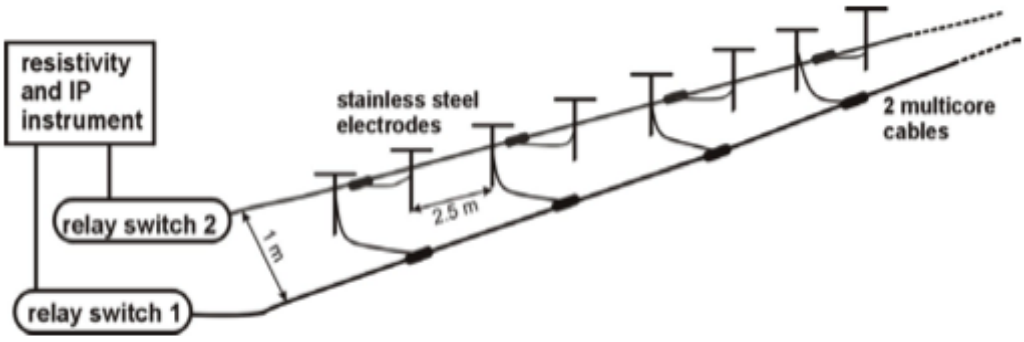

Fig 5.6. Example of the separated cable layout (Dahlin *et al.* 2003).

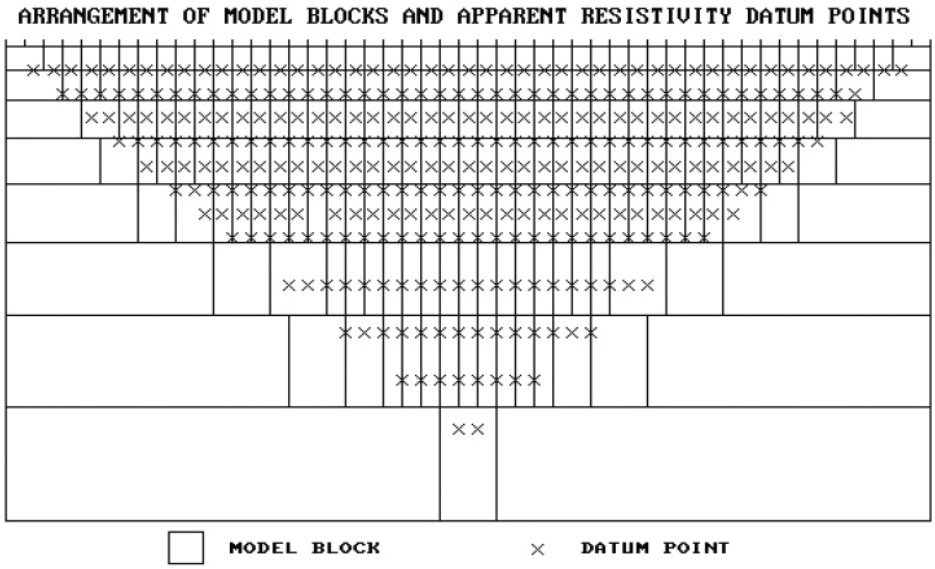

Fig. 5.7. Cell block arrangement (Loke 2003).

5.3 Modelling

Broad outline modelling of field data is a process where a 2D or 3D model is adapted to measured values. The model is divided into cell blocks, which often have a width of half the electrode spacing (Fig. 5.7). The cell block depths normally increase with 10% for every deeper layer. The modelling program is then trying to adjust the resistivity of the model blocks so that they agree with the measured values. This process is called inversion and is done several times, each time enhancing the agreement between measured and modelled values. The difference is quantified with the RMS (root-mean-squared) error (Geotomo Software 2006).

A common programme for 2D-modeling of field data is Res2Dinv. If present, topography shall be incorporated in the dat-files before inversion. Data points that are obviously erroneous, i.e. many times larger or smaller than the others, are deleted. Remaining outliers are deleted in Res2Dinv with the function "Exterminate bad data points". It has been shown that robust inversion gives the best results in most circumstances. The robust inversion attempts to find a model that minimizes the absolute values of the data misfit which makes it less sensitive to outliers in the data than the smoothness-constrained least squares inversion (Dahlin and Zhou 2004).

The vertical/horizontal flatness filter can be adjusted to emphasize vertical or horizontal structures. If the expected measurement target is a vertical structure, e.g. a dolerite dike, the flatness filter is given a higher value. If the expected target on the other hand is a horizontal structure, e.g. sedimentary layers, the flatness filter is given a lower value (Loke 2003).

Furthermore a modification called model refinement can be worth considering. This adjustment splits the model block cells into half the electrode spacing, reducing the model misfit when there are large resistivity contrasts in shallow data (Loke 2003).

The damping factor constrains the range of values the cellblocks can take (Loke 2003). Noisy data generally require a higher damping factor than data of good quality. The damping factor increases with depth since the resolution decreases in the lower parts of the inversion model. The change of damping factor with depth can be manually adjusted. For each modelling iteration the damping factor generally decreases, as the model response gets more and more similar to the measured values. However, a minimum value is set to stabilize the inversion process. The initial and minimum damping factors can be manually adjusted. The damping factor can also be optimized to give the lowest RMS error in each iteration (Geotomo Software 2006).

5.4 Merging protocols

Resolution differs from array to array, both horizontally and vertically. Some characteristics worth considering when choosing appropriate array may be the structure orientation, ground conductivity and depth penetration. One solution to this problem is to merge protocols from different arrays that combine their good qualities. There are though some questions to bear in mind when modelling the merged protocol. It has been shown that some arrays tend to dominate over others. To overcome this problem a weighting factor can be introduced in the algorithm. This seems to give a more accurate model than inverting all datasets without weighting. However, it is not always a good solution to merge protocols. If one of the arrays has significantly better data quality than the other merging of data might be a bad idea (Athanasiou *et al.* 2006). Merging of such datasets could yet be justifiable if for example good resolution at shallow depths and large depth penetration cannot be achieved in another way.

5.5 Analysis of data quality

To achieve knowledge about the data quality, an analysis of negative data can be made. According to chapter 4.4, dataset of low quality often contains negative values. Generally, this has to be taken with care because there are cases where the geological settings gives 'true' negative data (Sumner 1976).

However, by examine the difference between normal and separated cable layouts in terms of negative data amount and distribution of apparent chargeability in the IP pseudosections, the effect of capacitive coupling can be examined. Analysis of the decay curves will also contribute to understanding of capacitive coupling effects, but also the electromagnetic effects can be examined.

The electrode contact will be investigated by an electrode contact test, which is performed with a specially designed protocol.

6. Field tests – Test-line Lund

6.1 Fieldwork

To evaluate the quality of data in different types of arrays and measurement set-ups, four measurements of Induced Polarization with different electrode configurations and arrays were made. All profiles that were in the layout had a length of 108 to 116 m and were approximately in the same direction. In the layout, three multicore cables were used in the normal measurement (single multicore cable) and six cables in the special array of separated cables. All cables were connected to the inputs of the relay-switches. The instrument was placed between cable 1 and 2. Therefore, an extension cable was needed to reach cable 3. Since the length of the lawn limits the length of the array, exclusion of the last electrodes had to be done.

To evaluate the electrode contact, one measurement with a specially designed protocol was made and the same layout was used.

Also, both forward and reciprocal measurements were made. This gave us the difference between the normal and reciprocal measurement and an observation error was obtained.

The study examined two types of arrays, dipole-dipole and multiple gradient, with an electrode distance of 2 meter. In the separated cable layout, the electrode distance between a transmitting current electrode and a potential reading electrode was 1 meter. During the days when the measurements with dipole-dipole array were performed, the ground was very dry because the lack of rain during the period. When the measurement with the gradient array was performed, the ground was relatively moist due to heavy rain the days before. The protocols used are listed in Appendix 3.

6.2 Equipment

The equipment that was used is according Table 4.1 and the type of cable was 3X40 m multi-core, 2 m electrode distance, 21 take-outs.

6.3 Reference data

Earlier, Dr T. Dahlin has surveyed the site, where he examined charge-up effects. According to Dahlin (1999), it is obvious that the records from the site includes disturbance from electric power lines. This will probably influence the measurements that are made in this study.

6.4 Results

6.4.1 Difference between single cable array and separated cable array.

The results are presented in the form of pseudosections and graphs. The unit are apparent chargeability, mV/V. Note that the scale on each pseudosection is designed so that black represents negative data and light grey represents positive data.

The pseudosections show the first time window 10-30 ms. The total time is 310 ms and consists of 5 time window with an increasing factor of 20 ms on each window.

In Fig. 6.1a, the measured IP-pseudosection with one single cable is shown. The electrode configuration is dipole-dipole. The total amount of data points is 1021. The length of the profile is 110 m and the total amount of electrodes is 55. The pseudodepth is ca 24 m. The measurement cycle has been stacked maximum 5 times and minimum 2 times.

In Fig. 6.1b, the measured IP-pseudosection with separated cable is shown. Electrode configuration is dipole-dipole. The total amount of data points is 1071. The length of the profile is 114 m and the total amounts of electrodes are 57 (114). The pseudodepth is ca 24 m. The measurement cycle has been stacked twice.

In table 6.1 the amount of negative data in the different time windows is shown. The amount of negative data in M1 is decreasing with time, while in M2 is it increasing.

Table 6.1. Difference in negative values from measurements of test-line, Lund. Dipole-dipole array - Single (M1) and Separated cables (M2). Gradient array – Separated cables M3).

Time window (ms)	Dip.-Dip. Sing. (M1) (%)	Dip.-Dip. Sep. (M2) (%)	Grad. Sep. (M3) (%)
10-30	63	29	3.5
30-70	52	30	1.6
70-130	45	32	2.1
130-210	44	35	2.9
210-310	44	35	3.4

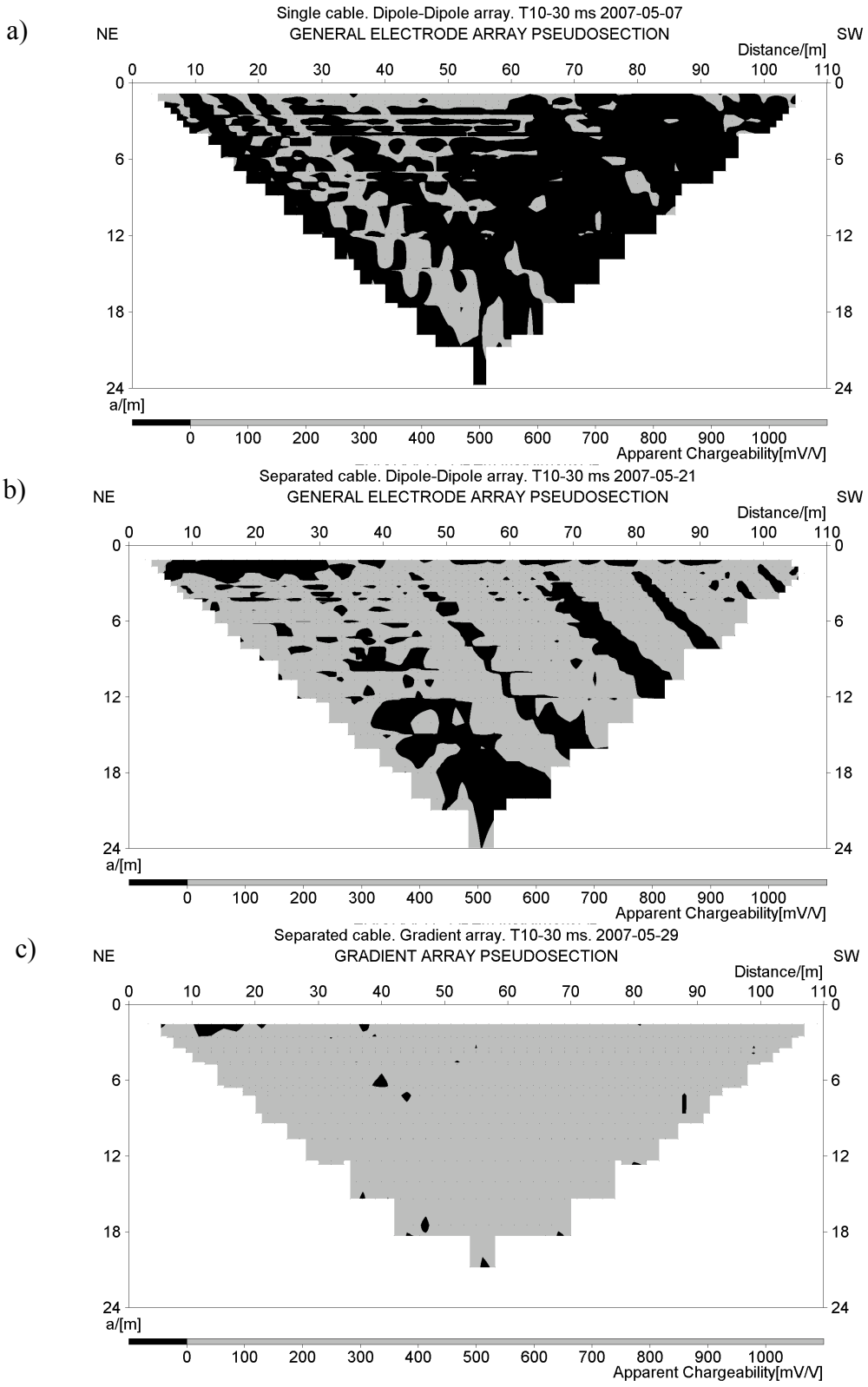

Fig. 6.1. Pseudosections of measured apparent chargeability with different electrode arrays. Time window 1 (10-30 ms). Note that black represents negative data and light grey represents positive data. (a) Single cable array, dipole-dipole array. (b) Separated cable array, dipole-dipole array. (c) Separated cable array, gradient array.

a)

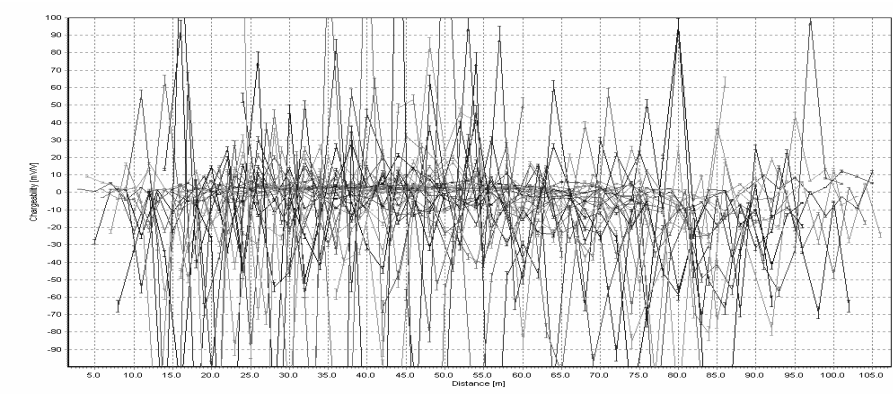

b)

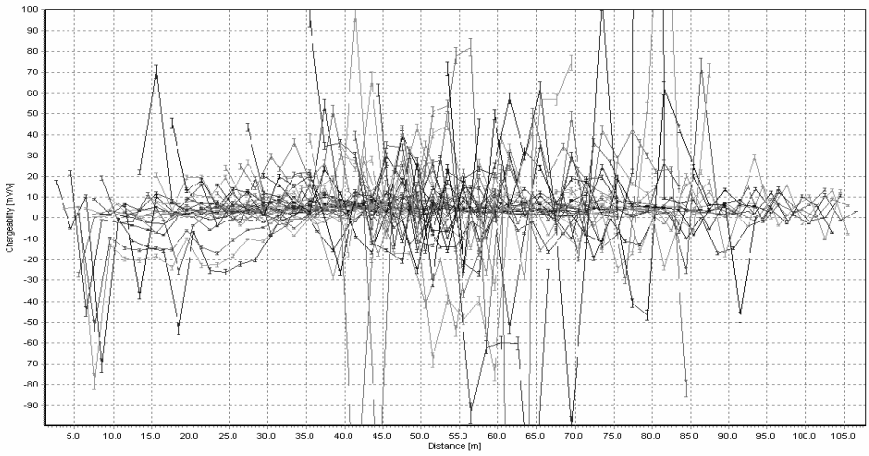

c)

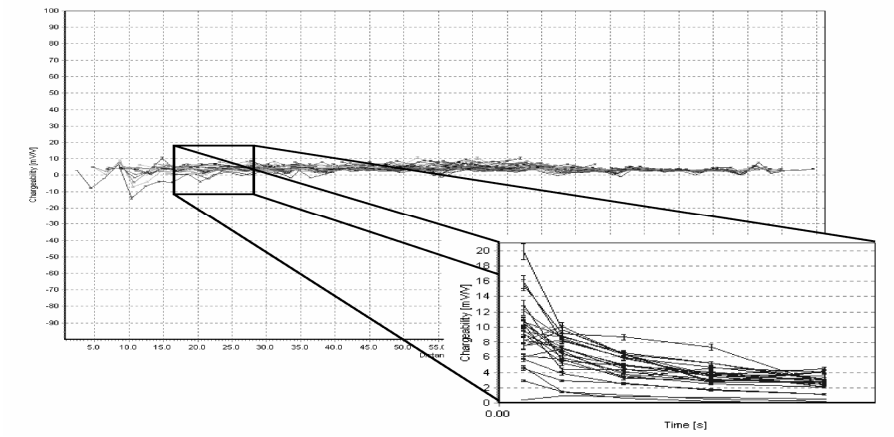

Fig. 6.2. Measured apparent chargeability with different array and electrode configuration. (a) Single cable, Dipole-Dipole array. (b) Separated cable, dipole-dipole array. (c) Separated cable array, multiple gradient array. The small window in (c) shows the decay curves of selected electrodes, each line representing one data point.

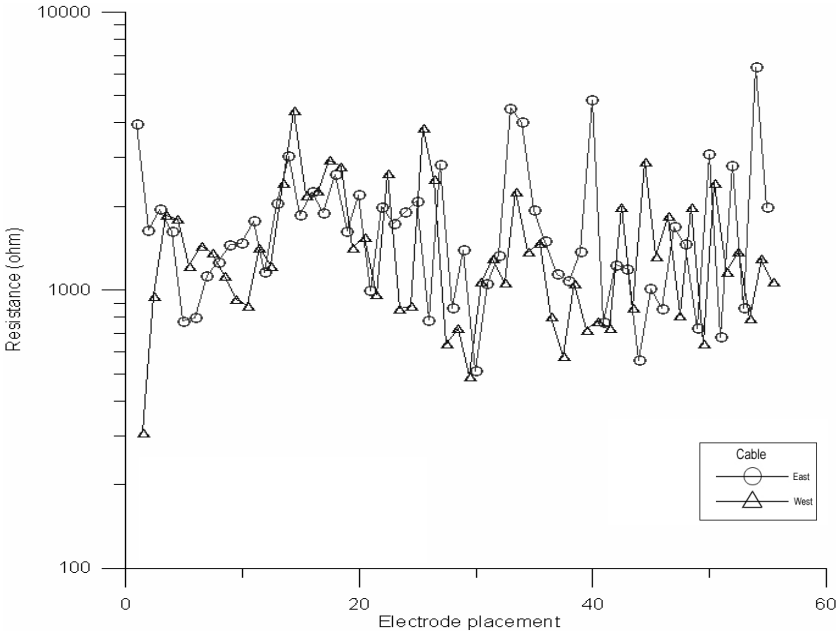

Fig. 6.3. Electrode resistance.

6.4.2 Difference between dipole-dipole array and gradient array

In Fig. 6.1c, the measured IP-pseudosection with separated cable is shown. The electrode configuration is gradient array. The length of the profile is 116 m and the total amount of electrodes is 58 (116). The pseudodepth is ca 20 m. The measurement cycle has been stacked 2 times.

In column M3 in Table 6.1, the amount of negative data points in the different time windows for measurement with gradient array and separated cables are shown.

Electrode resistance

The electrode contact is shown in Fig. 6.3 as two curves, which represent each cable in the separated cable array. The curve with circles represents cable east (usually used as current transmitting cable) and the curve with triangles represent cable west (usually used as potential reading cable). Each value is calculated according to Equation 4.11. The triangles are shifted a half step compared to the circles, this distance represent 1 m in the layout.

The highest recorded resistance is ca 7000 Ω on cable east, and the lowest recorded resistance is ca 300 Ω on cable west. Total amount of electrodes is 57 (114).

Apparent resistivity

The pseudosections in Fig. 6.4a, 6.4b and 6.4c show the apparent resistivity. The apparent resistivity in Fig. 6.4a ranges from 15 Ωm up to 100 Ωm, and the pseudodepth is ca 23 meters.

In Fig. 6.4b the apparent resistivity is ranging from 20 Ωm to 4400 Ωm, although the highest value is not seen in the pseudosection. The pseudodepth is maximum 24 meters.

Fig. 6.4c has an apparent resistivity from 15 Ωm up to 200 Ωm. The pseudodepth is maximum 20 meters. Note that the scales have different units for IP and for resistivity, mV/V and percent (%), respectively.

Observed error, chargeability

Fig. 6.5a shows observed error between forward and reciprocal measurement of Induced Polarization. Calculated mean value is ca 235 mV/V and median value is ca 106 mV/V. The pseudosection is missing data points in the NE direction, as a consequence of the measuring protocols used. Single cable layout is used in this measurement.

Fig. 6.5b shows the measurement when separated cables layout is used. Calculated mean value is ca 55 mV/V and median value is 22 mV/V. Also, here is some lack of data in the NE direction, but in less extension compared to Fig. 6.5a.

Observed error, resistivity

In Fig. 6.6a is observed error between forward and reciprocal measurement of apparent resistivity shown. Single cable layout is used and the calculated mean value is 4.5 % and median value is 1.2%. Fig. 6.6b shows observed error in measurement of resistivity where separate cables layout is used. The calculated mean value is 1.0 % and median value is 0.5%.

6.4.3 Inversions

The inverted resistivity section in Fig. 6.7a. shows that a layer from x = 8 meters goes through the whole profile. Its thickness is ca 5 meter and contains some inhomogeneities and the resistivities range from ca 13 Ωm up to 36 Ωm. Below this layer, a body with resistivities between 36 Ωm up to 130 Ωm is present. The depth of penetration is 22 m and the mean residual value is 1.8 %.

The inverted IP section in Fig. 6.7b shows an area in the NE part of the line where the chargeability is close to zero mV/V. Its extension is from x = 0 to ca x = 7 m. Otherwise the chargeability is increasing downwards up to ca 9 mV/V. The depth of penetration is 22 m and the mean residual value is 0.9 %.

Inversion parameters for the IP and resistivity models are shown in Appendix 1.

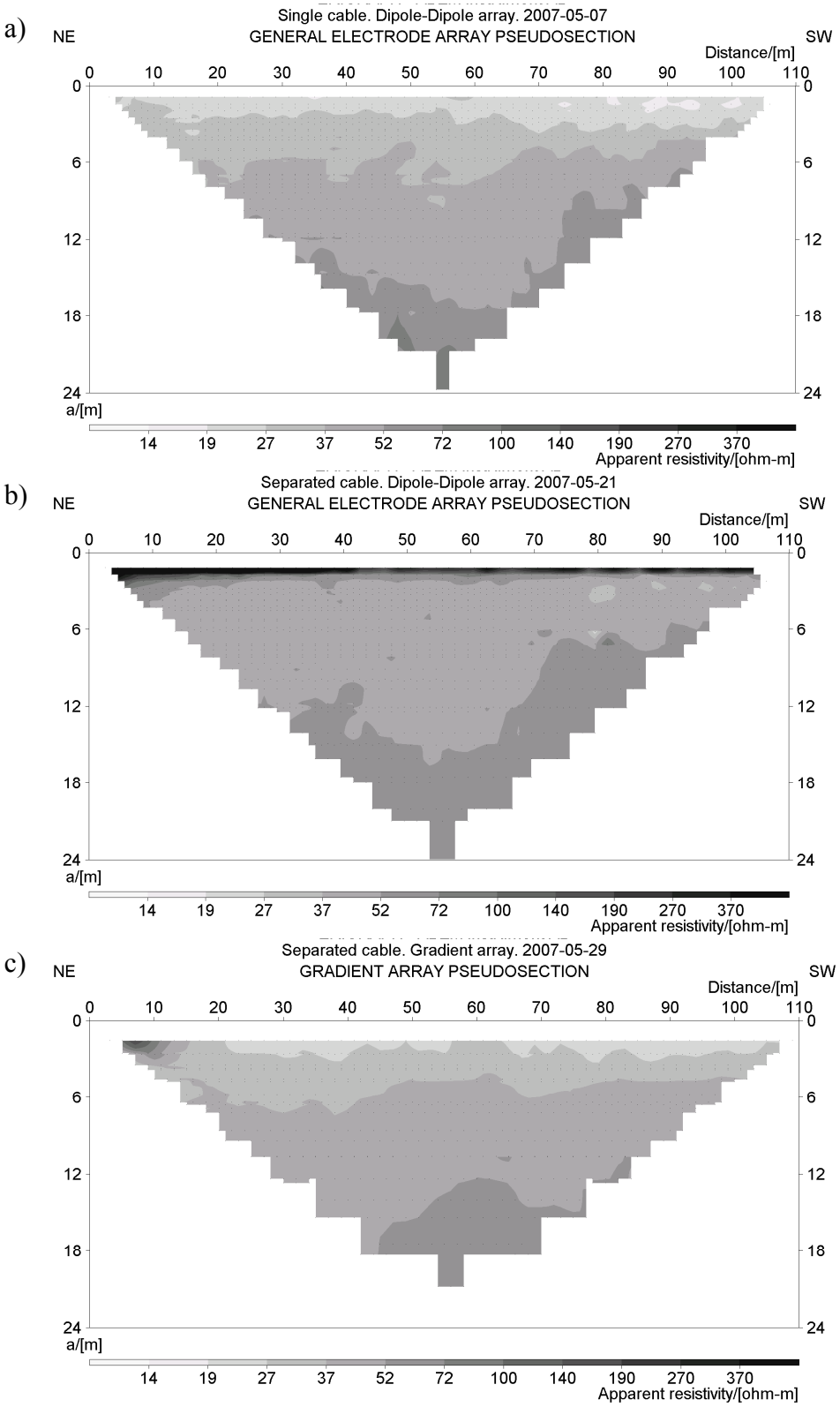

Fig. 6.4. Pseudosections of measured apparent resistivity with different electrode array. (a) Single cable array, dipole-dipole array. (b) Separated cables, dipole-dipole electrode configuration. (c) Separated cables, gradient array.

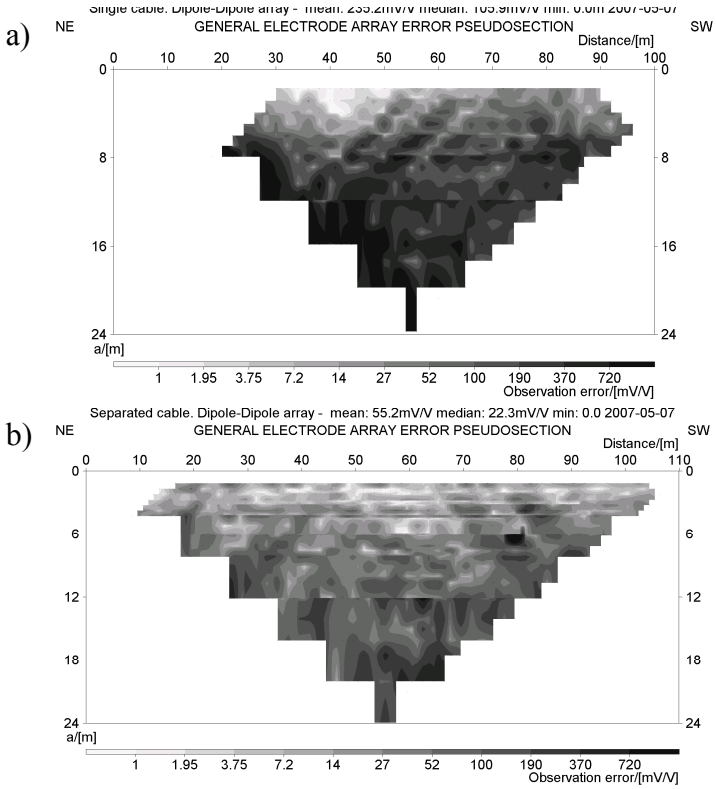

Fig. 6.5. Calculated errors of apparent chargeability between normal and reciprocal measurement. All time windows (10-110 ms) (a) Single cable, dipole-dipole array. (b) Separated cables, dipole-dipole array.

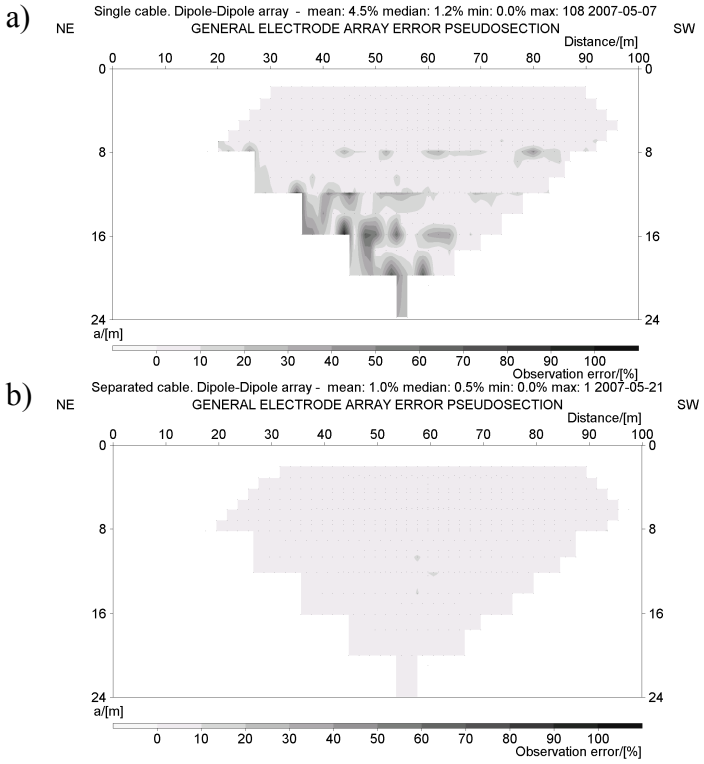

Fig. 6.6. Calculated errors of apparent resistivity between normal and reciprocal measurement. All time windows (10-110 ms)(a) Single cables, dipole-dipole array. (b) Separated cables, dipole-dipole array.

a)

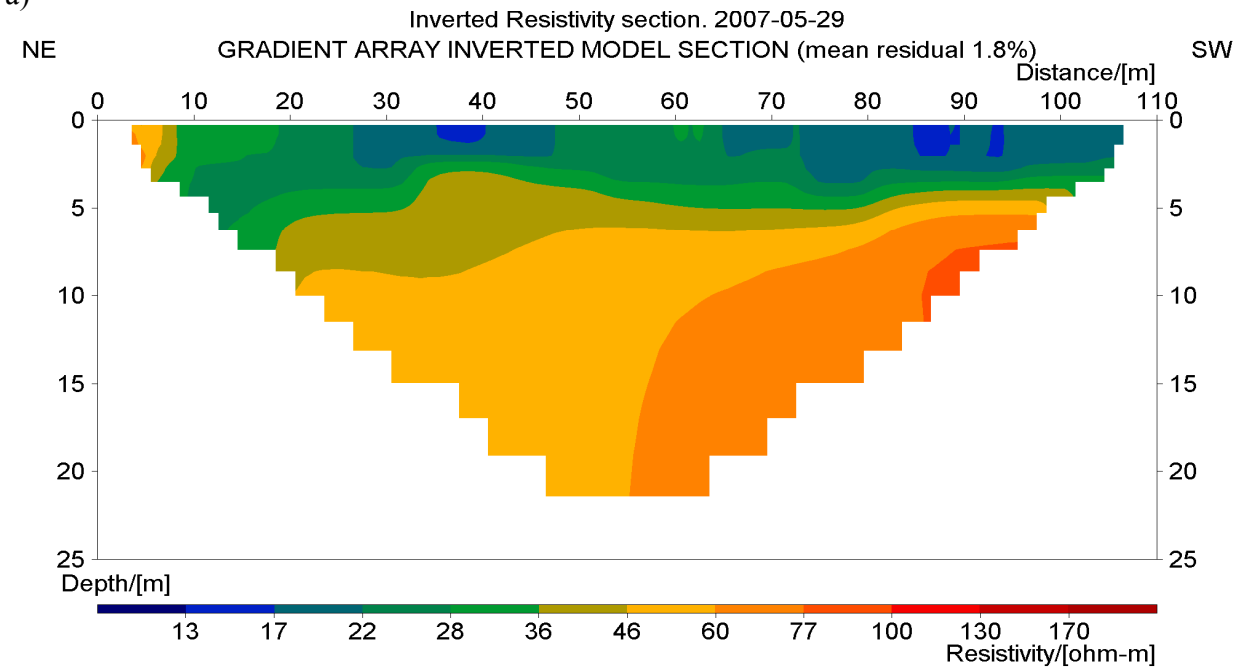

b)

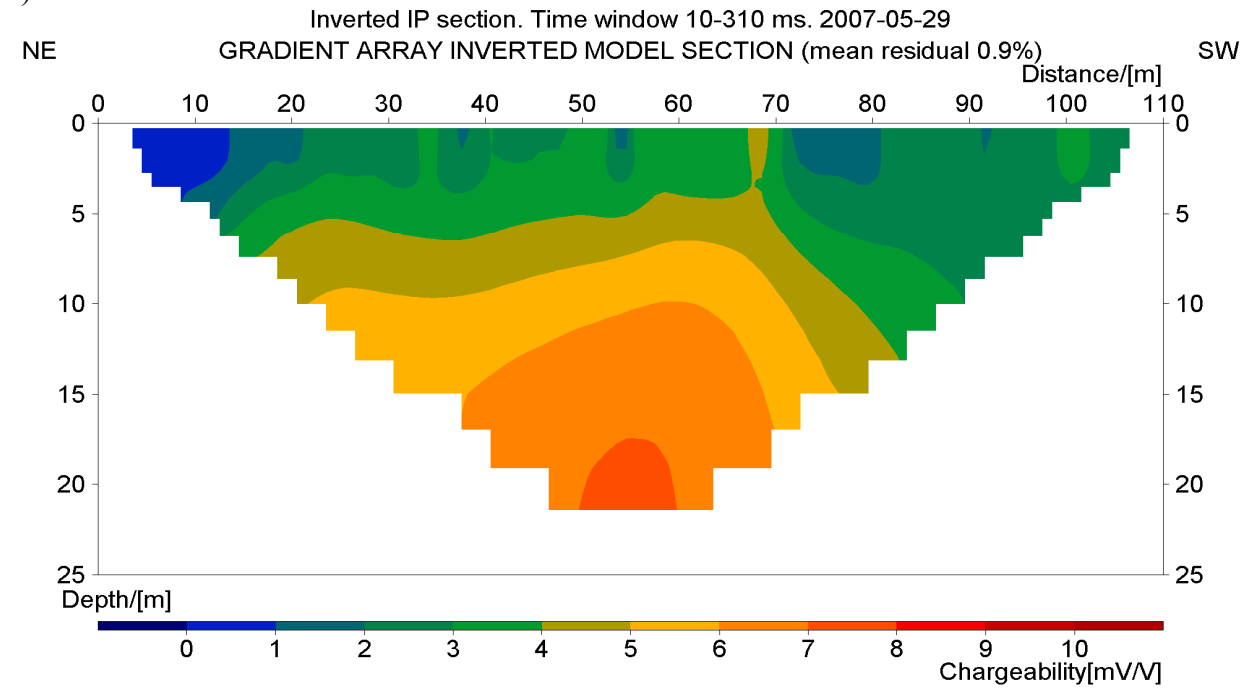

Fig. 6.7. Inverted sections. Gradient array. (a) Resistivity. (b) IP, all time windows (10-310 ms).

6.5 Discussion

By looking at pseudosections of IP, information can be found regarding the quality of the data.

The site that was investigated is a high noise area. This is quite clear in the pseudosections of the IP-measurements.

The presented sections include systematic bad data points and sharp transitions in the chargeabilities. Therefore, because of the large amount of negative values, only pseudosections of apparent chargeability are presented showing negative and positive data. No apparent value of chargeability is presented.

In a single cable array the noise level is higher than in a separated cable array and the measurements will be affected by several different type of noise sources. According to Dahlin (1999), it is important to consider adverse effects such as charge-up effects when a measurement of the potential is made recently after the electrode has been used for current transmitting. This can be done by separate current cable and potential reading cable, which will eliminate the charge-up effects.

Other effects, such as electrode polarization self-potentials, telluric currents, and electric power lines, have to be considered as well when an interpretation of a survey is going to be made. The investigated area contains some electric power cables that probably have affected the results (Dahlin 1999).

In Fig. 6.1a, the measurement with single cable array contains more negative data compared to Fig. 6.1b, which is measured with separated cables. According to Table 6.2 and Fig. 6.1b, the difference in the amount of negative data between the single cable array and separated array results in highest difference in the earlier time. However, by looking on each type of measurement, it seems that the amount of negative data is decreasing with time in the single cable array and increasing in the separated cable array. This may depend on other noise sources having a relatively stronger influence with time.

If we assume that the capacitive coupling has more or less no influence in the separated cable array, then other noise source, e.g. electric power lines, telluric noise, subsurface contains horizontally multilayered structures etc., will have a constant noise signal meanwhile the injected current is in its decay phase. This will result in a lower signal-to-noise-ratio with increasing decay time and the data will consist of more negative response in the later time.

In the single cable array the capacitive coupling has a large influence on the acquisition of data, (Sumner 1976), and will contribute to a "shadow effect" of the other noise sources behaviour as in separated cable array. This will be most pronounced at earlier times.

In this survey, the frequency of the negative data seems to differ much between the measurement with gradient and dipole-dipole array (Figs. 6.1b and 6.1c). According to Dahlin (2004), the dipole-dipole array is more sensitive than gradient array.

Fig. 6.1c shows the distribution of negative data in the gradient array with separated cables. According to table 6.2, the amount of negative data in the gradient measurement (Fig. 6.1c) is much smaller compared to the other measurement. The quality of the data is probably influenced beneficially by the precipitation the site was exposed to before the measurement took place. However, in this survey, the difference shows that using gradient array compared to dipole-dipole array gives a better quality of data.

The presented results seems to show that capacitive coupling frequently occurs as negative data in the measurement of IP. Sumner (1976) supports our conclusion when he claims that large negative values (compared to positive values) can be due to couplings effects. But, if it is capacitive and/or EMC, he leaves unmentioned. However, the positive data points should be affected of this phenomenon as well and will be shown by reciprocity analysis.

In this survey, the negative response seems also to be dependent on other things such as the electrode contact, EMC, external noise sources, measurement errors and of course human factor. This interpretation is based on the results of the separated cable array. Hence, there are still negative values in Fig. 6.1b and 6.1c when separated cables are used. The capacitive coupling due to direct coupling between the conductors is decreasing with a factor of distance in square (Dahlin, personal communication). Therefore, there should not be any negative data points when using separated cables. However, it may be capacitive coupling effect between the ground and the cables that contributes to negative data. This is not investigated in this study.

Important is that when the measurements of dipole-dipole array were made, the precipitation was more or less nonexistent, before and during the test weeks. Indeed, this will not promote good data quality because of bad contact. Therefore, the condition of the subsurface will also influence the quality of the data.

In Fig. 6.2, the chargeability variation is shown. Fig. 6.2a, dipole-dipole array and single cable, shows a very noisy measurement with high variation in chargeability's between the data points. It seems, when using separated cables, the variation is decreasing. However, still there is some noise in the data points. Therefore, the decay curves are not shown in Fig. 6.2a and 6.2b because it just shows noise behaviour.

The measurement with separated cables and gradient array shows a small variation (Fig. 6.2c). Also, the curves that are shown in Fig. 6.2c have a logarithmically decay form, which represents data of good quality. This is probably due to the fact that the area was exposed for precipitation as discussed before. This will contribute to a low resistivity in the surface which may be responsible to the big difference compared to the other measurements.

The measured contact resistance shows a large variation, from a couple of hundred Ω and up to several thousand Ω. Also between two closely spaced

electrodes, a significant variation is present. The result of the resistivity measurement contains some "bad" data point as well. These bad data points are not in the form of negative values. Instead, it is some kind of differences in the value of the measured apparent resistivity between the different types of measurement. Compared to the IP results, these sections are of better quality. This is because the measurement of resistivity is not so sensitive to noise as IP measurement, since the measurement of the resistivity is made at the same time as the current is injected, (Reynolds 1997).

The sections in Fig. 6.4a, 6.4b and 6.4c show almost the same type of apparent resistivity. The boundaries in the transitions are a little more disturbed in the single cable measurement compared to the other measurement with the separated cable array. In Fig. 6.4b, the apparent resistivity is very high in the top layer compared to the other sections. This may depend on the protocol design of the separated cables array, it can also be due to measurement errors. Fig. 6.4c represent probably the truest values because the ground contact was better due to heavy precipitation wetted the ground.

In Fig. 6.5a the observed error, estimated from reciprocal measurements, in the chargeabilities of the single cable array is shown. It is quite high values, which means a large difference between the normal and the reciprocal measurement. This is probably due to capacitive coupling effects, but may also depend on the EMC effects. The position of the calculated data points is displaced. This is due incompleteness of the protocol file. The section that shows the observed errors in the separated cable array, Fig. 6.5b, has a pattern of lower values. This difference, between the single cable array and the separated cable array is probably due to the charge-up effects, where capacitive coupling effect is reduced in the separated cable array. The EMC effect is probably still present in the data set of separated cables (Fig. 6.5b). According to Sumner 1976, the dipole-dipole array contributes to positive values, which are connected to EMC effects, hence the difference in the normal and reciprocal data set.

In the single cable array, the mean value is 235 mV/V; in the separated cable array it is 55 mV/V. This is a difference of a factor of 5. Also the median value has a difference of a factor of ca 5, 106 mV/V and 22 mV/V for the single cable array and separated cable array, respectively. The maximum value in the separated cable array is deviating compared to the other values. It has a difference of a factor of 5, approximately, compared to the second highest value. This data point will indeed influence the mean and median value.

In Figs. 6.6a and 6.6b, the reciprocal errors from in the measurement of the resistivity is shown. It is clear that the data of resistivity has a much better quality compared to the IP-data. There are really low mean and median values. But still, a difference between single cable array and separated cable is shown. The single cable array shows larger reciprocal errors than the separated cable array.

The inverted section of resistivity and IP of measurement M3 (separated cables, gradient array) presented in Fig. 6.7a and 6.7b, are of good quality. The mean residual value is 1.8 % and 0.9 %, respectively. According to Fig. 6.1c, the measurement has a small amount of negative data in the IP. This is probably due to, as earlier discussed, type of electrode configuration and separated cable array. However, also the electrode contact has a considerable influence on the data acquisition in the measurement. The modelled section shows an area in the NW part of the line, 5-15 meters in *x*-direction. On the surface in that area, filling material as macadam was observed. It seems to be a reasonable assumption because the area is shallow and the penetration is not more than 4 meters. The rest of the profile shows an increasing chargeability downwards. However, the chargeabilities are not very high, maximum, 9 mV/V, and it is a smooth transition from low to high values.

The resistivity is low with values ranging from about 13 Ohm to ca 180 Ohm. The top layer has the lowest values and the resistivity increase with depth. As discussed before, borehole data from LTH1 (Alm (Persson) 1985) indicate that the subsurface is made up of different types of clayey till and sand beds to a depth of ca 50 m. The penetration depth of the measurement is barely 25 meters. Clay does normally have a low resistivity (Palacky 1987, Reynolds 1997, Fetter 2001).

For obtaining good data quality, i.e. high signal strength, a high injection current is important. On the other hand the capacitive coupling effect will also increase more or less perpendicular to the increasing current (Dahlin, personal communication). But the other noise sources, such as telluric noise and self-potential as earlier discussed, will be weaker compared to the signal and the signal-to-noise ratio will therefore be better. In high resistivity areas, a high-injected current is difficult to achieve. In this survey the injected current is ranging from 20 mA up to 200 mA. That is a difference of factor 10 and has probably an effect on the IP-data. To examine this influence, further investigation has to be done.

6.6 Conclusions

It is obvious that the noise, mostly capacitive coupling, will decrease with increasing the distance between the transmitting current cable and the potential reading cable. This will give a higher quality data set. Of the presented results it seems that capacitive coupling gives negative data in the measurement of IP but also the positive data points may be affected by this noise.

The result of difference in normal and reciprocal measurements shows that the positive values differs and this might be caused by the EMC effect.

The user always wants to have data of good quality, therefore measurement with separated cables may be useful when measuring in high noise areas, such as urban environments, but also in normal areas is of in-

terest. Unfortunately, measuring arrays with separated cables is more time consuming and logistically complicated than standard data acquisition, but it may be worth the work.

A good idea is to make the measurement when the site of investigation has been exposed to precipitation, or water the area close to the electrode. This should indeed contribute to better quality of the data.

This survey has been concentrated on the results of induced polarization. But also good quality of the resistivity is important. However, a simple rule is that when IP data is of good quality, the quality of resistivity is in all likelihood sufficient

If the measurement of electrode contact was done before the data acquisition of IP is started, it would give somehow an idea of how the quality of the data will be. For good data quality, the electrode contact should be as good as possible, i.e. the resistance should be as low as possible. However, in field, it is very important to have good electrode contact. And this has to be considered when applying the electrodes into the ground.

7. Field tests – Test-line Aarhus

7.1 Fieldwork

Fieldwork took place during one day (the 11th of July 2007). The weather was rainy and it had rained a lot before and during the survey, thus the soil was very moist. The profile was 400 m long and the electrode separation was 5 m. One measurement with single cable layout and gradient protocol was carried out. The experience from the survey in Lund entailed that separated cables with gradient array was used. In addition pole-dipole array was used to obtain deeper penetration; this was also with separated cables. The remote electrode used in the pole-dipole measurement was placed approximately 700 m from the instrument (Fig 7.1).

The protocols used are listed in Appendix 3.

7.2 Equipment

The equipment is according Table 4.1 and the type of cable was 4X100 m multi-core (8X100 m in the separated cables layout), 5 m electrode distance, 21 take-outs. A remote cable was also used.

7.3 Reference data

The area has earlier been surveyed but no reports have been written. According to A. Viezzoli from Aarhus University it is an area that consist of till to a depth of a few meters to a few tens of meters. This till is overlying a thick layer of tertiary clay. The aquifer and the bedrock of limestone are on an unreachable depth for our measurement.

In the earlier investigations, an anomaly of high IP effect was obtained at around x = 300 m. This was interpreted as a pipeline.

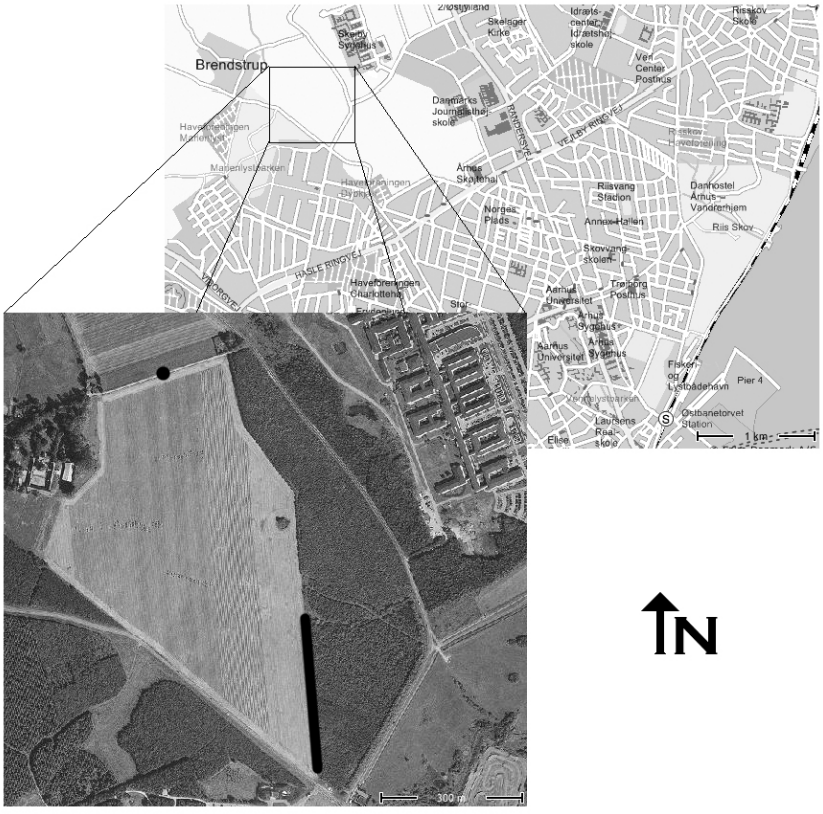

Fig. 7.1. Area of investigation, Aarhus, Denmark. The black line represents the cable layout and the black dot represent the remote electrode.

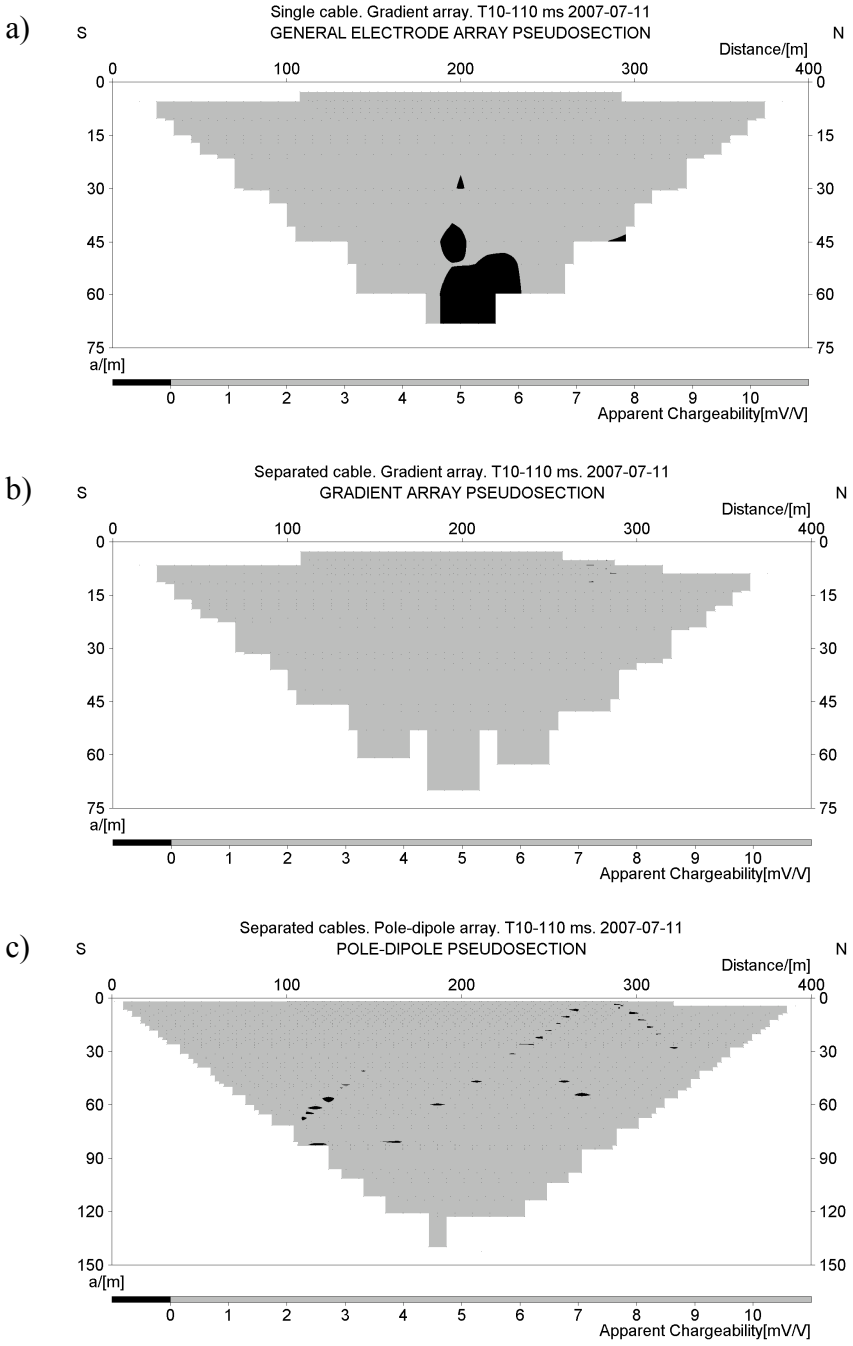

Fig. 7.2. Pseudosections of measured apparent chargeability with different electrode arrays. Time window 1 (10-110 ms), Test-line Aarhus, Denmark. Note that black represents negative data and light grey represents positive data. (a) Single cable, gradient array. (b) Separated cables, gradient array. (c) Separated cables, pole-dipole array.

a)

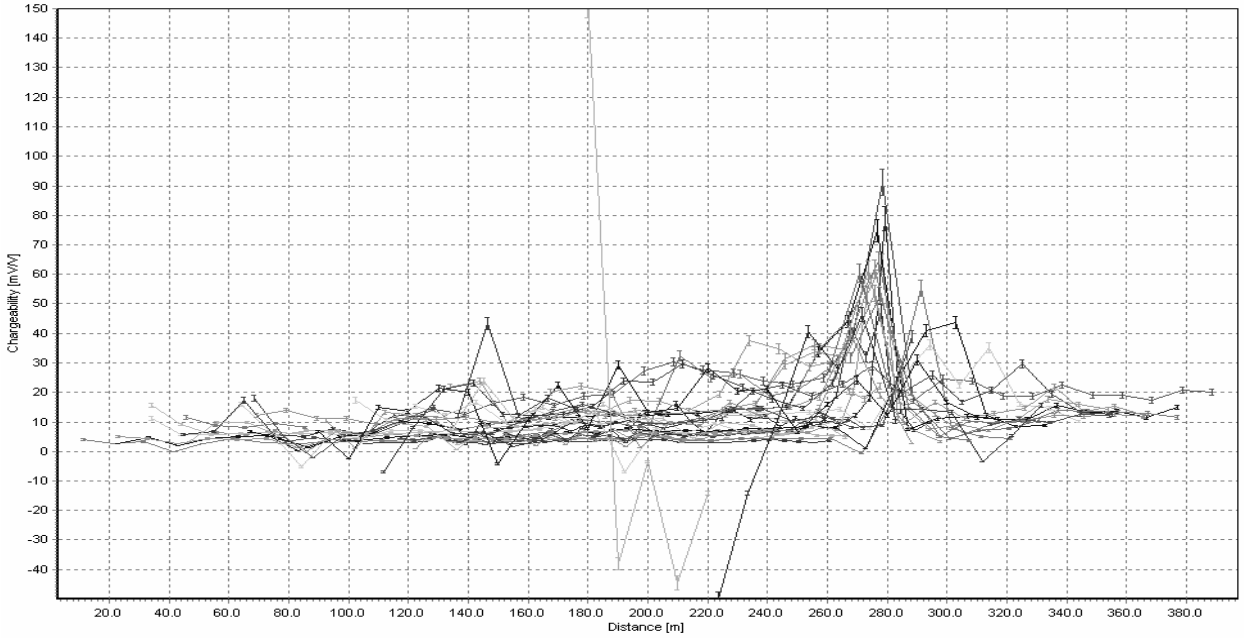

b)

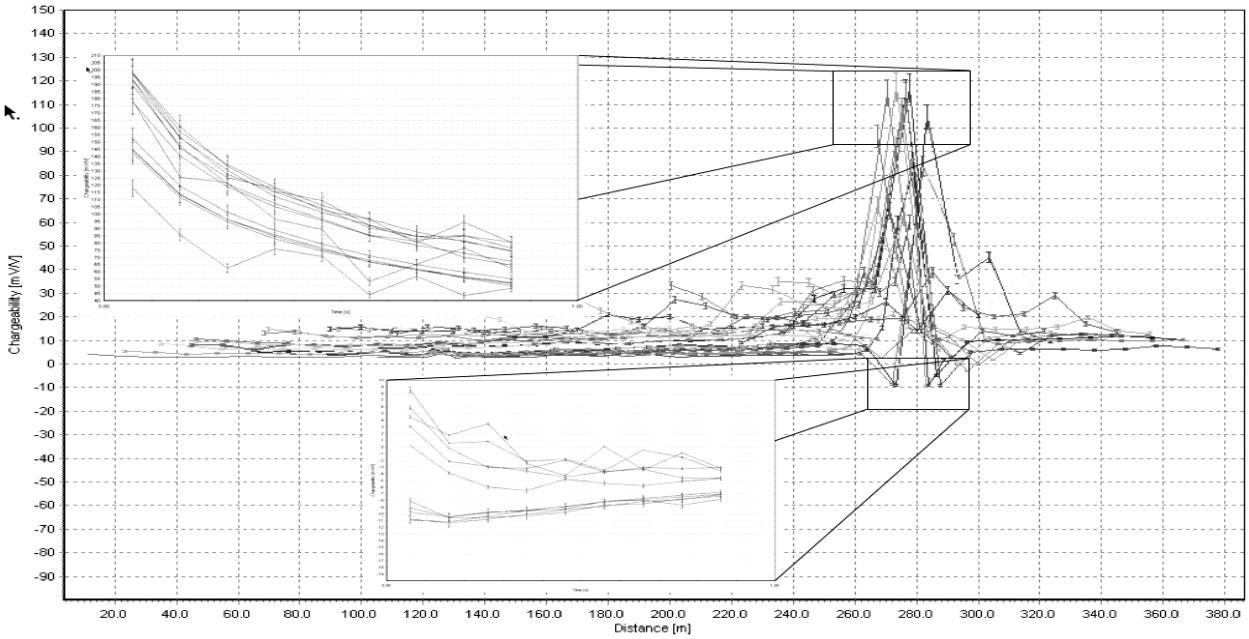

Fig. 7.3. Measured apparent chargeability with different cable layout. All time windows (10-910 ms). Test-line Aarhus, Denmark. (a) Single cable, gradient array. (b) Separated cables, gradient array. Small window in (b) shows the decay curves of selected electrodes, each line represent one data point.

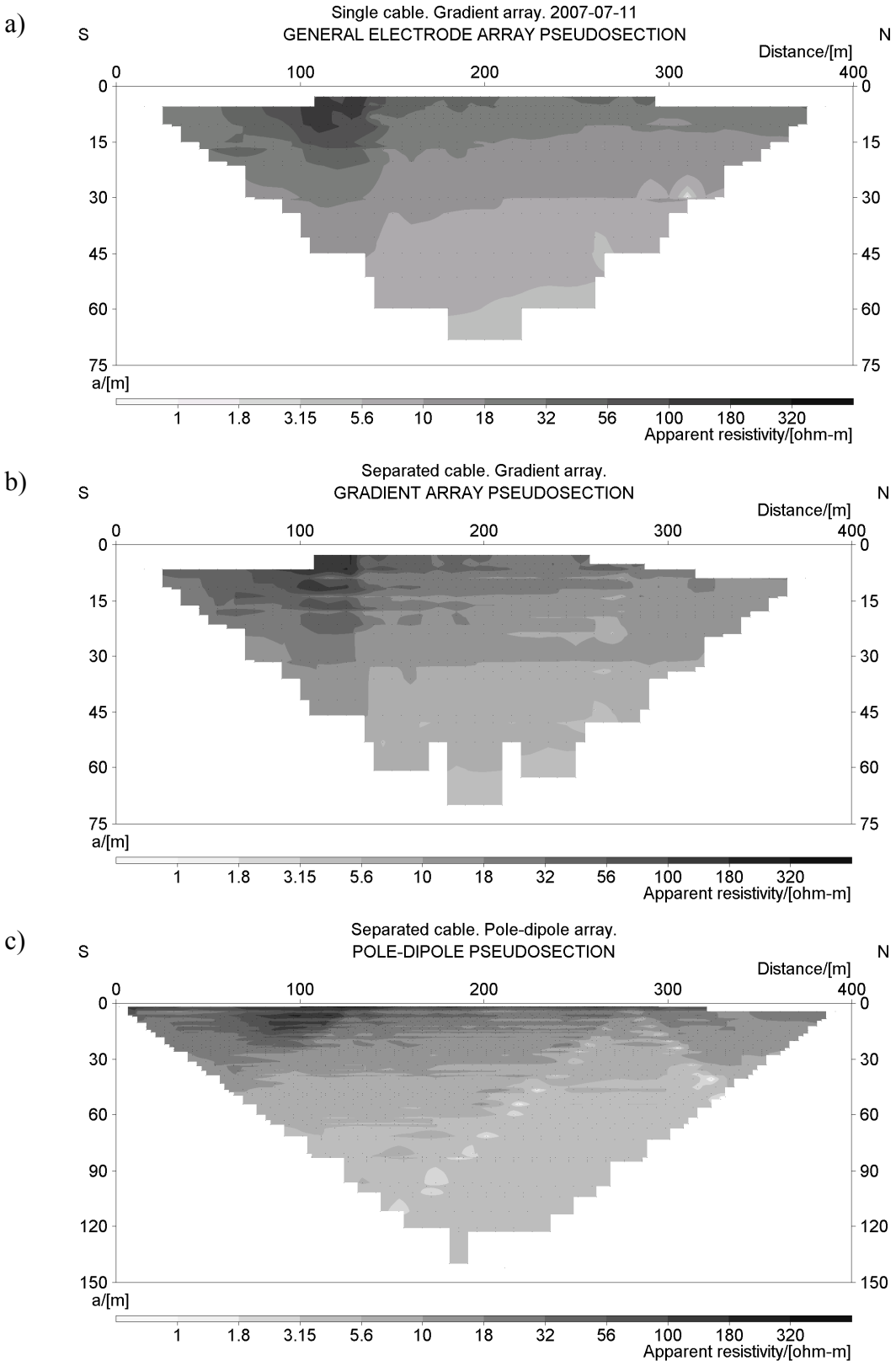

Fig. 7.4. Pseudosections of measured apparent resistivity with different electrode array. Test-line Aarhus, Denmark. (a) Single cable, gradient array. (b) Separated cable, gradient array. (c) Separated cables, pole-dipole array.

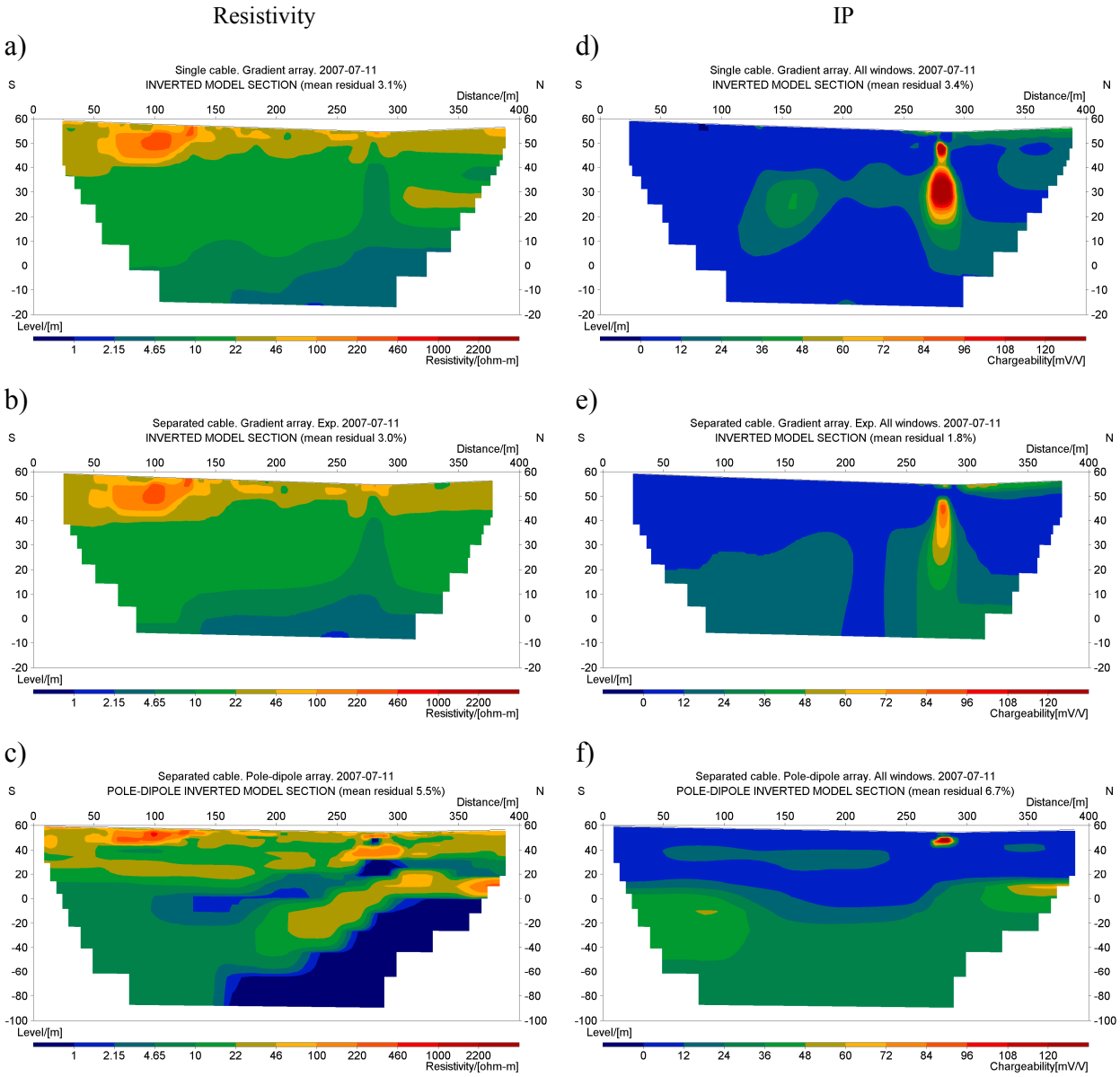

Fig. 7.5. Inverted sections, Test-line Aarhus, Denmark. (a) Single cable array, gradient array, resistivity. (b) Separated cables, gradient array, resistivity. (c) Separated cables, pole-dipole array, resistivity. (d) Single cable, gradient array, IP. (e) Separated cables, gradient array, IP. (f) Separated cables, pole-dipole array, IP.

7.4 Results

Note

When using separated cables, the current electrodes are shifted a half step relatively the potential electrodes. Therefore the penetration depth varies a bit, which leads to fewer data points on the same depth. The plot of a pseudosection is a linear interpolation between data points that are on the same depth. If the depth differs, it may result in gaps in the pseudosection. This phenomenon is visible in Fig. 7.2b-c, Fig. 7.4b-c and Appendix 2.

7.4.1. Difference between measurements using single cable, separated cables and different electrode configuration

The results are presented partly in the same way as in chapter 6, i.e. in form of pseudosections and graphs.

Chargeabilities and decay curves

The pseudosections in Fig. 7.2 show the first time window 10-110 ms. The total time is 910 ms and consists of 9 time windows adding 100 ms for each window.

All profiles that are presented have a length of 400 m and the total amount of electrodes is 81 (162 in the separated cables layout). The measurement cycle has been stacked twice. The pseudodepth is approximately 68 m for the gradient measurement and 140 m for the pole-dipole measurement.

In Fig. 7.2a the measured IP-pseudosection with one single cable is shown. The electrode configuration is gradient. Total amount of data points is 742. Negative values are concentrated to the longer electrode separation. In the separated cables measurement, Fig. 7.2b, is the total amount of data points 707.

In Fig. 7.2c, measured IP-pseudosection with separated cable is shown. Electrode configuration is pole-dipole. Total amount of data points is 2045. Negative values are situated at same places in the pole-dipole array as in the separated gradient array. In the pole-dipole there are also some more negative values scattered in the profile.

Fig. 7.3 shows the chargeability variation from the data set and also the decays for some positive and negative data points are shown. Unfortunately, the section of pole-dipole array is not presented, because the software presentation did not have the capability to read that type of protocols.

The pseudosections that are shown in Fig. 7.4 show the apparent resistivity. The apparent resistivity in Fig. 7.4a and 7.4b is varying from 2 Ωm up to over 320 Ω m. The pseudodepth is approximately 68 meters. Fig. 7.4c has an apparent resistivity from 1 Ωm up to 320 Ωm. The pseudodepth is around 140 meters.

7.4.2. Inversions

The inverted resistivity section in Fig. 7.5a-c has resistivities between 1-500 Ωm, where the highest values are situated on the upper part of the section. The depth of penetration in the gradient array is around 10 meter below sea level (m.b.s.l.) and the mean residual value is 2.7 %. In the pole-dipole array the depth of penetration is approximately 100 m.b.s.l. and the mean residual value is 11.2 %.

In the inverted IP section (Fig. 7.5d-f) is the highest chargeability situated at x = 280 m. The chargeability is varying between 0-450 mV/V. The maximum chargeability in the scale is set to 120 mV/V. Therefore, the highest values in Fig. 4f are not visualized in the section. The depth of penetration is the same as in the resistivity sections (Fig. 7.5a-c).

Inversion parameters for the IP and resistivity models are shown in Appendix 1

7.5 Discussion

When using separated cables, the amount of negative data in the IP section seems to be, except for a few, almost nonexistent. The negative values that are present in Fig. 7.2b and 7.2c are probably most connected to 2D-effects, which are caused by the high anomaly in the chargeability. This is especially seen in Fig. 7.3b where the negative values are very close to the high chargeability, at x = 280 m. This negative effect and high chargeability are present in all pseudosections except in the measurement with the single cable (Fig. 7.3a). The 2D effect is probably present but due to the noise level it is not so obvious.

The difference between the amount of negative data in later and earlier times seems not to be so significant, therefore it is not discussed in this work.

The area with negative data in the deepest part of the single cable measurement (Fig. 7.1a) is probably due to coupling effects. Based on experience from the measurement in Lund our suggestion is that the coupling effect is mostly capacitive, since the effect is almost totally absent when using separated cables.

Because the small amount of negative values, pseudosections of apparent chargeability is presented in Appendix 2, where the distribution is shown.

The transitions in the gradient single cable measurement are more jagged than the measurement with the separated cables. Also, in the gradient single cable measurement, the chargeabilities are overall of lower values, especially where the predicted anomaly is situated. In the pole-dipole measurement, the values are very scattered and the chargeabilities are very high.

In the pole-dipole measurement, the transition in the apparent resistivity seems to be a little more disturbed (Fig. 7.4c). However, the differences in apparent resistivities between the single and separated cables array are not so significant (Figs. 7.4a and 7.4b). The pseudosection and inverted section shows both much the same anomalies and transition in the values. This is probably due to the moderate ground resistivity.

In the inverted resistivity section the mean residual value is larger (3.0 %) in the gradient separated cables measurement, compared to the gradient single cable array (3.1 %) (Figs. 7.5a and 7.5b). However, the mean residual value is in a reasonable magnitude.

In the inverted IP sections of the gradient measurements, the mean residual value is as low as 3.4 % (single cable measurement) and 1.8 % (separated cables measurement), which indeed are very good for further interpretation (Figs. 7.5d and 7.5e).

The resistivity and IP section of the pole-dipole measurement (Figs. 7.5c and 7.5e) shows a higher mean residual value (5.5 % in the resistivity measurement and 6.7 % in the IP measurement) compared to the gradient measurement. This is probably because the depth penetration is larger and the quality of data is decreasing with depth.

The presented inverted sections show a top layer of relatively high resistivity. In the section with separated cables and gradient array (Fig. 7.5b), the area from x = 0 m to 150 m the layer is close to 20 m thick. Further north the thickness of the layer is a slightly smaller, ~ 10 m. This layer has a resistivity of 40-460 Ωm. This large difference is probably caused by a varying content of clay in the till (Sørensen *et al.* 2003) According to Fig. 4.2 and observation in field this resistivity probably represents a till. Downwards in the section the resistivities are decreasing. This may be due to the layer of tertiary clays and the surface of it seems to be situated in contact with the till layer, i.e. 30 m.a.s.l. in the south and 50 m.a.s.l. in the north. According to Parasnis (1997), clay has resistivities of 1-120 Ωm. The presented section shows resistivities of 1 Ωm to 10 Ωm and chargeability's of 10-60 mV/V.

The area contains thick layers of glacial formations and the bedrock surface may be on a depth that is larger than the penetration depth of the sections (Sørensen *et al.* 2003). Therefore, the low resistivity layer is probably clay, as discussed before.

In the pole-dipole section (Fig. 7.5c) a square shaped area of very low resistivity is present from x = 275 to 300 m on a depth of 20 to 30 m.a.s.l. In the IP section (Fig. 7.5f), it is shown that the area does not have any significant IP anomaly. However, this may be a result of different sensitive patterns of the arrays (Dahlin and Zhou 2006). It might also be a lens of clay with another kind of mineral composition that causes the lower resistivity. Another possibility is if the pipeline contains, or has been containing, some geoelectrical responding medium. It may also be an inversion problem. Most probable it may be a result of a 2D or a 3D effect.

Below this is a large area of low resistivity, x = 150 m to 375 m. This may be a layer of clay with another mineral composition, which is more conductive. Or, it is a result of inversion problems.

The boundary between the layers at a depth of about 20 m.a.s.l. (x = 325-400 m), a relatively high chargeability is present (~ 60 mV/V). Around 280 m a very high chargeability is present in the top layer. In the gradient array using single cable the area is split up in two circle-shaped formations. In the gradient section using separated cables the area has a drawn-out form, while in the pole-dipole section it is more shaped as a circle. This may be a pipeline. Why the gradient array using single cable gives two anomalies and the gradient array using separated cables gives a stretched formation may depend on the high 2D-effect, mentioned earlier.

7.6 Conclusion

In this survey the use of separated cables results in a higher quality of the data compared to single cable measurements. However, the difference is not so large.

In the use of pole-dipole array, a much higher penetration depth is obtained, around twice as deep. Important is that the resolution is decreasing with depth and the quality will be affected as well.

The area has a higher resistivity in the top layer, which is probably a till, and is more conductive with depth. The surface of the tertiary clay layer is interpreted to be about 30 m.a.s.l. in the south and at about 50 m.a.s.l. in the north. The bedrock is situated on a greater depth and is therefore not present in these sections.

The high chargeability anomaly at x = 280 m is probably the pipeline that was assumed earlier, and it is lying quite shallow (~ 5 m). By looking at the decay curves (Fig. 7.3b), the shape of the negative chargeability close to the high positive chargeability is likely to be a result of a 2D-effect, but it also can be a 3D effect depending on how the pipeline is orientated.

Below this anomaly, approximately 20 m.a.s.l., a low resistivity is present. This may have different explanations. It might be a lens with clay of a different type of mineral composition compared to the surrounding clay material, or, it may be something geoelectrically responding medium from the pipeline. However, most probable is it a result of 2D or 3D effects and maybe inversion problems. Further down a large area of a more conductive material is present. This could be a clay with another type of mineral composition. To obtain a more exact interpretation of these formations, more investigations have to be done, e.g. drilling.

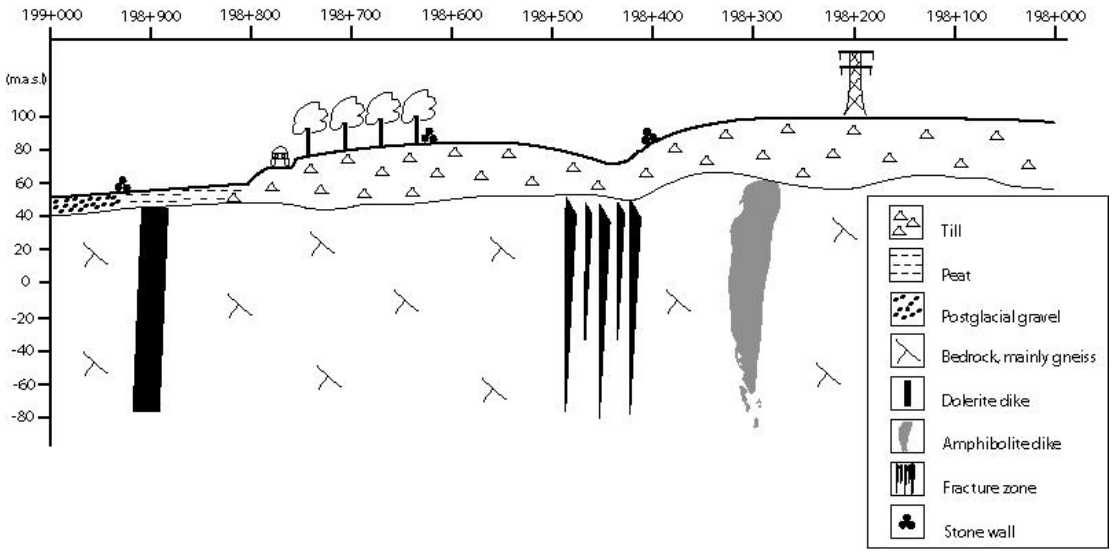

Fig. 8.1. Expected geological model of Site 1 and Site 2 at the Hallandsås Horst. Coordinates according to Banverket.

8 Field tests – The Hallandsås Horst

8.1 Fieldwork

Site 1

The first measurement took place on the 5th and 6th of June 2007. A meadow close to the southern connection of the tunnel had been chosen as the first site to investigate. The north side of the meadow was moist while the southern end was drier. A stone wall marks the boundary between the moist ground and the drier ground. The profile was 200 m long with 5 m electrode spacing. The profile was situated between the western and the eastern tunnel and was parallel with the tunnel direction, i.e. 34˚ E. Roll-along technique was not necessary because of the short distance.

Measurements were carried out with gradient and pole-dipole arrays. Separated cables were used but the gradient array was additionally done with single cable layout. The protocols used are listed in Appendix 3.

The pole-dipole measurement was carried out with a remote electrode distance of about 600 m. That is too short for a profile length of 200 m and data should therefore be critically evaluated.

Site 2

The next measurement session at the Hallandsås Horst took place the 12th and 13th of September 2007. 700 m was done with roll-along technique. The same electrode arrays as during the first measurement occasion were used, i.e. gradient array with single cable layout, gradient array with separated cables and pole-dipole array with separated cables. The profile was laid out between the eastern and the western tunnels, parallel with the tunnel direction. The profile started at the tunnel coordinate 198+748 just north of the road that ended the first measurement occasion. The profile ended at 198+048. The remote electrode in the pole-dipole measurement was placed as far away as possible but limited by the railroad and roads in the area. The distance between the remote electrode (C2) and current electrode (C1) varied between 400 – 550 m during the roll-along. One stonewall crossed the profile at about 120 m and another stonewall at about 345 m. A power line is present at 550 m.

8.2 Equipment

Equipment used at the Hallandsås Horst is according to Table 4.1 and the type of cable was 4X100 m multicore (8X100 m in the separated cables layout), 5 m electrode distance, 21 take-outs. A remote cable was also used.

8.3 Reference data

Documentation done while constructing the tunnel using drill and blast is used as reference. The data is supplied by Banverket, the Swedish Railroad Department. Mapping data from the tunnels show rock type, fractures and rock quality at approximately 30 m.a.s.l. The bedrock surface is interpreted from refraction seismic measurements (Banverket 1999). Groundwater data were taken from the Banverket internet site (www.banverket.se). Maps of bedrock, structure geology and Quaternary deposits have also been used in the geological interpretation (Wikman and Henkel 1979b, Wikman and Bergström 1987, Ringberg 2000, Ringberg 1995)

Earlier resistivity measurements have shown that resistivity in the SMZ is low, below 300 Ωm. It is however difficult to tell from just resistivity data if the rock is water bearing or clay weathered with low water content (Danielsen *et al.* 2004). The SMZ consist mainly of heavily clay weathered rock but there are also more unweathered parts (Sturk *et al.* 2005). Resistivity at the ends of the SRZ is low enough to indicate that the rock is fractured and water bearing (Dahlin *et al.* 1999).

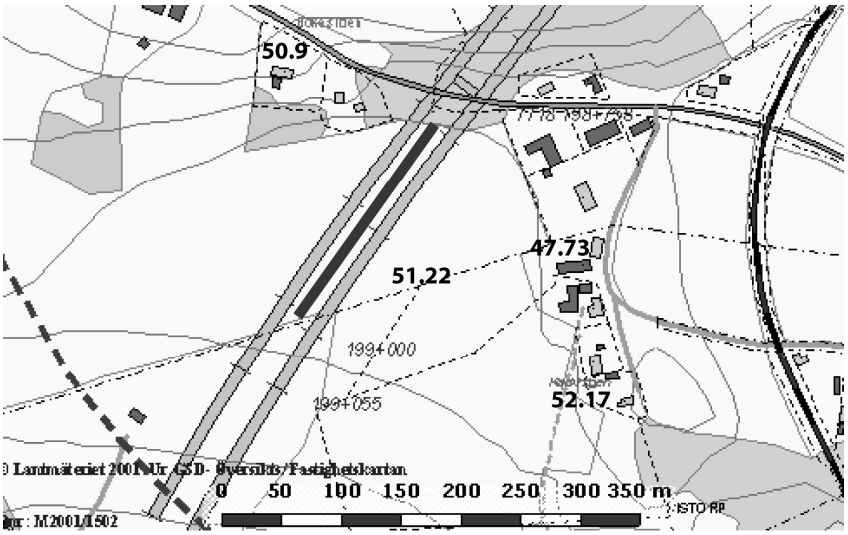

Fig. 8.2. Map showing groundwater levels and position of measured line at Site 1. Black numbers are groundwater levels in m.a.s.l. Measurements were done 2007-05-29. Data are taken from the Banverket internet site (www.banverket.se)

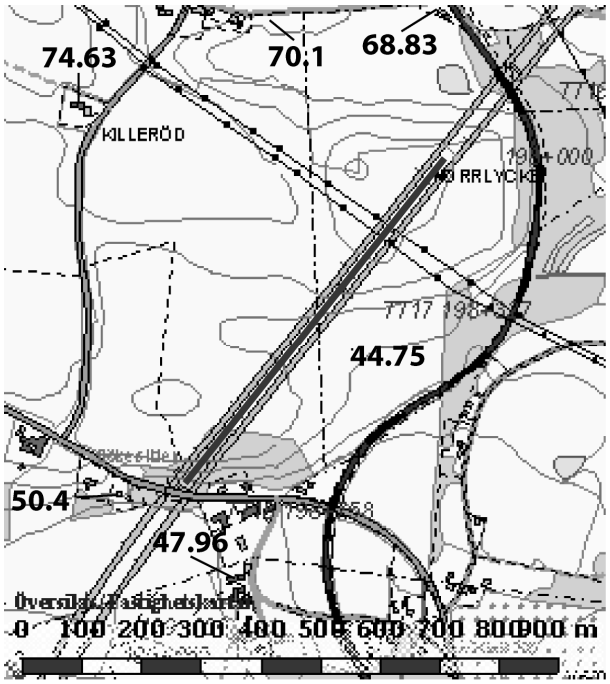

Fig. 8.3. Map showing ground water levels and position of measured line at Site 2. Black numbers are groundwater levels in m.a.s.l. Measurements were done 2007-08-22. Data are taken from the Banverket internet site (www.banverket.se).

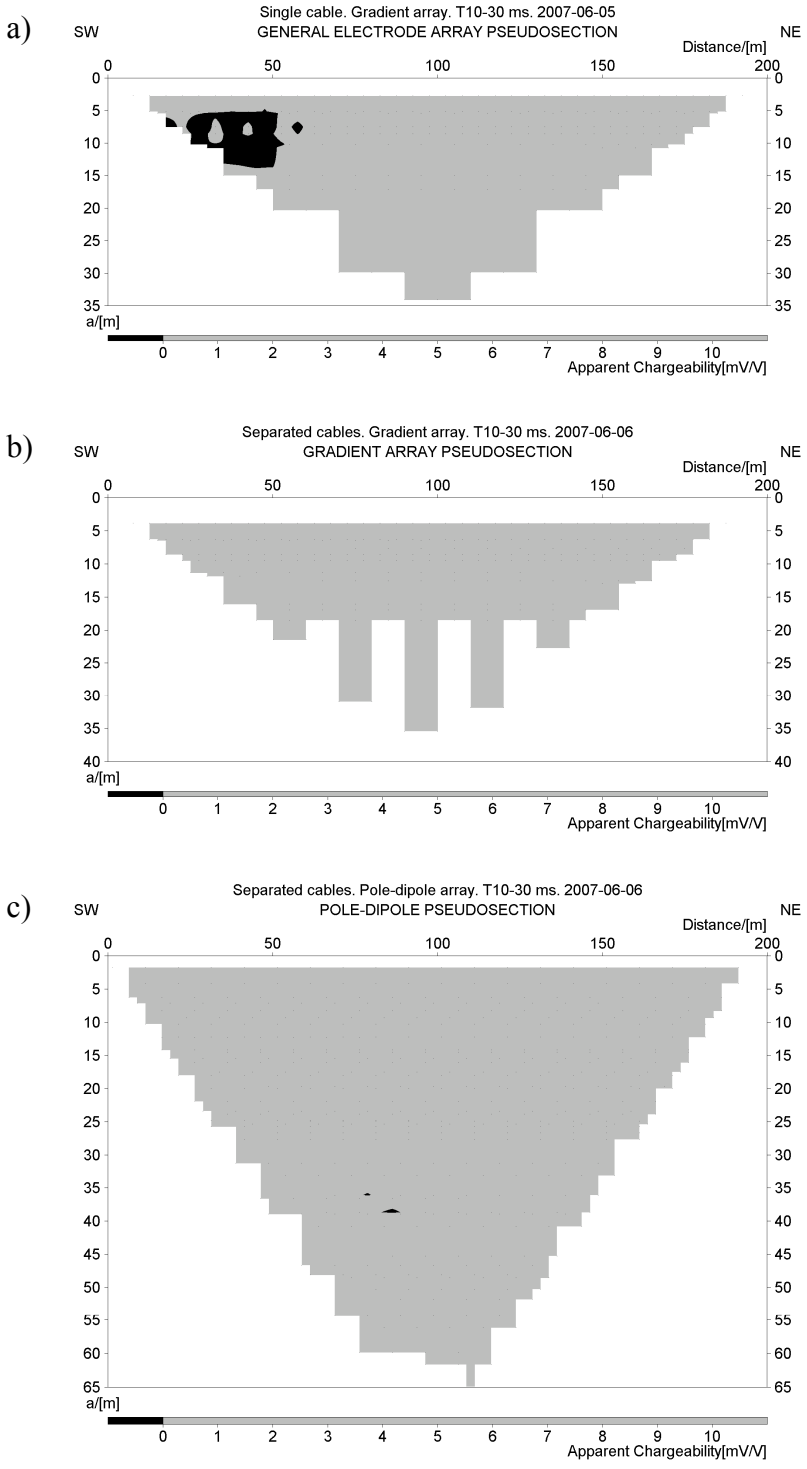

Fig. 8.4 Pseudosections of measured apparent chargeability with different electrode arrays, Site 1, Hallandsås Horst. Time window 1 (10-30 ms). Note that black represents negative data and light grey represents positive data. (a) Single cable, gradient array. (b) Separated cables, gradient array. (c) Separated cables, pole-dipole array.

The different types of reference data are compiled in the following two chapters, Site 1 and Site 2. This information is then used for the interpretation and discussion of the results. A model of the expected geology in the area was also made and is presented in Fig. 8.1.

A summary of the most fractured areas in the tunnels along the profile (Site 1 and 2) is listed below. Data were taken from the Tunnel documentation (Banverket 1999).

198+925 – 198+830: Gneiss and dolerite. A dolerite dike of 45 m width crosses the tunnels at approximately 198+900. Increased fracturing in the whole area.

198+520 – 198+385: Gneiss, amphibolite and dolerite. A dolerite body is present in the western tunnel and an amphibolite body is present in the eastern tunnel. Increased fracturing in connection with dolerite and amphibolite.

198+205 – 198+180: Amphibolite. In the eastern tunnel the amphibolite border on gneiss to the south and in the western tunnel the amphibolite border on gneiss to the north. Fractured and bad rock.

Site 1

From the reference data it is seen that the bedrock at site 1 mainly consists of gneiss. Approximately the middle of the profile a dolerite dike is present (Wikman and Henkel 1979b). Soil type in the first part of the profile is postglacial gravel and in the second part swamp peat (Ringberg 2000). There are probably till beneath the gravel and the peat.

At this site the depth to the tunnel roof is approximately 25 m according to Banverket (1999). The surface slopes gently from 52 m.a.s.l. in the southern end of the profile to 56 m.a.s.l. in the northern end. Soil depth is about 10 m. Tunnel documentation (Banverket 1999) confirms that main rock type is gneiss and that a dolerite dike crosses the profile at 198+900. There are also increased fracturing in the contact zone between dolerite and gneiss. The bedrock surrounding the dolerite is of poor quality. In the western tunnel some thin parts of amphibolite are present north of the dolerite dike, but they are not present in the eastern tunnel. Water leakage is almost zero in the southern part but increases at 70 m to about 150 l/min (Banverket 1999).

Groundwater data showed that the groundwater level in late May 2007 varied in the area between 48 and 52 m.a.s.l. (Fig 8.2). This is approximately 2 – 6 m below ground level.

Site 2

The reference data shows that the bedrock mainly consists of gneiss. An amphibolite dike crosses the profile at approximately 198+300 (Wikman and Henkel 1979b). The map of structural geology shows a fracture zone at about 198+450. The soil consists of till (Ringberg 2000), which according to Ringberg (1995) could overlay glacifluvial sediment, see chapter 3.3.

The ground level in the profile varies between 64 and 82 m.a.s.l. and soil depth is 13 – 26 m. Groundwater levels in late August varied between 45 and 75 m.a.s.l. in the area. This is approximately 2 – 20 m below ground level. There is a gradient decrease towards southeast (Fig. 8.3).

8.4 Results

8.4.1 Difference between measurements using single cable, separated cables and different electrode configuration.

Note

The presented pseudosections (Fig. 8.4b-c, Fig. 8.5.b-c and Appendix 2) show the same interpolation problem as in the Aarhus result.

Site 1

Three pseudosections from site 1 were obtained, gradient array using single cable, gradient array using separated cables and pole-dipole array using separated cables. The unit is apparent chargeability, mV/V.

The pseudosections in Fig. 8.4 show the first time window, i.e. 10 – 30 ms. The length of the profile is 200 m. The measurement cycle has been stacked two times.

Fig. 8.4a shows single gradient array. The total amount of data points is 329. The total time is 310 ms and consists of 5 time windows with an increasing factor of 20 ms on each window. The total amount of electrodes is 41. The pseudodepth is approximately 34 m.

In Fig. 8.4b and 8.4c the pseudosections using separated cables are seen. In both cases the total time is 910 ms and consists of 9 time windows with an increasing factor of 20 ms on each window. The total amount of electrodes is 82. The separated gradient array (Fig. 8.4b) has 297 data points and the pseudodepth is about 35 m. The pole-dipole array (Fig. 8.4c) has 512 data points and the pseudodepth is roughly 60 m.

In Appendix 2, the pseudosections of apparent chargeability is shown.

Negative data are very rare at Site 1 and are therefore not presented as detailed as at Site 2. The measurement using single cable has some negative data in the first time window in the left corner of the pseudosection (Fig. 8.4a). The negative values percentage is then decreasing with time. The measurements using separated cables have almost no negative data (Figs. 8.4b and 8.4c). There are some single negative values in later time windows though. The pseudosections in Fig 8.5 shows the apparent resistivity. The apparent resistivity in Fig. 8.5a and 8.5b is varying from 80 Ωm up to 1000 Ωm. The pseudodepth is about 35 m. Fig. 8.5c has an apparent resistivity from 10 Ωm up to 2000 Ωm. The pseudodepth is about 60 m.

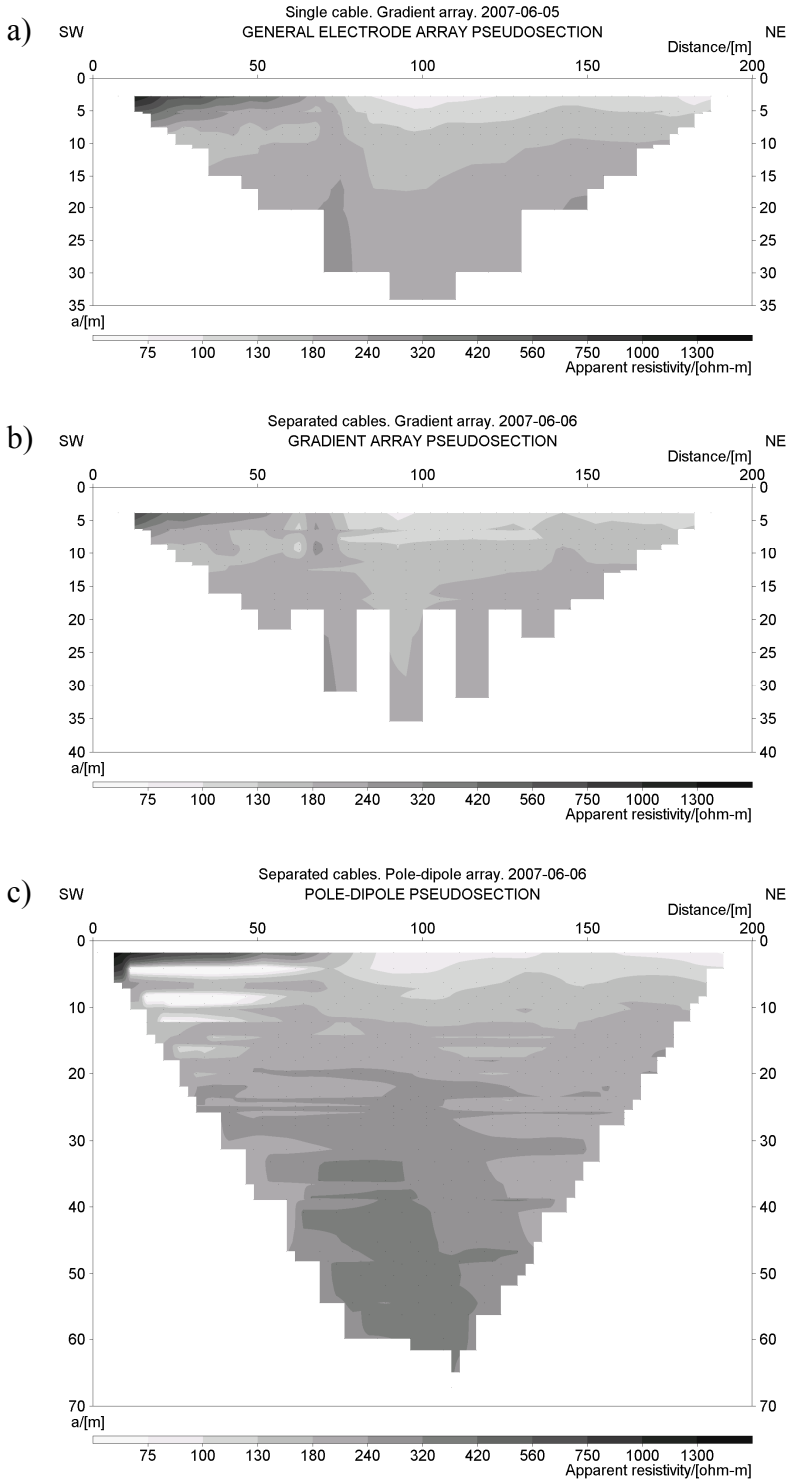

Fig. 8.5. Pseudosections of measured apparent resistivity with different electrode arrays, Site 1, Hallandsås Horst. (a) Single cable, gradient array. (b) Separated cables, gradient array. (c) Separated cables, pole-dipole array.

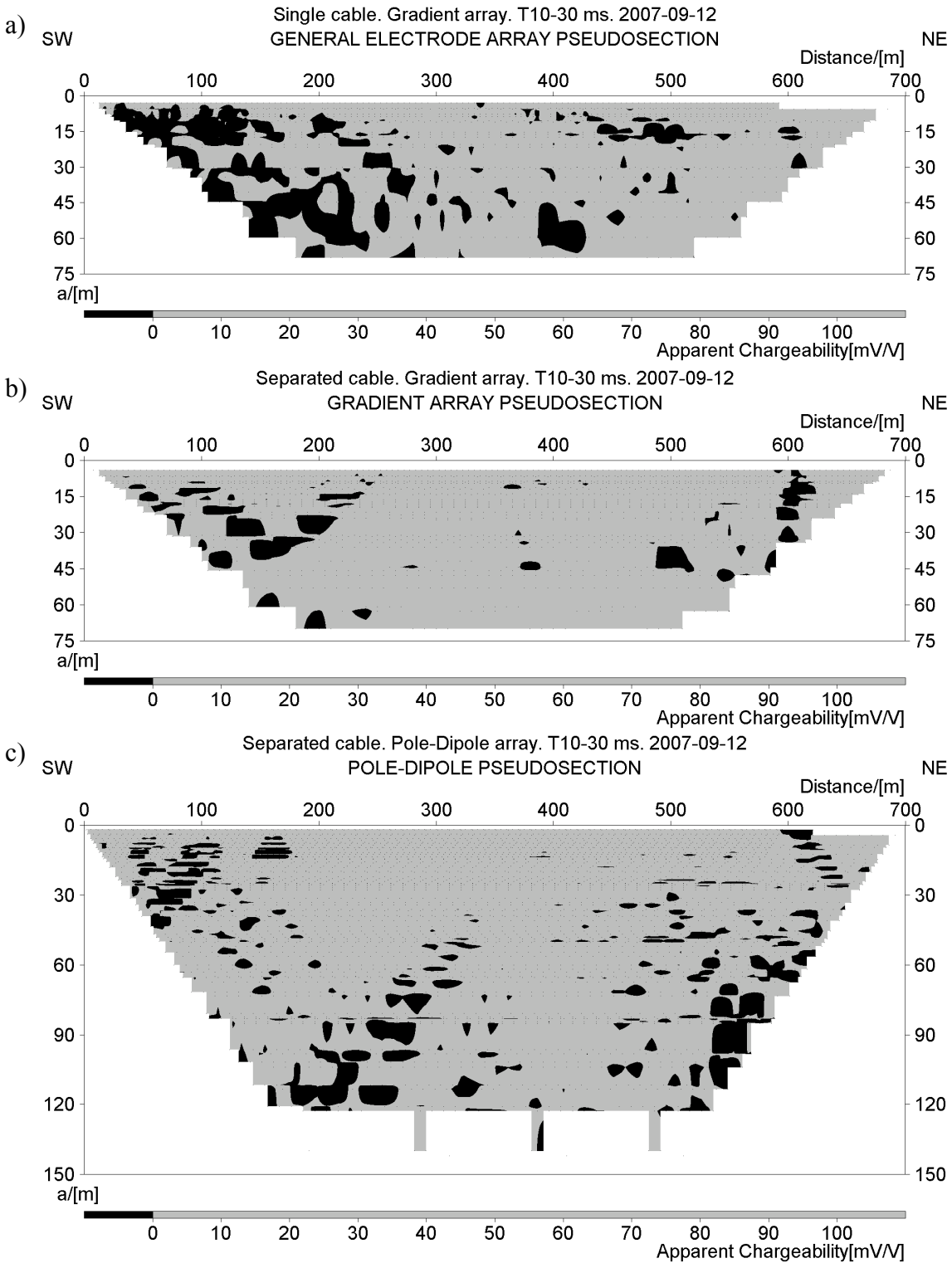

Fig. 8.6. Pseudosections of measured apparent chargeability with different electrode arrays, Site 2, Hallandsås Horst. Time window 1 (10-30 ms). Note that black represents negative data and light grey represents positive data. (a) Single cable, gradient array. (b) Separated cables, gradient array. (c) Separated cables, pole-dipole array.

The highest apparent resistivity is found in the upper left corner in all three pseudosections (Fig. 8.5). The area extends to x = 70 m in the separated gradient array, x = 40 m in the single gradient array and x = 10 m in the pole-dipole array. The single gradient array and pole-dipole array has higher apparent resistivity than the separated gradient array in this area. The lowest apparent resistivity is found in the upper middle and upper right parts of the sections. The pole-dipole array shows lower values than the gradient arrays. Further down, to about 35 m pseudodepth, the three sections have an apparent resistivity interval of about 150 – 300 Ωm. In the bottom of the pole-dipole array the apparent resistivity is roughly 300 – 400 Ωm.

Site 2

Three pseudosections with the same arrays as at Site 1 were obtained. In Appendix, the apparent chargeability is shown.

The pseudosections in Fig. 8.6 show the first time window, 10 – 30 ms. The total time is 910 ms consisting of 9 time windows with an increasing factor of 20 ms on each window. The length of the profile is 700 m and the total amount of electrodes is 162. The measurement cycle has been stacked one time. Gradient array single cable (Fig. 8.6a) has 1991 data points and the pseudodepth is around 70 m. Gradient array separated cables (Fig. 8.6b) have 1986 data points and slightly larger pseudodepth. Pole-dipole array (Fig. 8.6c) has 5845 data points and the pseudodepth is approximately 140 m.

The gradient array using single cable shows a significantly higher degree of negative data in the first time window than gradient array using separated cables (Fig. 8.6). The negative values in the single cable measurement are mostly located to the left part of the section, whereas the separated cables measurement has most negative values towards both sides of the section. The pole-dipole measurement has negative values preferably on the sides and the lower parts of the section. The amount of negative data are somewhere between the gradient sections.

Table 8.2 shows how the percentage of negative values changes with time during measurement. There are less negative values in the measurements using separated cables (Table 8.2). The negative values decrease in the first time-windows but increase in later time-windows. In the single measurement the negative values decrease at earlier times and then stabilize. The pole-dipole measurement has a negative values percentage that is almost as low as for the gradient array using separated cables.

Fig. 8.7 shows IP-values integrated over the whole time spectrum and decay curves for some negative data in the gradient arrays. It is seen that IP-values in the gradient array using single cable is significantly noisier than IP-values in the gradient array using separated cables. Also, the negative data points in the single cable measurement have noisier decay curves than the separated cables measurement. Decay curves in the separated cables measurement have a significant rise in the first time window. The curves then go up and down in an abnormal pattern. In the profile centre of the separated cables measurement a strong negative anomaly is situated just beside a strong positive anomaly. Strong anomalies are also present in the right corner.

Table 8.2. Difference in negative values from Site 2 at the Hallandsås Horst. Gradient array using single and separated cables. Pole-dipole array using separated cables.

Time window (ms)	Grad. Single. (%)	Grad. Sep. (%)	Pole-dipole Sep. (%)
10-30	20	6.1	9.7
30-70	16	4.6	9.2
70-130	14	3.8	6.7
130-210	13	5.0	7.7
210-310	13	2.9	4.9
310-430	14	3.0	5.2
430-570	15	6.6	10
570-730	13	6.3	11
730-910	14	8.0	11

The pseudosections in Fig. 8.8 show the apparent resistivity. The apparent resistivity in Fig. 8.8a and 8.9b is varying from 80 Ωm up to 2000 Ωm. The pseudodepth is about 70 m. Fig. 8.8c has an apparent resistivity from 50 Ωm up to 3000 Ωm. The pseudodepth is about 140 m.

There are no large differences between single cable and separated cables when it comes to apparent resistivity. The pseudosections from measurements using separated cables are slightly less, though. The gradient arrays show highest apparent resistivity (about 400 – 2000 Ωm) near the surface. The centre area, x = 330 – 470 m, is an exception where the apparent resistivity is low (about 100 – 180 Ωm). At pseudodepths of 10 – 30 m the apparent resistivity is roughly 200 Ωm. Apparent resistivity then gradually increases downwards to about 400 Ωm at the bottom. The pole-dipole array has approximately the same appearance in the depth interval of the gradient arrays. Further down the data is a little bit more scattered. Some small spots of high apparent resistivity with systematically distribution are present, preferentially in the right part of the section. In the lower left corner the apparent resistivity is about 70 – 200 Ωm.

8.4.2 Inversions

Inversion was only made on the datasets with separated cables because they have shown better data quality than the measurements using single cable. The whole time span was selected because it gives a good compromise between signal strength and noise contamination.

At the first measurement site the expected geology was a more or less vertical dolerite dike surrounded by

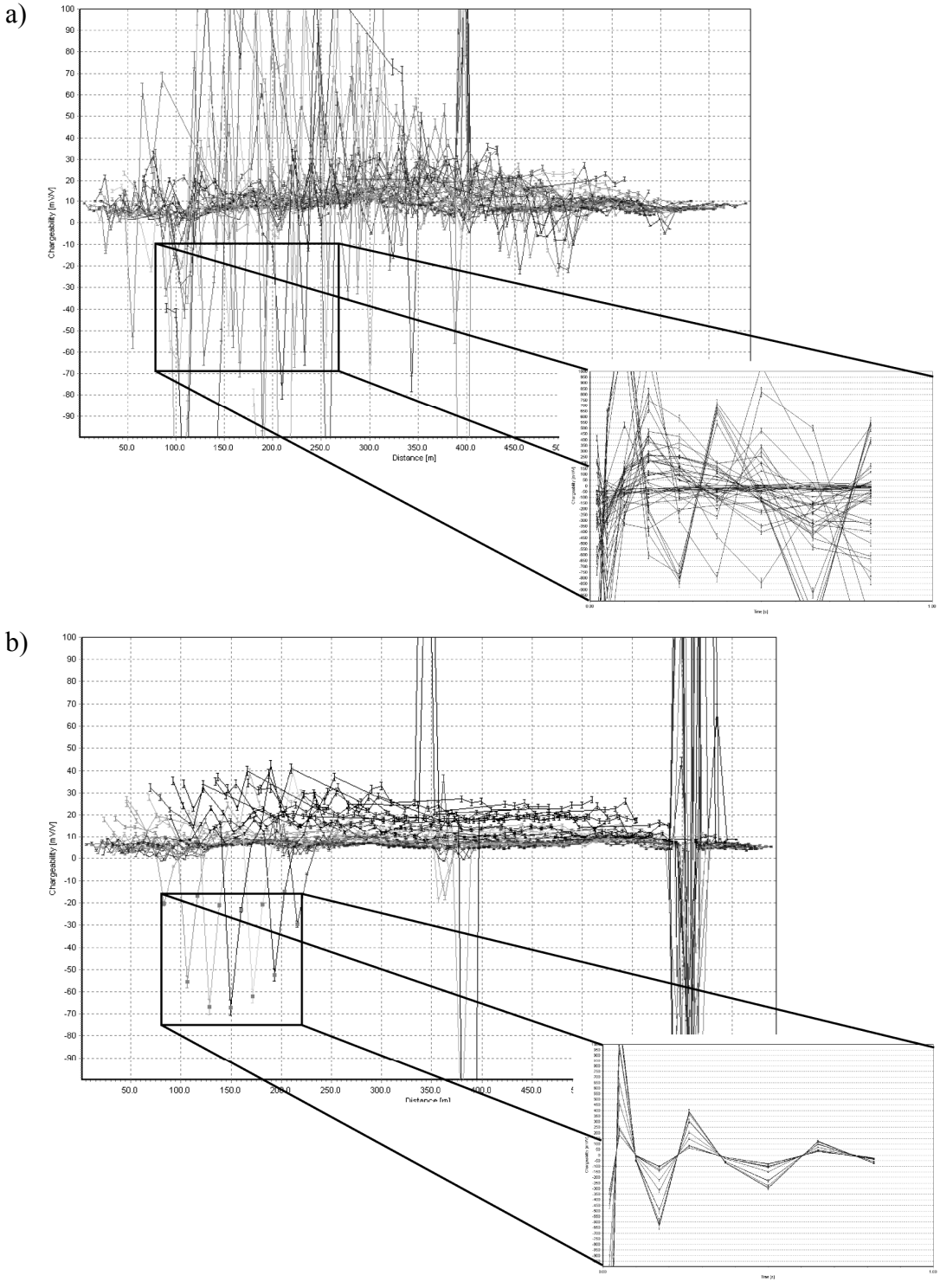

Fig. 8.7. Measured apparent chargeability and decay curves of negative values in gradient array. (a) Single cable. (b) Separated cables. Small windows shows the decay curves of selected electrodes, each line representing one data point.

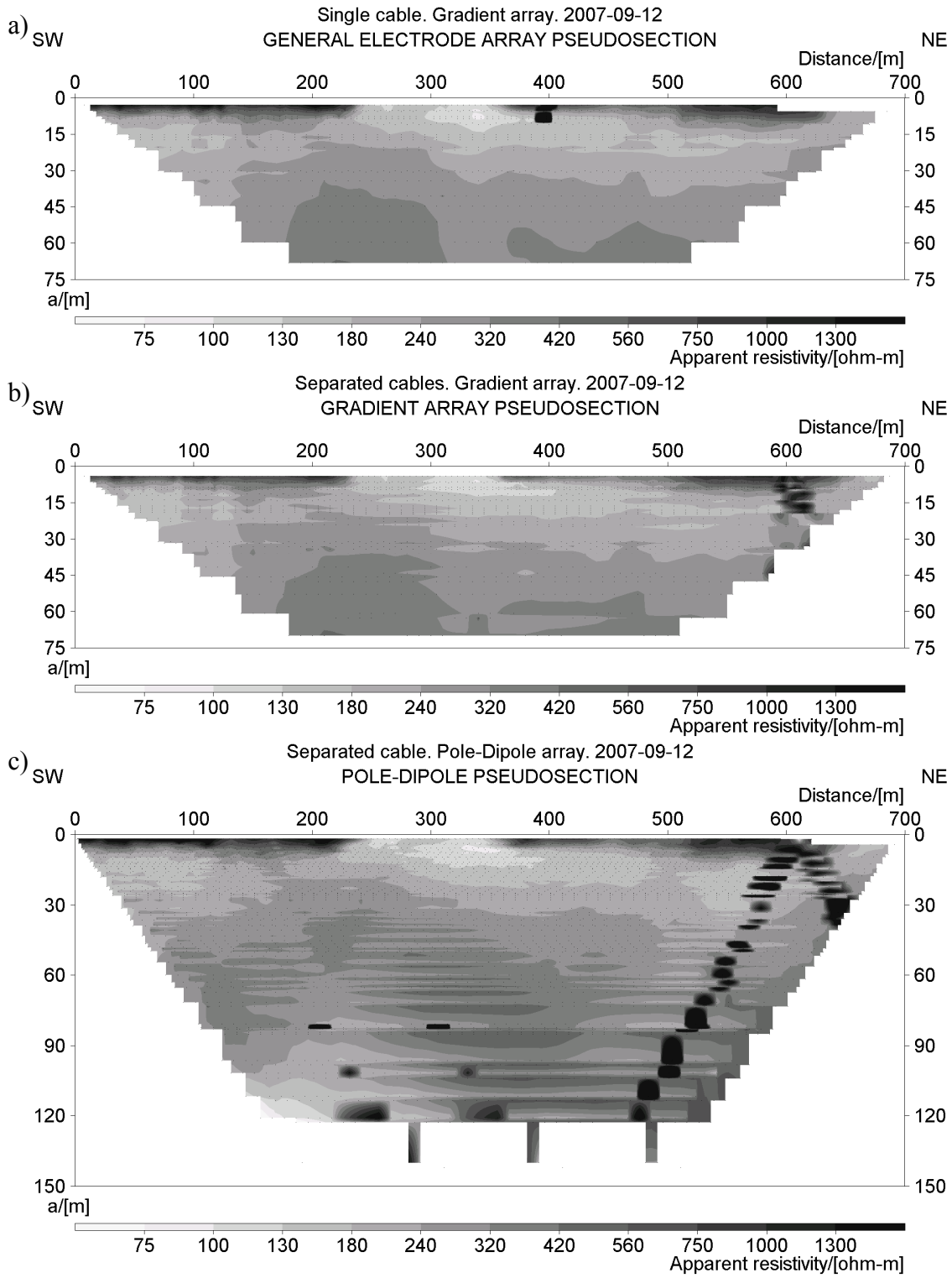

Fig. 8.8. Pseudosections of measured apparent resistivity with different electrode arrays, Site 2, Hallandsås Horst, Sweden. (a) Single cable, gradient array. (b) Separated cables, gradient array. (c) Separated cables, pole-dipole array.

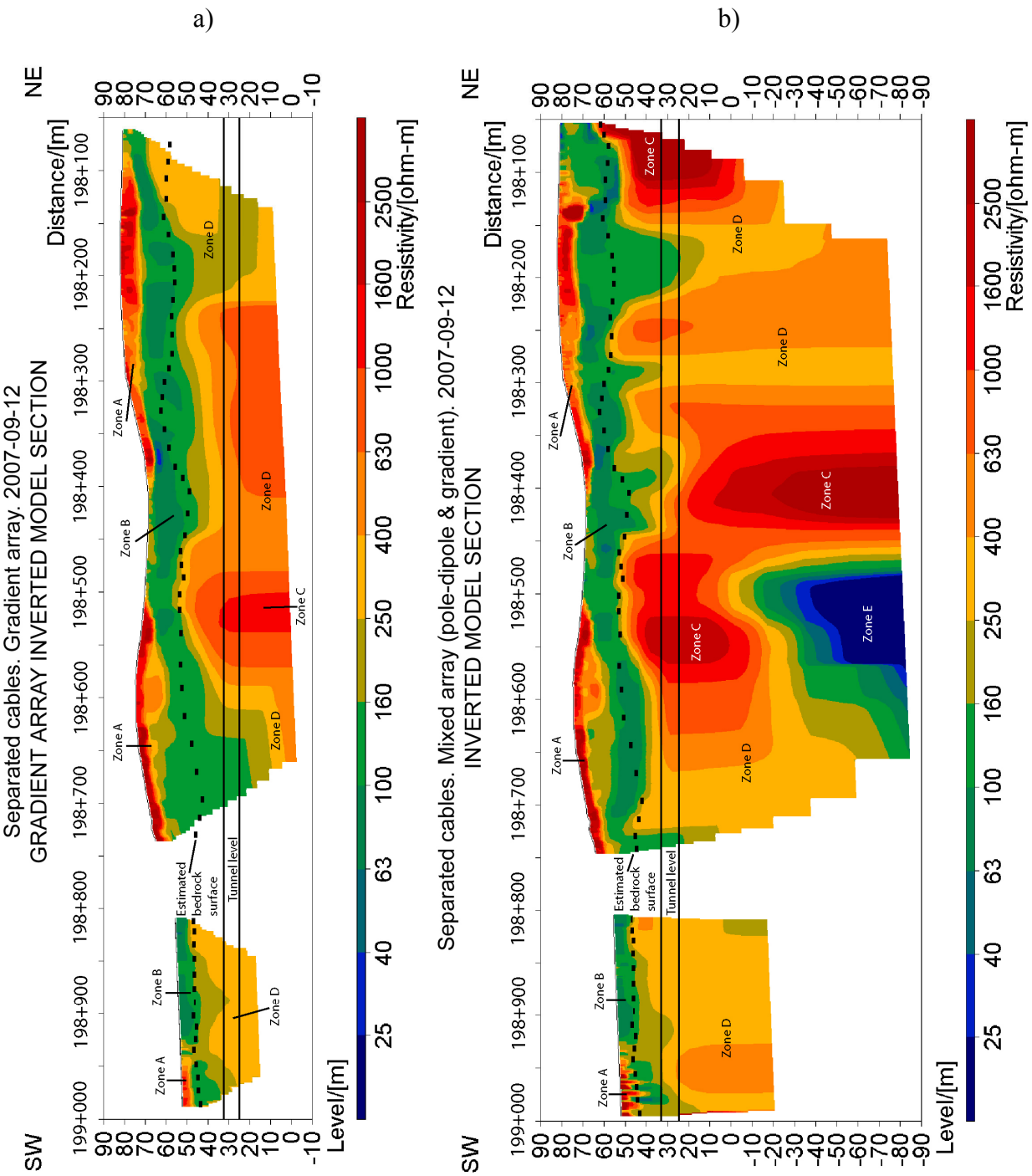

Fig. 8.9. Resistivity models from Site 1 (left part) and Site 2 (right part) at the Hallandsås Horst. Separated cables. (a) Gradient array. (b) Mixed array in the left part and pole-dipole array in the right part.

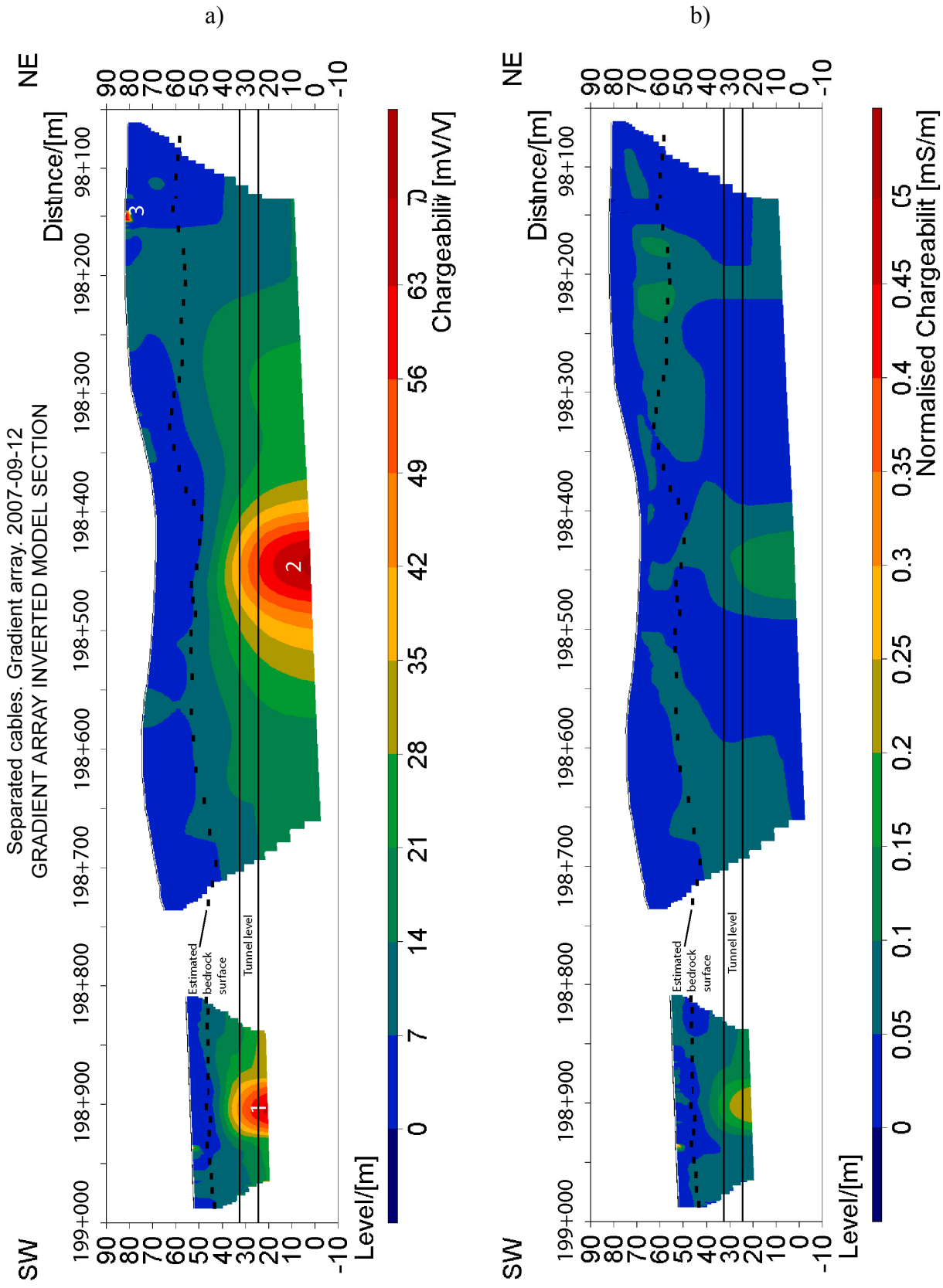

Fig. 8.10. IP and normalized IP models from Site 1 (left part) and Site 2 (right part) at the Hallandsås Horst. Separated cables. All time windows (10-910 ms). (a) IP, gradient array. (b) Normalized IP, gradient array.

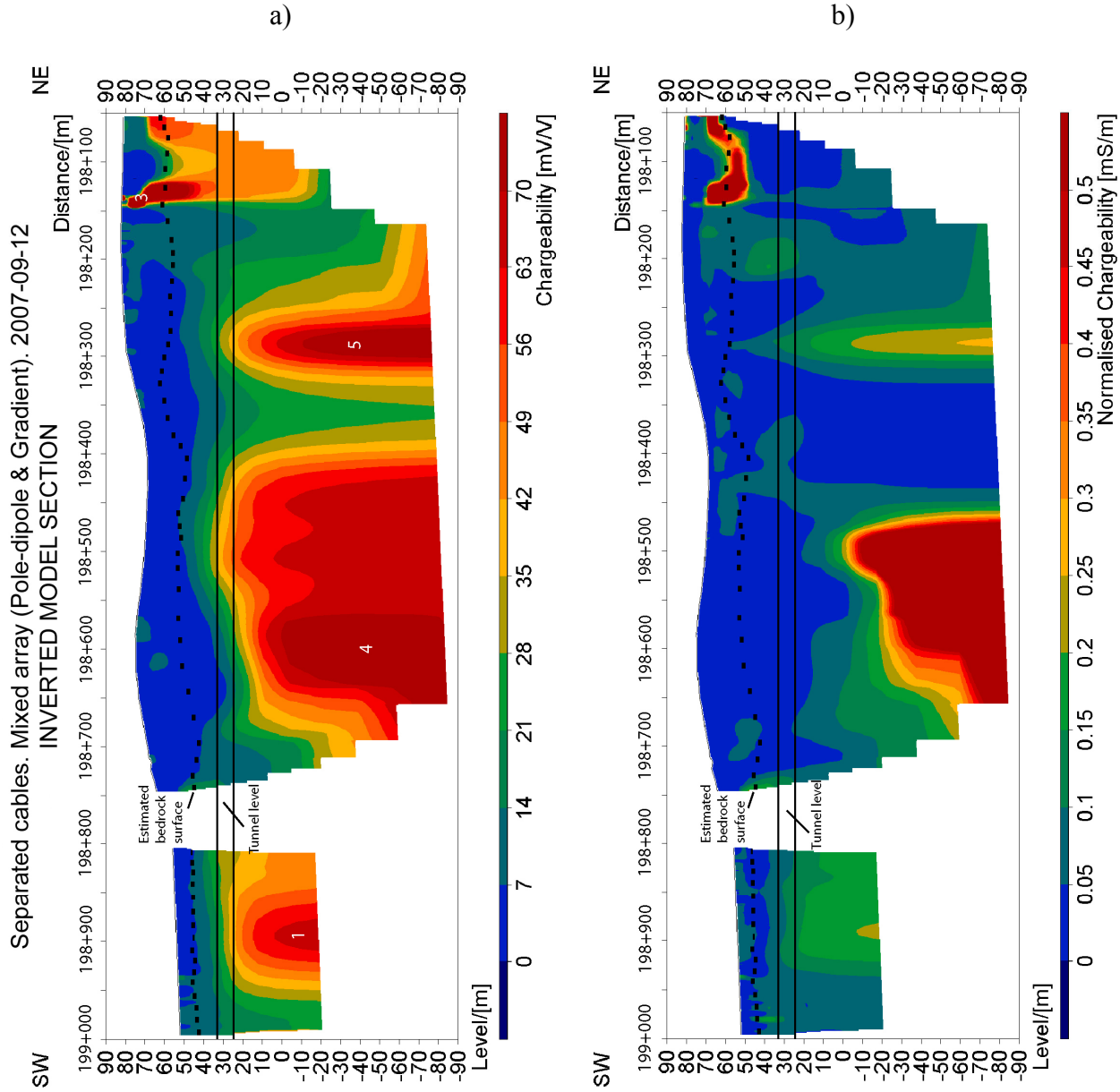

Fig. 8.11. IP and normalized IP models from Site 1, mixed array (left part) and Site 2, pole-dipole array (right part) at the Hallandsås Horst. Separated cables. All time windows (10-910 ms). (a) IP. (b) Normalized IP.

Table 8.4. Mean errors from the Hallandsås Horst inversions.

Site	Gradient (%)	Gradient (%)	Pole-dipole (%)	Pole-dipole (%)	Merge (%)	Merged (%)
	Res	IP	Res	IP	Res	IP
1	3.7	1.7	-	-	12.9	2.3
2	2.1	3.2	5.3	8.0	-	-

fissured gneiss (Banverket 1999). Therefore the vertical/horizontal flatness filter was set to 2.0 to emphasize the vertical component in the data. In the inversions from the second measurement site the flatness filter was set to 1.0 (default).

Pole-dipole data has greater depth penetration then gradient data. Since there are missing data points in the pole-dipole section from Site 1 the resolution at shallow depths are better in the gradient section. To get both good resolution and depth penetration merging of pole-dipole and separated gradient data was done. This resulted in a model with mixed arrays from Site 1.

After inversion the gradient models from Site 1 and Site 2 were put together. The model with mixed arrays from Site 1 and the pole-dipole model from Site 2 were also put together and presented in profiles stretching over the whole measured area.

Fig. 8.9 shows resistivity models from the Hallandsås Horst. The uppermost region where resistivity is high, >1000 Ωm, is named Zone A. This layer is about 10 – 15 m thick. There is a zone with resistivity values below 150 Ωm that is found beneath Zone A and at the surface at 198+940 - 198+800 and 198+500 – 198+400. This is named Zone B. There is one area with high resistivity, > 1000 Ωm, in the lower part of Fig. 8.9a. In Fig. 8.9b there are three high resistivity areas. The southern area has resistivity up to about 2000 Ωm. The middle area has resistivity up to about 4000 Ωm and the northern area has resistivity up to about 8000 Ωm. These areas are named Zone C. The areas in between have resistivities on 200 – 700 Ωm and is named Zone D. One area with very low resistivity in Fig.8.9b sticks out. This area is named Zone E.

Fig. 8.10 and 8.11 shows IP and normalized IP models. The IP models show high chargeability (50-70 Ωm) at 198+900, anomaly 1 (Fig. 8.10a and 8.11a). The model in Fig. 8.11a has a stronger and wider anomaly. The gradient model shows IP-effect at 198+450 (anomaly 2) with highest values (70 Ωm) in the bottom of the model (Fig. 8.10a). The model in Fig. 8.11a shows high chargeability (> 70 Ωm) in an area stretching from 198+650 to 198+550 with a maximum around 198+600 (anomaly 4). Anomaly 5 is also strong (> 70 Ωm) and has small lateral spread. It is situated at 198+290. Anomaly 3 (> 70 Ωm) is seen on shallow depths at 198+150 (Fig. 8.11a). Anomaly 3 is not that clear in the gradient model but still visible and a few negative values are also present in this region (Fig. 8.10a).

The normalized IP in the gradient model has three weak anomalies (Fig. 8.10b). One is located in the bottom of the model at approximately 198+900. The second one is located in the bottom of the model at 198+450. The third one is located at approximately 198+200 at 65 m.a.s.l. The normalized IP in Fig 8.11d has one clear anomaly in the bottom of the model at 198+875. The anomaly between 198+670 and 198+460 is very strong (over 10mS/m). At 198+300 and 198+200 there are also anomalies, the latter quite strong.

8.5 Discussion

Pseudosections

The quality of the resistivity data from the gradient measurements does not differ much between single and separated cable layout. Pole-dipole data are slightly more scattered and uneven than gradient data (Figs. 8.5 and 8.8). The short pole-dipole protocol at Site 1 is missing due to measuring errors. Hence, data is missing in the upper part of the section, leading to low resolution at shallow depths. The difference between gradient and pole-dipole data in the upper part of the section is therefore expected (Fig. 8.5).

Apparent chargeability sections are presented in Appendix 2.

There are rather large differences in IP-data quality between single cable and separated cables using gradient array at Site 1. This is especially obvious in the first time window (Appendix 2 Fig. A2.2). The separated section has smoother boundaries and more even distribution of IP values. Data quality in the pole-dipole section is relatively poor, since IP values have a more scattered distribution (Appendix 2 Fig. A2.2).

In the IP sections from Site 2 there are also significant differences between single and separated cables (Appendix 2 Fig. A2.3). The separated gradient array is more even and has less sharp transitions in IP value. The pole-dipole data has a rather scattered distribution at depths. The upper part of the section is more even and comparable to the separated gradient array.

One interesting feature is that the negative values percentage in the pole-dipole array, change in time more or less in the same way as separated gradient array (Table 8.2). This may indicate that the negative values are caused by something else than capacitive coupling, and that the capacitive coupling have been significantly reduced, as expected.

Site 2 shows a significantly higher degree of negative data than Site 1 (Figs. 8.4 and 8.6). This could be due to increased coupling effects or a higher degree of external noise, such as a power line. If it is coupling effects, one explanation is that the uppermost ground has a higher resistivity at Site 2, which could lead to increased capacitive coupling (Dahlin et. al. 2002). Another possible explanation is that the layout at Site 2 was much longer and therefore more prone to coupling effects.

The strikingly noisier appearance of the single cable measurement compared to the separated cable measurement could indicate that the capacitive coupling is stronger in the gradient array using single cable (Fig. 8.7). The distinct rise of the decay curves in the first time window of the separated cables measurement might be a sign of inductive coupling (Sumner 1976). However, the curves are fluctuating and deviate very much from a logarithmic decaying response. It is possible that external noise contaminate the data, perhaps some electrical arrangements in the tunnel. It also might be connected to bad electrode contact. This was attempted to examine. But it was too complex to define because the four responsible electrodes resulted, in different combinations, in a large amount of both positive and negative data.

The anomaly in the centre of the profile in Fig. 8.7 b looks like a 2D geometric effect and might be caused by a fracture zone as discussed later. The strong anomalies in the right corner are probably due to external noise effects from the power line.

Difference in negative values between single cable and separated cables using gradient array are larger in earlier times, i.e.10 - 430 ms (Table 8.2). Approximately the same pattern was seen in the measurements made in Lund. As discussed in chapter 6, this is probably due to decreasing capacitive coupling and signal-to-noise-ratio with time.

Geological interpretation of resistivity models

The bedrock surface is not clear in the resistivity models (Fig. 8.9). If the seismic data are correctly interpreted the upper part of the bedrock seems to be very weathered since the resistivity is lower than 200 Ωm. It could also be an effect of uncertainties in resistivity and/or seismic data. As indicated from the map of Quaternary deposits, the first part of the profile should consist of postglacial gravel. The resistivity in this area is high, which support the expected geological model. The area at shallow depths between 199+000 and 198+940 is therefore interpreted as postglacial gravel. The area at shallow depths between 198+940 and 198+800 should be peat. The low resistivity and observed wetness support this interpretation. There may be till underneath the gravel and the peat since they are both postglacial formations. It is however hard to tell from the resistivity models. Zone A in the area from 198+750 to 198+050 is probably till due to reference data (Ringberg 1995). Zone B in the same area (Site 2) could be water saturated till or glaciofluvial sediments as discussed in chapter 3.3. The relatively low resistivity indicates that the soil in any way has a high water content.

Zone C is most likely rock with less joints or just slightly fissured rock. The resistivity values in Zone D are very low for fresh rock (200-700 Ωm). This is in the resistivity range for fissured rock, and several resistivities are even low enough to indicate substantial clay weathering (Jeppsson 2003). The tunnel documentation shows some fracturing in the area and rather poor rock quality, although not as severe as in the SMZ (Banverket 1999). Zone E could be the fracture zone that is located on the map of structural geology at 198+450.

There are some differences in resolution at tunnel level between gradient and mixed/pole-dipole arrays (Fig. 8.9a and 8.9b). Data from gradient measurement does not correlate as well with the tunnel documentation as data from pole-dipole measurement, especially not in the last part of the profile (Banverket 1999). The explanation for that is probably that the resolution at tunnel level is lower in the gradient model than the pole-dipole model. Therefore, comparison only between tunnel documentation and the mixed/pole-dipole model is presented.

Resistivity contrasts are larger and anomalies generally higher in Fig. 8.9b. The first 200 m has resistivities between 150 and 450 Ωm. Tunnel documentation (Banverket 1999) shows quite poor rock quality, especially in the eastern tunnel. Bedrock between 198+750 and 198+600 has low resistivity (100 – 400 Ωm). Tunnel documentation (Banverket 1999) shows gneiss of relatively good quality in the eastern tunnel but more fractured gneiss in the western tunnel. Between 198+600 and 198+500 there is high resistivity at tunnel level (400 – 2000 Ωm). In the tunnel documentation there is gneiss with good quality except for the last 20 m where some amphibolite and fractures are present (Banverket 1999). At 198+500 – 198+210 there is moderate resistivity (300 – 700 Ωm) with lower values between 198+450 and 198+350. This correlates well with the presence of amphibolite and fracturing in the eastern tunnel. The pole-dipole array shows lower resistivity between 198+210 and 198+150. This correlates well with the presence of fracturing in the contact zone between gneiss and amphibolite in the tunnel. The resistivity at tunnel level increases through the last part of the profile. The rock quality increases, as expected, in the corresponding tunnel part.

Geological interpretation of IP models

The high chargeability anomaly (anomaly 1) that is seen in the IP models at 198+900 could be the dolerite dike expected at this location (Figs. 8.10a and 8.11a). The normalized IP models have also anomalies at approximately 198+900 (Figs. 8.10b and 8.11b). That indicates that the anomalies are effects of structural changes and not only conductivity changes, which further support the interpretation of a dolerite dike.

The tunnels do not go through the IP-anomalies in the pole-dipole model (Fig. 8.11a). Anomaly 2 in the gradient model (Fig. 8.10a) is though correlating rather well with a fracture zone in the contact between gneiss and amphibolite in the tunnels. In the western tunnel even dolerite is present (Banverket 1999). The map of structural geology also shows a fracture zone at this location (Wikman 1979a). Resistivity in this area (198+450) is relatively low (ca 500 Ωm) as expected in a fracture zone (Fig. 8.9). The high IP-effect could

indicate that the fracture zone is clay weathered (Fig. 8.10a). Anomaly 2 also shows normalized IP-effect (Fig. 8.10b), which indicates a structural change.

It is likely that anomaly 3 is caused by the power line. The negative values in the gradient model indicate noise effects that further strengthen this interpretation (Fig. 8.10a).

It is possible that anomaly 2 and 4 are parts of the same fracture zone that is seen on the map of structural geology. Anomaly 4 lies just next to an area with very low resistivity, Zone E (Fig. 8.9b), which also could be connected to the fracture zone as mentioned earlier. The lowest resistivity could then indicate an area with heavy fracturing, but weathering and clay development may be most prevalent in the area with highest IP-effect, i.e. the southern part of the fracture zone, anomaly 4. The normalized chargeability is high in the area between 198+650 and 198+450, below 0 m.a.s.l. (Fig. 8.11b). However, the highest values (over 10 mS/m) are located between 198+550 and 198+500. This could also be an indication that the fracture zone is most prominent here and that the high IP-effect in anomaly 4 (Fig. 8.11a) is in higher degree affected by conductivity changes caused by weathering and clay formation. The boundary of this zone is sharp in the normalized IP model compared to the IP model (Figs. 8.11a and 8.11b).

The bedrock map shows an amphibolite dike at approximately 198+300 where anomaly 5 is present (Fig. 8.11a). Tunnel documentation also shows a high amphibolite content in the area. Fracturing and clay weathering in the contact zone of the amphibolite dike probably cause the IP-effect. The normalized chargeability of anomaly 5 is relatively low compared to anomaly 4 (Fig. 8.11b). This could mean that the structural change of anomaly 5 is not as large as anomaly 4, e.g. a weaker fracture zone. The chargeability on the other hand is high, which could indicate severe weathering.

8.6 Conclusions

Capacitive coupling is significantly reduced when using separated cables. Earlier time windows give the best data quality in measurements with separated cables. That is probably due to decreasing signal strength with time. The measurements with single cable layout on the other hand have better data quality in later time windows. That is probably because the capacitive coupling is decreasing with time. This seems to have a larger effect on data quality than decreasing signal-to-noise-ratio.

The electromagnetic coupling increases with increasing cable length. This could be one explanation for the low amount of negative values at Site 1. Another explanation could be that the grounding resistances are lower than at Site 2, leading to lower capacitive coupling.

The bedrock of the investigated area seems to be very fractured. Three major structures are found. The first one is connected to a dolerite dike that crosses the profile at 198+900. The second one is probably a fracture zone that stretches from 198+650 to about 198+450 and is most prevalent below sea level. This fracture zone distinguishes itself by showing much higher normalized IP than the others and the resistivity is also exceptionally low. That could indicate an area of substantial fracturing and perhaps water-bearing rock. The southern end of this fracture zone, which shows higher IP, might be heavy clay weathered. The degree of fracturing most likely decrease upwards but the zone seems to extend up to tunnel level. The third structure is located at 198+300 and is probably a clay weathered fracture zone containing amphibolite.

The soil layer consists of postglacial gravel, peat and till. A boundary between high and low resistivity in the soil layer was found that probably represents a transition from dry till to wet till or glaciofluvial sediment.

9 Conclusions

9.1 Data quality

This study shows that the acquired IP data is of higher quality when using separated cables. This is significant in all measurements. It is shown that the capacitive coupling mostly causes noise manifested by negative data, as well as anomalously high data values, but also other effects such as 2D effects give negative data.
The quality is better if the area of investigation has a low to moderate top surface resistance. This is shown in the survey in Lund where the results has a significant difference when the area was exposed by heavy precipitation but also where the area has a moderate ground resistivity.

The ground surface at the Hallandsås Horst was generally more resistive than in Aarhus. Simultaneously, the difference in negative values between single and separated arrays was larger at the Hallandsås Horst. Also, the distribution of IP-values were more scattered in the single cable measurement compared to the separated cables measurements at the Hallandsås Horst. Therefore, regarding data quality, separated cables have been a good choice at the Hallandsås Horst but may have been overambitious in Aarhus. It is also important to bear in mind that the use of separated cables are a logistically complicated and time consuming method.

It is also shown that the measurements of resistivity are not much affected of using single multicore cables. This is because the resistivity measurements start a relatively long time (200-500 ms) after the start of current injection. Compare this with the IP integration, which is started very recently (10 ms) after current switch-off and last during the decay of the depolarization. A good rule is when having high quality of IP data; the data of resistivity is as well with high probability of good quality.

Finally conclusions regarding data quality:

- Layout with separated cables contributes to better quality of data in surveys of Induced Polarization.
- The capacitive coupling generates negative data, as well as anomalously high.
- The capacitive coupling increase with increasing ground resistance.
- 2D-effects may generate negative data.
- The electromagnetic coupling (inductive coupling) may increase with increasing length of the layout.

To obtain data of good quality in a disturbed and/or highly resistive area when measuring Induced Polarization, following actions should be performed.

- Use layout with separated cables.
- Make sure that the contact between electrode and ground are good.
- Use protocols that are designed for minimizing charge-up effects.

9.2 Geological interpretation

Aarhus

The thickness of the upper layer consisting of a till reaches a depth of about 30 m.a.s.l in the south and about 50 m.a.s.l. in the north. Under this a thick layer of Tertiary clays is situated. The profile of the pole-dipole measurement reaches a depth of about 100 m. The bedrock is situated on a greater depth than the penetration depth of the measurement. The high chargeability anomaly at x = 280 m is probably the pipeline that was assumed earlier. It has chargeability values of 60-100 mV/V and resistivity value of 5-20 Ωm. The upper part of the "pipeline" is lying about 5 m below surface.

The Hallandsås Horst

The study shows that there are three major structures in the bedrock. These are:

- Dolerite dike at x = 198+900, crossing the tunnel. There is no significant anomaly in the resistivity data. Chargeability values are 50-70 mV/V.
- Probable fracture zone between x = 198+650 and x = 198+450. The southern part of the fracture zone could be more weathered and less water bearing than the northern part. The upper boundary of this zone is situated on a depth about 10-30 m below the tunnel. The resistivity values vary between 1-60 Ωm, the chargeability values are around 70 mV/V and the normalized chargeability values are 1-10 mS/m.
- Clay weathered fracture zone which probably contains amphibolite. It is situated at x =198+300. It may cross the tunnel. There is no significant resistivity anomaly in this area. The chargeability values are around 70 mV/V but the normalized chargeability does only reach 0.25 mS/m.

The soil layer consists of postglacial gravel, peat and till. There may also be glacifluvial sediments present.

10 Acknowledgements

First of all we would like to thank our supervisors Torleif Dahlin and Berit E. Danielsen for all help and the time they spent to make this work as good as possible. It has been a really nice time working with you.

We would also like to thank Andrea Viezzoli for all help and advices when the measurements in Aarhus was performed, and when you showed us where the best espresso in town was.

Thank you to all personals from Engineering Geology, for all help with all kind of information and pleasant coffee breaks, Henrik Arver for the help of carrying heavy cables and electrodes at the Hallandsås Horst, Tobias Karlsson for interesting discussions in the office and Robert Sturk for helping us with accommodation during the field work at Hallandsås. Per Möller and Carl-Erik Magnusson for all answers of our questions during the work.

Finally we would like to thank our fellow students and teachers for a really nice time in Lund and our families for all support at home.

References

Athanasiou E. N., Tsourlos P. I., Papazachos C. B., Tsokas G.N., 2006. Combined weighted inversion of electrical resistivity data arising from different array types. *Journal of Applied Geophysics 62 (2007) 124-140.*

Banverket, Södra Banregionen, 2002. Projekt Hallandsås Kontraktshandling, Handling 8.3, Geologisk-hydrogeologisk prognos.

Banverket, Södra Banregionen, 1999. Skottorp-Förslöv, Ny järnväg. Tunnlar genom Hallandsås. Uppdaterad bedömning av berggrundsförhållanden. Resultat av kompletterande geoundersökningar åren 1998-99. Erfarenheter från utförd tunneldrivning. Bilaga 4:4 och 4:5.

Bertin J. Loeb J. 1976. *Experimental and Theoretical Aspects of Induced Polarization Volume 1. presentation and Application of the IP Method. Case Histories.* Geoexploration monographs 1. 250 p.

Butler D. K., 2005. *Near-surface geophysics*. SEG Investigations in Geophysics Series No. 13., ISBN 1-5608-0130-1, 732 p.

Çağlar I., 2000. A Method to Remove Electromagnetic Coupling from Induced Polarization Data for an "Exponential" Earth Model. *Pure appl. geophys. 157 (2000) 1729 – 1748.*

Charters R.A., Dosso. H. W., Best M. E., Nienaber, W., 1989, Inductive coupling for a conductive dyke in a resistive Earth. *Physics of the Earth and Planetary Interiors, Volume 54, Issue 1-2, 140-148.*

Dahlin T. 1999. Short note on electrode charge-up effects in DC resistivity data acquisition using multi-electrode arrays. *Geophysical Prospecting, 2000, 48, 181-187.*

Dahlin T., Leroux V., Nissen J., 2002. Measuring techniques in induced polarisation imaging. *Journal of Applied Geophysics 50 (2002) 279 – 298.*

Dahlin T., Zhou B., 2005. Multiple-gradient array measurement for multichannel 2D resistivity imaging. *Near Surface Geophysics, 2006, 113-123.*

Dahlin T., Zhou B., 2004. A numerical comparison of 2D resistivity imaging with ten electrode arrays. *Geophysical Prospecting 52, 379-398.*

Dahlin.T., Bjelm.L., Svensson.C., 1999. Use of electrical imaging in site investigationsfor a railway tunnel through the Hallandsås Horst, Sweden. *Quarterly Journal of Engineering Geology, 32, 163-172.*

Danielsen J .E., Dahlin T., 2004, The applicability of geoelectrical imaging as a tool for design and construction in rock: A pre-study. Engineering Geology, Lund University. Report No. LUTVDG/TVTG—7027—SE.

Danielsen B. E., 2007. *The applicability of geoelectrical imaging as a tool for construction in rock*. Licentiate Thesis 2007. Engineering Geology, Lund University, ISBN 978-91-976848-1-1.

Danielsen B. E. Literature study. Not published.

Fetter C. W., 2001. *Applied Hydrogeology. 4th edition*. ISBN 0-13-122687-8, 598 p.

Geotomo Software, 2006. RES2DINV ver. 3.55 for Windows 98/Me/2000/NT/XP. *Rapid 2-D Resistivity & IP inversion using the least-squares method Wenner (a,b,g), dipole-dipole, inline pole-pole, poledipole, equatorial dipole-dipole, Wenner-Schlumberger, gradient and non-conventional arrays. On land, underwater and cross-borehole surveys.* 136 p.

Hennig T., Wellera A., Canhb T., 2005. The effect of dike geometry on different resistivity configurations. *Journal of Applied Geophysics 57 (2005) 278 – 292.*

Jeppsson H. 2006. Kompendium i Geofysiska undersökningsmetoder, GEL 546. Lunds Universitet. Not published.

Larsen G., Kronborg C., 1994. *Geologisk set, Det mellemste Jylland, En beskrivelse af områder af national geologisk interesse*. Geografforlaget, Miljøministeriet, Skov- og Naturstyrelesen. ISBN 87-7702-132-0.

Leroux V., Dahlin T., 2003. Site conditions requiring extra precautions for induced polarisation measurements. Procs. *9th Meeting of Environmental and Engineering Geophysics, Prague, Czech Republic, 31 August-4 September 2003. O-052.*

Loke, M. H., 2003. Tutorial: 2D and 3D electrical imaging surveys, 134 p. www.geoelectrical.com.

Loke, M. H., 2006. RES2DINV ver. 3.55 for Windows 98/Me/2000/NT/XP: Rapid 2-D Resistivity & IP inversion using the least-squares method, Geotomo Software, Malaysia, 136 p.

Marescot L., Rigobert S, Lopes S. P., Lagabrielle R., Chapellier D. 2005. A general approach for DC apparent resistivity evaluation on arbitrarily shaped 3D structures. *Journal of Applied Geophysics 60*

(2006) 55–67.
Martinho E., Almeida F., 2006. 3D behaviour of contamination in landfill sites using 2D resistivity/IP imaging: case studies in Portugal. *Environ Geol (2006) 49: 1071–1078.*
Palacky, G.I., 1987. *Resistivity characteristics of geological targets.* In: Nabighian, M. (Ed.), *Electromagnetic Methods in Applied Geophysics-Theory*. Society of Exploration Geophysicists, Tulsa, OK, pp. 53– 129.
Parasnis D. S., 1997. *Principles of applied geophysics. 5th edition*, ISBN 0-412-80250-3, 429 p.
Partha S. Routh, Douglas W. Oldenburg 2000. Electromagnetic coupling in frequency-domain Induced Polarization data: a method for removal. *Geophys. J. Int. (2001) 145, 59–76.*
Persson (Alm), P-G. 1985. *The Temperature Log as an Indicator of Permeable Zones and Fractures in Wells,* Dept. of Engineering Geology, Lund, Sweden, LUTVDG/(TVTG-3009)/1-94.
Reynolds J. M. 1997. *An Introduction to applied and environmental geophysics.* John Wiley & Sons Ltd, West Sussex, England. ISBN 10-0471-96802-1, 796 p.
Ringberg B., 1995. Description to the Quaternary Map: Halmstad SV, Scale 1:50 000, Sveriges geologiska undersökning. Ae 121, ISBN 91-7158-537-0, 52 p.
Ringberg B., 2000: Map of the Quaternary Deposits 4C Halmstad SV, Scale 1:50 000, Sveriges geologiska undersökning Ae 121.
Sharma, P. V., 1997. *Environmental and engineering geophysics*. Cambridge University UK. ISBN 0-521-57632-6, 475 p.
Slater L. D., Lesmes D., 2002. IP interpretation in environmental investigations. *Geophysics. Vol. 67. NO. 1 (January-February 2002): p. 77-88.*
Sturk. R, Annertz. K, von Matérn. M, Tunnelling through a regional weakness zone with extremely poor rock at the Hallandsås project. *SveBeFo, Bergmekanikdag 2005 Föredrag, p. 149-159.*
Sumner J. S. 1976. *Principles of Induced Polarization for geophysical exploration.* Elsevier scientific publishing company, ISBN 0-444-41481-9, 277 p.
Sørensen K.I., Auken E., Christensen N. B., Pellerin L., 2003. An Integrated Approach for Hydrogeophysical Investigations: New Technologies and a Case History. *Near Surface Geophysics, 2003, Part 2: Applications and Case Histories.*
Vinegar H. J., Waxman M. H., 1984. Induced Polarization of shaly sands. *Geophysics, Volume 49, Issue 8, pp. 1267-1287*
Wikman.H, Bergström.J, 1987. Description to the map of solid rocks: Halmstad SV, scale 1:50 000. Sveriges geologiska undersökning. Af 133. ISBN 91-7158-415-3
Wikman H, Henkel., 1979a. Map of Structure Geology: 4C Halmstad SV, scale 1:50 000. Sveriges geologiska undersökning Af nr 133.
Wikman H., Henkel H., 1979b. Map of Solids Rocks: 4C Halmstad SV, scale 1:50 000. Sveriges geologiska undersökning Af nr 133.

Internet sources

www.banverket.se
www.banverket.se/sv/Amnen/Aktuella-proekt/Projekt/1869/Hallandsas/Projektdatabas/Sok-matdata.aspx, downloaded 2007-09-25.
www.kabrna.com/cpgs/stratigraphy/strat_column.htm, downloaded 2007-11-20.

Appendix 1

Inversion parameters

Test-line Lund, Sweden

Filename: ideon7_b_c_east_1-5ed.INV
INITIAL DAMPING FACTOR 0.160
MINIMUM DAMPING FACTOR 0.015
VERTICAL TO HORIZONTAL FILTER RATIO 1.00
Flatness filter is directly used on model parameters.
Jacobian matrix is recalculated after each iteration.
Normal nesh used.
Factor to increase damping factor with depth is 1.05
Damping factor is optimised for each iteration
Robust constrain used on data with epsilon factor 0.0500
Robust constrain used on model with epsilon factor 0.0050
Finite-difference method was used in forward modelling.
Logarithm of apparent resistivity values used as inversion parameter.
Limit imposed on range of model resistivity values
Average model resistivity used as reference resistivity
Upper and lower range limits are 50.000 and 0.020
Effect of side blocks is severely reduced
Simultaneous inversion of IP data
Relative change in RMS error for convergence is 5.0000
Minimum change in RMS error for line search is 0.4000
Ratio of maximum number of model blocks to data points 20.00
Factor to increase model depth range is 1.00
Position of electrodes are not rounded to nearest unit electrode spacing.
Position of electrodes for dipole-dipole array are automatically switched
Recalculation of Jacobian matrix is not restarted in quasi-Newton steps.
Standard Gauss-Newton inversion method used
Width of model cells is 1.00 times the unit electrode spacing
Number of nodes between adjacent electrodes is 2

Test-line Aarhus, Denmark

Filename: grad_l_s_singel_lund_aw025.INV
INITIAL DAMPING FACTOR 0.160
MINIMUM DAMPING FACTOR 0.015
VERTICAL TO HORIZONTAL FILTER RATIO 0.25
Flatness filter is directly used on model parameters.
Jacobian matrix is recalculated after each iteration.
Normal nesh used.
Factor to increase damping factor with depth is 1.05
Damping factor is optimised for each iteration
Robust constrain used on data with epsilon factor 0.0500
Robust constrain used on model with epsilon factor 0.0050
Finite-element method was used in forward modelling.
Logarithm of apparent resistivity values used as inversion parameter.
Limit imposed on range of model resistivity values
Average model resistivity used as reference resistivity
Upper and lower range limits are 50.000 and 0.020
Effect of side blocks is severely reduced
Simultaneous inversion of IP data
Relative change in RMS error for convergence is 5.0000
Minimum change in RMS error for line search is 0.4000
Ratio of maximum number of model blocks to data points 20.00
Factor to increase model depth range is 1.00
Position of electrodes are not rounded to nearest unit electrode spacing.
Position of electrodes for dipole-dipole array are automatically switched
Recalculation of Jacobian matrix is not restarted in quasi-Newton steps.

Incomplete solution Gauss-Newton inversion method used with convergence limit 0.005
Width of model cells is 1.00 times the unit electrode spacing
Number of nodes between adjacent electrodes is 2

Filename: grad_sl_sep_lund_electfixed_aw025.INV
INITIAL DAMPING FACTOR 0.160
MINIMUM DAMPING FACTOR 0.015
VERTICAL TO HORIZONTAL FILTER RATIO 0.25
Flatness filter is directly used on model parameters.
Jacobian matrix is recalculated after each iteration.
Normal nesh used.
Factor to increase damping factor with depth is 1.05
Damping factor is optimised for each iteration
Robust constrain used on data with epsilon factor 0.0500
Robust constrain used on model with epsilon factor 0.0050
Finite-element method was used in forward modelling.
Logarithm of apparent resistivity values used as inversion parameter.
Limit imposed on range of model resistivity values
Average model resistivity used as reference resistivity
Upper and lower range limits are 50.000 and 0.020
Effect of side blocks is severely reduced
Simultaneous inversion of IP data
Relative change in RMS error for convergence is 5.0000
Minimum change in RMS error for line search is 0.4000
Ratio of maximum number of model blocks to data points 20.00
Factor to increase model depth range is 1.00
Position of electrodes are not rounded to nearest unit electrode spacing.
Position of electrodes for dipole-dipole array are automatically switched
Recalculation of Jacobian matrix is not restarted in quasi-Newton steps.
Incomplete solution Gauss-Newton inversion method used with convergence limit 0.005
Width of model cells is 0.50 times the unit electrode spacing
Number of nodes between adjacent electrodes is 2

Filename: poledipole_s_l_sep_lund_electfixed_aw.INV
INITIAL DAMPING FACTOR 0.300
MINIMUM DAMPING FACTOR 0.030
VERTICAL TO HORIZONTAL FILTER RATIO 0.25
Flatness filter is directly used on model parameters.
Jacobian matrix is recalculated after each iteration.
Normal nesh used.
Factor to increase damping factor with depth is 1.05
Damping factor is optimised for each iteration
Robust constrain used on data with epsilon factor 0.0500
Robust constrain used on model with epsilon factor 0.0050
Finite-element method was used in forward modelling.
Logarithm of apparent resistivity values used as inversion parameter.
Limit imposed on range of model resistivity values
Average model resistivity used as reference resistivity
Upper and lower range limits are 50.000 and 0.020
Effect of side blocks is severely reduced
Simultaneous inversion of IP data
Relative change in RMS error for convergence is 5.0000
Minimum change in RMS error for line search is 0.4000
Ratio of maximum number of model blocks to data points 20.00
Factor to increase model depth range is 1.00
Position of electrodes are not rounded to nearest unit electrode spacing.
Position of electrodes for dipole-dipole array are automatically switched
Recalculation of Jacobian matrix is not restarted in quasi-Newton steps.
Standard Gauss-Newton inversion method used
Width of model cells is 1.00 times the unit electrode spacing

Number of nodes between adjacent electrodes is 2

The-Hallandsås Horst

Site 1

Filename: M1_sep_b_w1-9.INV
INITIAL DAMPING FACTOR 0.300
MINIMUM DAMPING FACTOR 0.030
VERTICAL TO HORIZONTAL FILTER RATIO 2.00
Flatness filter is directly used on model parameters.
Jacobian matrix is recalculated after each iteration.
Normal nesh used.
Factor to increase damping factor with depth is 1.05
Damping factor is optimised for each iteration
Robust constrain used on data with epsilon factor 0.0500
Robust constrain used on model with epsilon factor 0.0050
Finite-element method was used in forward modelling.
Logarithm of apparent resistivity values used as inversion parameter.
Limit imposed on range of model resistivity values
Average model resistivity used as reference resistivity
Upper and lower range limits are 50.000 and 0.020
Effect of side blocks is severely reduced
Simultaneous inversion of IP data
Relative change in RMS error for convergence is 5.0000
Minimum change in RMS error for line search is 0.4000
Ratio of maximum number of model blocks to data points 20.00
Factor to increase model depth range is 1.00
Position of electrodes are not rounded to nearest unit electrode spacing.
Position of electrodes for dipole-dipole array are automatically switched
Recalculation of Jacobian matrix is not restarted in quasi-Newton steps.
Incomplete solution Gauss-Newton inversion method used with convergence limit 0.005
Width of model cells is 0.50 times the unit electrode spacing
Number of nodes between adjacent electrodes is 2

Filename: merging_pd_grad.INV
INITIAL DAMPING FACTOR 0.300
MINIMUM DAMPING FACTOR 0.030
VERTICAL TO HORIZONTAL FILTER RATIO 2.00
Flatness filter is directly used on model parameters.
Jacobian matrix is recalculated after each iteration.
Normal nesh used.
Factor to increase damping factor with depth is 1.05
Damping factor is optimised for each iteration
Robust constrain used on data with epsilon factor 0.0500
Robust constrain used on model with epsilon factor 0.0050
Finite-element method was used in forward modelling.
Logarithm of apparent resistivity values used as inversion parameter.
Limit imposed on range of model resistivity values
Average model resistivity used as reference resistivity
Upper and lower range limits are 50.000 and 0.020
Effect of side blocks is severely reduced
Simultaneous inversion of IP data
Relative change in RMS error for convergence is 5.0000
Minimum change in RMS error for line search is 0.4000
Ratio of maximum number of model blocks to data points 20.00
Factor to increase model depth range is 1.00
Position of electrodes are not rounded to nearest unit electrode spacing.
Position of electrodes for dipole-dipole array are automatically switched
Recalculation of Jacobian matrix is not restarted in quasi-Newton steps.
Incomplete solution Gauss-Newton inversion method used with convergence limit 0.005
Width of model cells is 0.50 times the unit electrode spacing

Number of nodes between adjacent electrodes is 2

Site 2

Filename: grad_sep_exp_topo_w1-9_merge.INV
INITIAL DAMPING FACTOR 0.160
MINIMUM DAMPING FACTOR 0.015
VERTICAL TO HORIZONTAL FILTER RATIO 1.00
Flatness filter is directly used on model parameters.
Jacobian matrix is recalculated after each iteration.
Normal nesh used.
Factor to increase damping factor with depth is 1.05
Damping factor is optimised for each iteration
Robust constrain used on data with epsilon factor 0.0500
Robust constrain used on model with epsilon factor 0.0050
Finite-element method was used in forward modelling.
Logarithm of apparent resistivity values used as inversion parameter.
Limit imposed on range of model resistivity values
Average model resistivity used as reference resistivity
Upper and lower range limits are 50.000 and 0.020
Effect of side blocks is severely reduced
Simultaneous inversion of IP data
Relative change in RMS error for convergence is 5.0000
Minimum change in RMS error for line search is 0.4000
Ratio of maximum number of model blocks to data points 20.00
Factor to increase model depth range is 1.00
Position of electrodes are not rounded to nearest unit electrode spacing.
Position of electrodes for dipole-dipole array are automatically switched
Recalculation of Jacobian matrix is not restarted in quasi-Newton steps.
Incomplete solution Gauss-Newton inversion method used with convergence limit 0.005
Width of model cells is 0.50 times the unit electrode spacing
Number of nodes between adjacent electrodes is 2

Filename: poldipol_sep_topo_w1-9_merge.INV
INITIAL DAMPING FACTOR 0.160
MINIMUM DAMPING FACTOR 0.015
VERTICAL TO HORIZONTAL FILTER RATIO 1.00
Flatness filter is directly used on model parameters.
Jacobian matrix is recalculated after each iteration.
Normal nesh used.
Factor to increase damping factor with depth is 1.05
Damping factor is optimised for each iteration
Robust constrain used on data with epsilon factor 0.0500
Robust constrain used on model with epsilon factor 0.0050
Finite-element method was used in forward modelling.
Logarithm of apparent resistivity values used as inversion parameter.
Limit imposed on range of model resistivity values
Average model resistivity used as reference resistivity
Upper and lower range limits are 50.000 and 0.020
Effect of side blocks is severely reduced
Sequential inversion of IP data
Relative change in RMS error for convergence is 5.0000
Minimum change in RMS error for line search is 0.4000
Ratio of maximum number of model blocks to data points 20.00
Factor to increase model depth range is 1.00
Position of electrodes are not rounded to nearest unit electrode spacing.
Position of electrodes for dipole-dipole array are automatically switched
Recalculation of Jacobian matrix is not restarted in quasi-Newton steps.
Incomplete solution Gauss-Newton inversion method used with convergence limit 0.005
Width of model cells is 0.50 times the unit electrode spacing
Number of nodes between adjacent electrodes is 2

Appendix 2

Pseudosections

Test-line Aarhus, Denmark

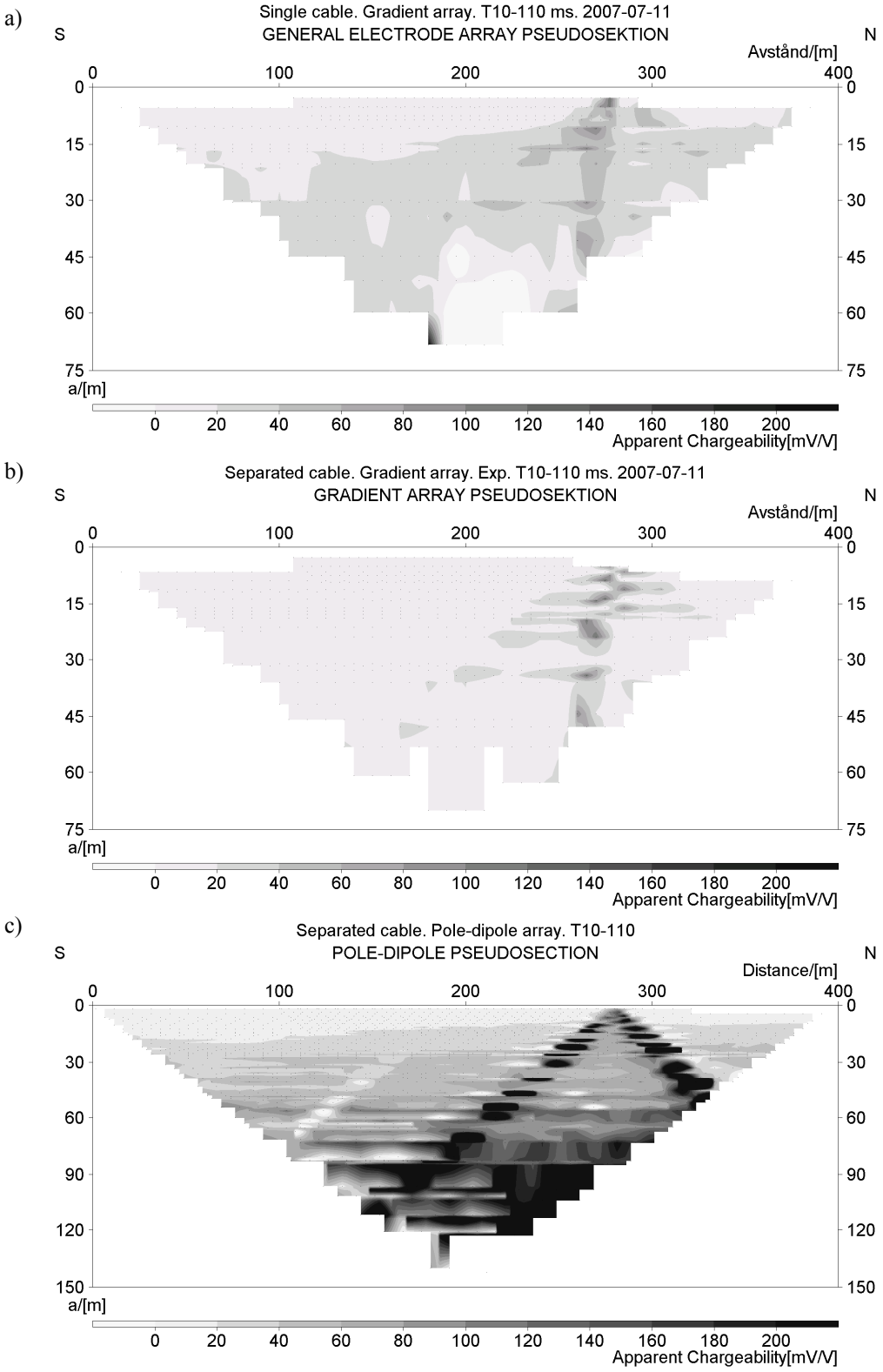

Fig. A2.1. Apparent chargeability. Test line Aarhus, Denmark. Time window 10-110 ms. (a) Single cable, gradient array. (b) Separated cable, gradient array. (c) Separated cables, pole-dipole array.

a)

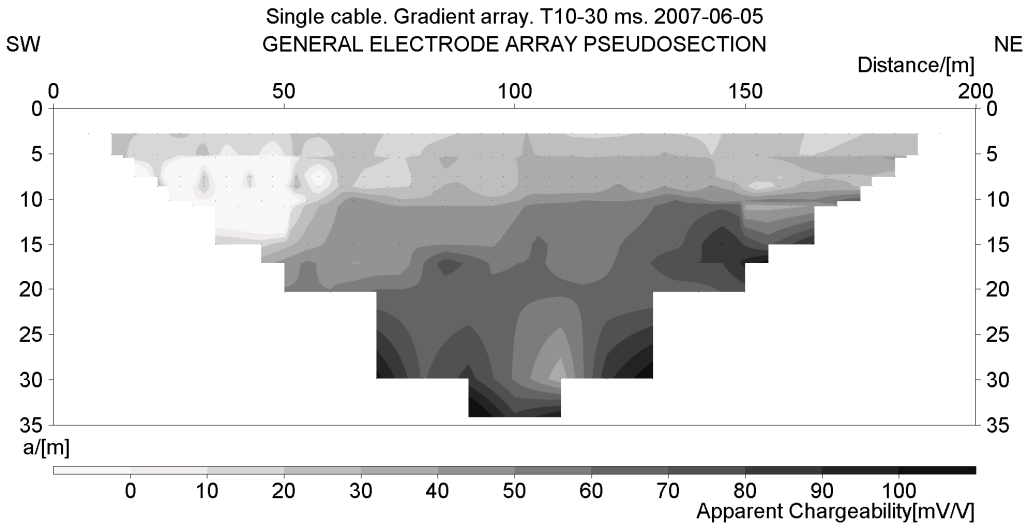

b)

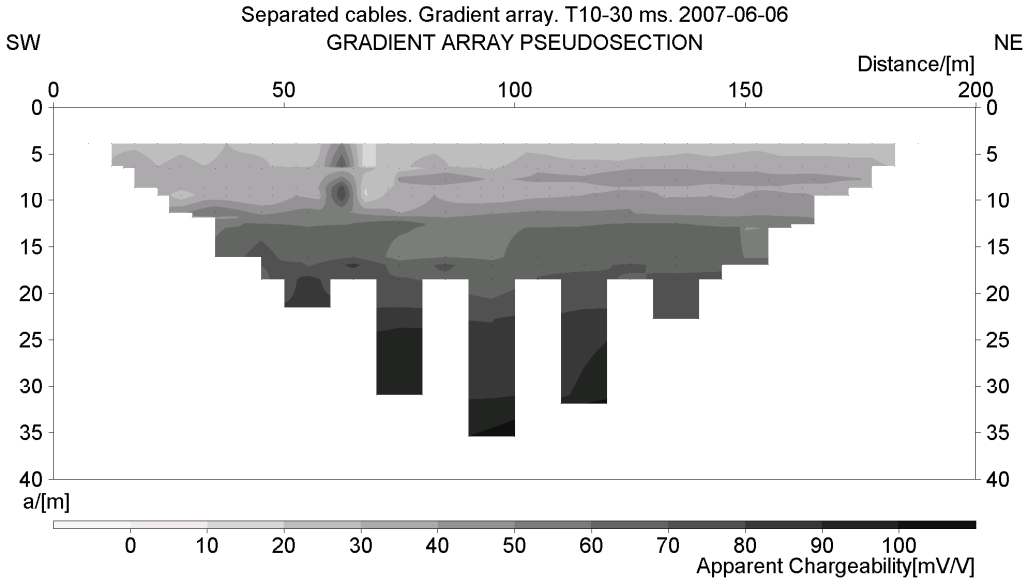

c)

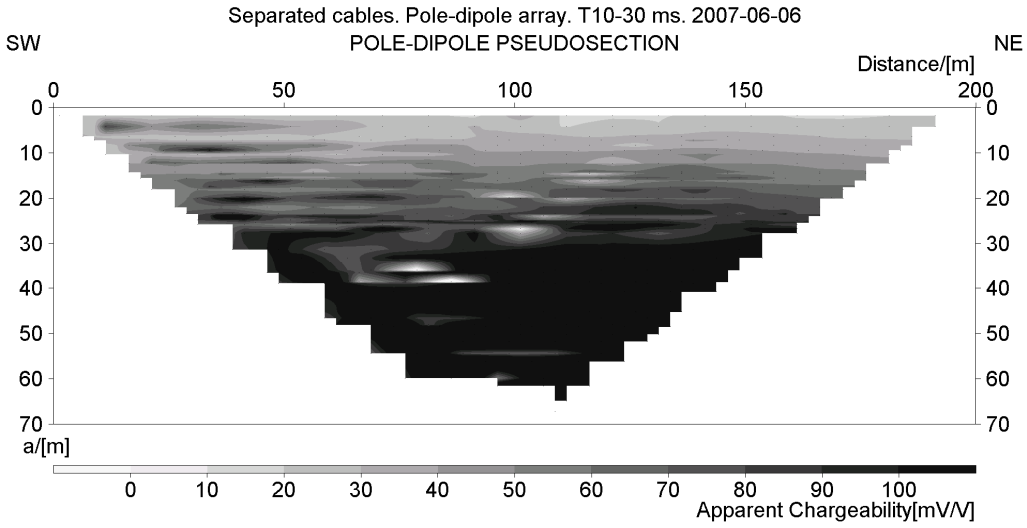

Fig. A2.2. Apparent chargeability, Test line Hallandsås Horst, Site 1. Time window 10-30 ms. (a) Single cable, gradient array. (b) Separated cables, gradient array. (c) Separated cables, pole-dipole array.

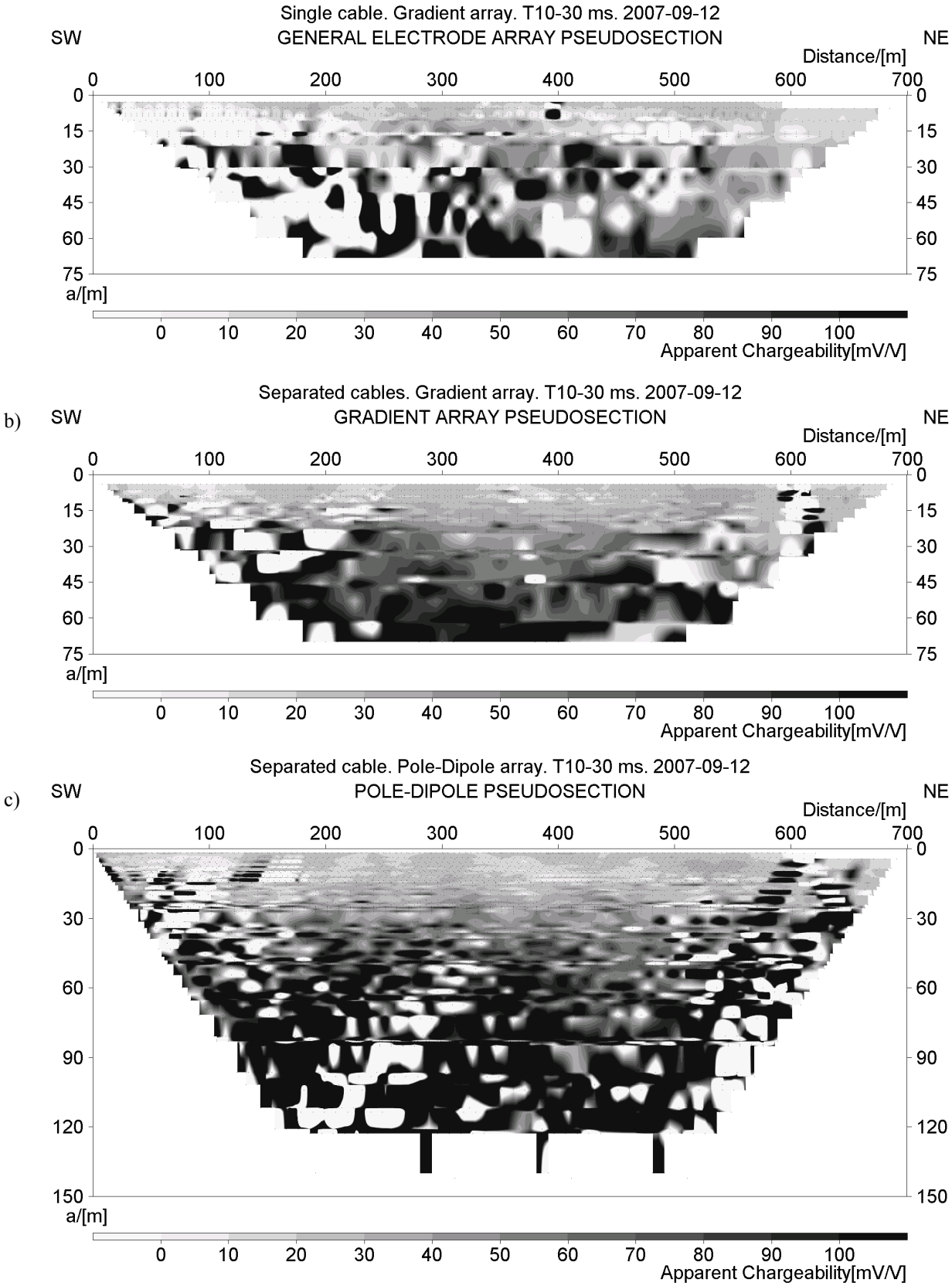

Fig. A2.3. Apparent chargeability, Test line Hallandsås Horst, Site 2. Time window 10-30 ms. (a) Single cable, gradient array. (b) Separated cables, gradient array. (c) Separated cables, pole-dipole array.

Appendix 3

Protocol-files

Test-line Lund, Sweden

Single cable, dipole-dipole array
DIDI7F3L.org
DIDI7F3S.org
DIDI7R3L.org
DIDI7R3S.org

Separated cables, dipole-dipole array
DIDI7F3L.org
DIDI7F3S.org

Separated cables, gradient array
GRD7_3_shift_exp.org

Electrode contact test
CONTACT3.org

Test-line Aarhus, Denmark

Single cable, gradient array
GRAD7S.org
GRAD7S.org

Separated cables, gradient array
Grad7L_shift_exp.org
Grad7S_shift_exp.org

Separated cables, pole-dipole array
POLDIP7L_shift.org
POLDIP7S_shift.org

Test-line Hallandås Horst, Sweden

Single cable, gradient array
GRAD7S.org
GRAD7S.org

Separated cables, gradient array
Grad7L_shift_exp.org
Grad7S_shift_exp.org

Separated cables, pole-dipole array
POLDIP7L_shift.org
POLDIP7S_shift.org

Tidigare skrifter i serien "Examensarbeten i Geologi vid Lunds Universitet":

171. Ekestubbe, Jonas, 2004: $^{40}Ar/^{39}Ar$ geokronologi och implikationer för tolkningen av den Kaledoniska utvecklingen i Kebnekaise.
172. Lindgren, Paula, 2004. Tre sensvekofenniska graniter: kontakt- och åldersrelationer samt förekomst av metasedimentära enklaver.
173. Janson, Charlotta, 2004. A petrographical and geochemical study of granitoids from the south-eastern part of the Linderödsåsen Horst, Skåne.
174. Jonsson, Sara, 2004: Structural control of fine-grained granite dykes at the Äspö Hard Rock Laboratory, north of Oskarshamn, Sweden.
175. Ljungberg, Carina, 2004: Belemniters stabila isotopsammansättning: paleomiljöns och diagenesens betydelse.
176. Oster, Jessica, 2004: A stratigraphic study of a coastal section through a Late Weichselian kettle hole basin at Ålabodarna, western Skåne, Sweden.
177. Einarsson, Elisabeth, 2004: Morphological and functional differences between rhamphorhynchoid and pterodactyloid pterosaurs with emphasis on flight.
178. Anell, Ingrid, 2004: Subsidence in rift zones; Analyzing results from repeated precision leveling of the Vogar Profile on the Reykjanes Peninsula, Southwest Iceland.
179. Wall, Torbjörn, 2004: Magnetic grain-size analyses of Holocene sediments in the North Atlantic and Norwegian Sea – palaeoceano-graphic applications.
180. Mellgren, Johanna, S., 2005: A model of reconstruction for the oral apparatus of the Ordovician conodont genus *Protopanderodus* Lindström, 1971.
181. Jansson, Cecilia, 2005: Krossbergskvalitet och petrografi i den kambriska Hardebergasandstenen i Skåne.
182. Öst, Jan-Olof, 2005: En övergripande beskrivning av malmbildande processer med detaljstudier av en bandad järnmalm från södra Dalarna, Bergslagen.
183. Bragée, Petra, 2005: A palaeoecological study of Holocene lake sediments above the highest shoreline in the province of Västerbotten, northeast Sweden.
184. Larsson, Peter, 2005: Palynofacies och mineralogi över krita-paleogengränsen vid Stevns Klint och Kjølby Gaard, Danmark.
185. Åberg, Lina, 2005: Metamorphic study of metasediment from the Kangilinaaq Peninsula, West Greenland.
186. Sidgren, Ann-Sofie, 2005: $^{40}Ar/^{39}Ar$-geokronologi i det Rinkiska bältet, västra Grönland.
187. Gustavsson, Lena, 2005: The Late Silurian Lau Event and brachiopods from Gotland, Sweden.
188. Nilsson, Eva K., 2005: Extinctions and faunal turnovers of early vertebrates during the Late Silurian Lau Event, Gotland, Sweden.
189. Czarniecka, Ursula, 2005: Investigations of infiltration basins at the Vomb Water Plant – a study of possible causes of reduced infiltration capacity.
190. G³owacka, Ma³gorzata, 2005: Soil and groundwater contamination with gasoline and diesel oil. Assessment of subsurface hydrocarbon contamination resulting from a fuel release from an underground storage tank in Vanstad, Skåne, Sweden.
191. Wennerberg, Hans, 2005: A study of early Holocene climate changes in Småland, Sweden, with focus on the '8.2 kyr event'.
192. Nolvi, Maria & Thorelli, Gunilla, 2006: Extraterrestrisk och terrestrisk kromrik spinell i fanerozoiska kondenserade sediment.
193. Nilsson, Andreas, 2006: Palaeomagnetic secular variations in the varved sediments of Lake Goœci¹¿, Poland: testing the stability of the natural remanent magnetization and validity of relative palaeointensity estimates.
194. Nilsson, Anders, 2006: Limnological responses to late Holocene permafrost dynamics at the Stordalen mire, Abisko, northern Sweden.
195. Nilsson, Susanne, 2006: Sedimentary facies and fauna of the Late Silurian Bjärsjölagård Limestone Member (Klinta Formation), Skåne, Sweden.
196. Sköld, Eva, 2006: Kulturlandskapets förändringar inom röjningsröseområdet Yttra Berg, Halland - en pollenanalytisk undersökning av de senaste 5000 åren.

197. Göransson, Ammy, 2006: Lokala miljöförändringar i samband med en plötslig havsyteförändring ca 8200 år före nutid vid Kalvöviken i centrala Blekinge.
198. Brunzell, Anna, 2006: Geofysiska mätningar och visualisering för bedömning av heterogeniteters utbredning i en isälvsavlagring med betydelse för grundvattenflöde.
199. Erlfeldt, Åsa, 2006: Brachiopod faunal dynamics during the Silurian Ireviken Event, Gotland, Sweden.
200. Vollert, Victoria, 2006: Petrografisk och geokemisk karaktärisering av metabasiter i Herrestadsområdet, Småland.
201. Rasmussen, Karin, 2006: En provenansstudie av Kågerödformationen i NV Skåne – tungmineral och petrografi.
202. Karlsson, Jonnina, P., 2006: An investigation of the Felsic Ramiane Pluton, in the Monapo Structure, Northern Moçambique.
203. Jansson, Ida-Maria, 2006: An Early Jurassic conifer-dominated assemblage of the Clarence-Moreton Basin, eastern Australia.
204. Striberger, Johan, 2006: En lito- och biostratigrafisk studie av senglaciala sediment från Skuremåla, Blekinge.
205. Bergelin, Ingemar, 2006: $^{40}Ar/^{39}Ar$ geochronology of basalts in Scania, S Sweden: evidence for two pulses at 191-178 Ma and 110 Ma, and their relation to the breakup of Pangea.
206. Edvarssson, Johannes, 2006: Dendrokronologisk undersökning av tallbestånds etablering, tillväxtdynamik och degenerering orsakat av klimatrelaterade hydrologiska variationer på Viss mosse och Åbuamossen, Skåne, södra Sverige, 7300-3200 cal. BP.
207. Stenfeldt, Fredrik, 2006: Litostratigrafiska studier av en platåformad sand- och grusavlagring i Skuremåla, Blekinge.
208. Dahlenborg, Lars, 2007: A Rock Magnetic Study of the Åkerberg Gold Deposit, Northern Sweden.
209. Olsson, Johan, 2007: Två svekofenniska graniter i Bottniska bassängen; utbredning, U-Pb zirkondatering och test av olika abrasionstekniker.
210. Erlandsson, Maria, 2007: Den geologiska utvecklingen av västra Hamrångesynklinalens suprakrustalbergarter, centrala Sverige.
211. Nilsson, Pernilla, 2007: Kvidingedeltat – bildningsprocesser och arkitektonisk uppbyggnadsmodell av ett glacifluvialt Gilbertdelta.
212. Ellingsgaard, Óluva, 2007: Evaluation of wireline well logs from the borehole Kyrkheddinge-4 by comparsion to measured core data.
213. Åkerman, Jonas, 2007. Borrkärnekartering av en Zn-Ag-Pb-mineralisering vid Stenbrånet, Västerbotten.
214. Kurlovich, Dzmitry, 2007: The Polotsk-Kurzeme and the Småland-Blekinge Deformation Zones of the East European Craton: geomorphology, architecture of the sedimentary cover and the crystalline basement.
215. Mikkelsen, Angelica, 2007: Relationer mellan grundvattenmagasin och geologiska strukturer i samband med tunnelborrning genom Hallandsås, Skåne.
216. Trondman, Anna-Kari, 2007: Stratigraphic studies of the Taniente Palet bog at the north-western corner of Isla de los Estados, Tierra del Fuego, South America.
217. Månsson, Carl-Henrik & Siikanen, Jonas, 2007: Measuring techniques of Induced Polarization regarding data quality with an application on a test-site in Aarhus, Denmark and the tunnel construction at the Hallandsås Horst, Sweden.
218. Ohlsson, Erika, 2007: Classification of stony meteorites from north-west Africa and the Dhofar desert region in Oman.

LUNDS UNIVERSITET

Geologiska institutionen
Gentrum för GeoBiosfärsvetenskap
Sölvegatan 12, 223 62 Lund